An investigation into the influence of stent strut thickness on in-stent restenosis using the finite element method

by

Fariza Fida Basir, BEng

A thesis submitted to Dublin City University in partial fulfilment of the requirement for the degree of

Masters in Engineering

Supervisors
Dr. Caitriona Lally, BEng, MEng, PhD
Professor M.S.J. Hashmi, Phd, DSc

School of Mechanical and Manufacturing Engineering
Dublin City University

November 2005

DECLARATION

I hereby certify that this material, which I now submit for assessment on the programme of study leading to the award of Masters in Engineering, is entirely my own work and has not been taken from the work of others save and to the extent that such work has been cited and acknowledged within the text of my work.

Signed: ---------- ID No: 97194735

Fariza Fida Basir

Date: 8th November 2005

ACKNOWLEDGEMENTS

I would like to take this opportunity to thank my supervisors, Dr. Caitriona Lally and Prof. M.S.J. Hashmi, for their help and guidance throughout the research study. I would like to extend my gratitude especially towards Dr. Caitriona Lally who went the extra mile and past her responsibilities to ensure that I achieve a good standard in my work; I thank her, for her endless support, guidance and encouragement throughout the study. I am forever grateful.

I would like to thank my technician, Keith Hickey for his assistance in accommodating the technical resources the project needed.

And to my friends; my best friend Jaycey, for her constant support and for having faith in me. Shuborna who shared many things with me, Aneela, my gym friend when studying got so overwhelming. To Darragh, Mary and Barbara, I thank them for their friendship over the years. To the lads in the lab, John, Declan and Dave, for making my life in college a good one with their little stories and humour. To Angah and Amy, I would like to extend my appreciation for their kindness and generosity. And to Jameel, I would like to thank him for listening patiently to the pains and laughters, let it be study or personal throughout the years.

Most of all, my love and thank to the most important people in my life, to my mother who has done so much, from cooking my favourite meal to supporting me financially and emotionally. I thank her for having constantly praying for my success and well-being. To my sister and also my best friend Farrah, who has never failed to be there for me. It would not be possible to return her endless support and sacrifices. Let us look forward to the new beginning that lies ahead.

An investigation into the influence of stent strut thickness on in-stent restenosis using the finite element method

Fariza Fida Basir

Abstract

In-stent restenosis represents the major limitation for stenting procedures. In-stent restenosis is the renarrowing of the artery lumen within a stent predominantly due to excessive growth of neointimal hyperplasia. Clinical studies have found that stent design is a key determinant in the propensity of stents to cause restenosis, indicating a vital link between the biomechanics of stents and the development of the disease. The ISAR-STEREO Trial specifically assessed the effect of strut thickness on restenosis outcome and found that for the same stent design, a thinner strut stent was associated with a significant reduction of angiographic and clinical restenosis compared to the same stent with a thicker strut. The main objective of this study is to use the finite element method to simulate these stenting procedures, and to examine the stresses induced within the stented arterial vessel walls by the stents, thus enabling the mechanical stimuli for in-stent restenosis to be identified.

Finite element models of thin and thick strut stents were developed and the stents were deployed in various stenosed vessel geometries such that the stresses induced within the stented vessels by the two stents could be compared. The stresses were examined at the end of stent deployment, to determine the mechanical stimuli for acute damage, and again at stent unloading, to determine the long term stimuli for in-stent restenosis. The stress analyses were used to determine the level of vascular injury caused to the artery by different strut thickness stents.

The finite element studies successfully identified differences between the mechanical loading of the arterial tissue in the vessels stented with the two different stents. The higher restenosis rate of the thicker strut stent, reported in the ISAR-STEREO clinical study, was found to be the result of the higher luminal gain achieved by the thicker strut stent, due to the lower recoil of the stent structure when both stents were expanded to the same initial lumen diameter. Further stenting analyses, however, found that the thicker strut stent resulted in a lower percentage of volume stressed at high levels compared with the thinner strut stent when it was expanded to the same final lumen diameter. This suggests that a thicker strut stent may in fact have the potential to be expanded to an optimal diameter whereby the in-stent restenosis is minimised. Therefore, it is proposed that the use of preclinical testing tools, such as finite element modelling, could be used to predetermine the deployment protocol and optimum luminal gain of a particular stent design in order to minimise the mechanical stimuli for in-stent restenosis.

TABLE OF CONTENTS

NOMENCLATURE

Roman Letters

a_{ij}	Material constants
E	Green-Lagrangian strain tensor
L	Length
R	Radius
S	Component of the second Piola-Kirchoff stress tensor
W	Strain energy

Greek Letters

I_1, I_2, I_3	Stretch invariants
$\lambda_1, \lambda_2, \lambda_3$	Principal stretches
Ø	Diameter
σ	von Mises stress
$\sigma_1, \sigma_2, \sigma_3$	Principal stresses
$\dot{\varepsilon}^{pl}$	Plastic strain rate tensor
$\dot{\varepsilon}_{eqv}$	Equivalent plastic strain

LIST OF FIGURES

LIST OF TABLES

Chapter 1

INTRODUCTION

1.1 Cardiovascular Disease

Cardiovascular disease (CVD) is a general description for a variety of disorders and conditions that can affect the circulatory system where the arteries of the body become blocked due to a build up of plaque. CVD is a major health and economic burden throughout the world, especially in most developed countries where it is the leading cause of death. In 1997, cardiovascular disease caused 43% of deaths worldwide [1]. In Ireland, CVD is the highest single cause of death and it caused between 38-40% of deaths in 2004 [2].

In general, there has been a drop in premature deaths from CVD across almost all EU countries (with the exception of Latvia) over the years from 2000 to 2002, see Figure 1.1 [3]. This drop in death rate is partly due to advances in medical care such as the development of alternative non-invasive treatments for cardiovascular disease treatment, such as balloon angioplasty and stenting. It is also as a result of increased health awareness. However, it is important to note that this drop still constitutes less than 10% of total deaths from CVD and it is therefore still vital that further measures to reduce the mortality rate from CVD be employed.

Throughout the world, private and funded research organisations have been playing a vital role in researching the causes, preventive measures, treatments and diagnostic procedures for CVD, and in particular heart disease. There are several treatments for CVD with the most common being artery bypass

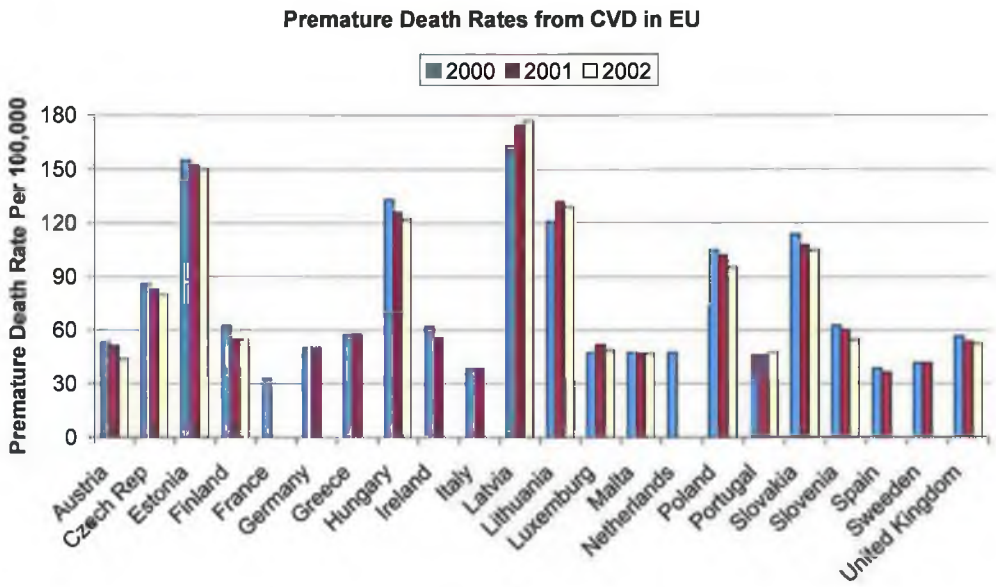

Figure 1.1 Graph of premature death rates from cardiovascular disease across EU countries, [3].

surgery, balloon angioplasty, stent implantation, atherectomy and laser vaporisation techniques [4]. Since their introduction in 1994, the use of stents has dramatically increased over the years for the treatment of CVD. In 1997, the use of stents in many countries ranged from 30%-65% of the total cases of coronary heart disease, where France was found to have the highest, and Brazil the lowest, use of stents [5].

1.2 Coronary Heart Disease

Coronary heart disease is a condition which develops due to a build up of deposits in the wall of the coronary arteries, known as plaque. Plaque builds up on the walls of the coronary arteries and causes hardening and narrowing of the arteries, see Figure 1.2. This process, called artherosclerosis, may significantly reduce or block blood flow to the heart, ultimately leading to a myocardial infarction, see Figure 1.2. Heart disease represents the majority of CVD cases in Ireland and it was responsible for 51% of total CVD cases in 2004 [2].

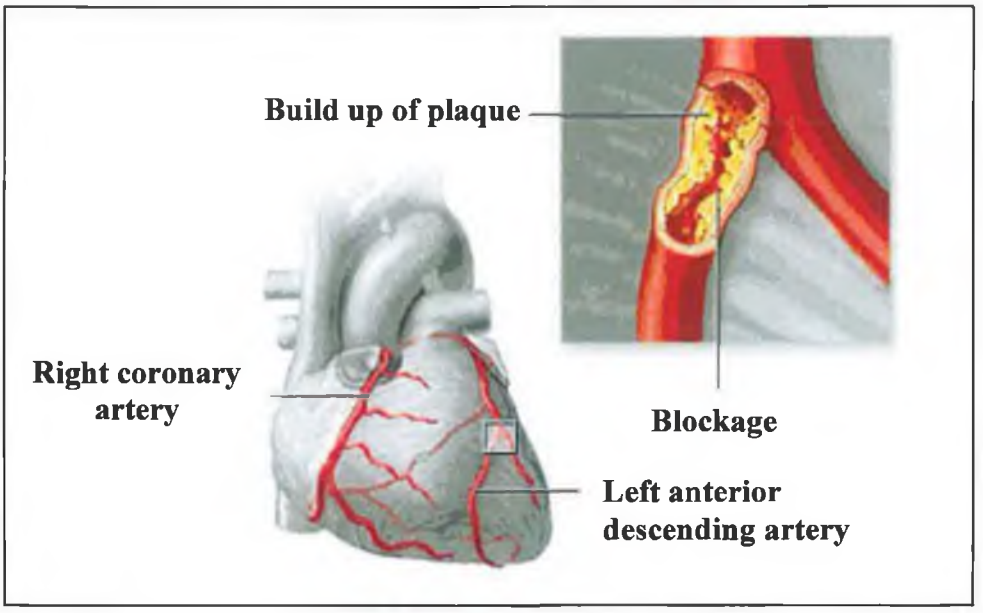

Figure 1.2 Illustration of artherosclerosis in the coronary arteries [adapted from Medline], [7].

Coronary heart disease may be treated in a number of ways, which depends on the severity of the disease. The main purpose of treatment is to restore blood flow to the heart. Early stages of the disease may be improved by lifestyle changes, e.g. cessation of smoking, exercise program, reduction of stress. In the most severe cases bypass surgery is required to restore blood flow.

Coronary artery bypass grafting (CABG) is a surgical procedure that involves detouring blood around a blockage in a coronary artery by taking a segment of a blood vessel from another part of the body or an artificial graft. According to AHA, CABG is the most commonly performed surgery in the United States and around the world, with over 571,000 CABG procedures performed in 1999 [6]. This procedure is generally very successful, with less than 5% chance of heart damage and less than 2% morbidity in most cases [4]. However, it is the most invasive vascular treatment, and consequently it is lengthy and costly. As a result, CABG is limited to treatment of the most severe cases of coronary heart disease.

The introduction of Percutaneous Transluminal Coronary Angioplasty (PTCA) in 1977 [8], was an attempt to non-invasively treat CVD. The frequent occurrence of restenosis post angioplasty led to the development of other catheter-based techniques, including atherectomy, excimer laser and balloon angioplasty combined with stenting [4]. Atherectomy is a catheter-based procedure to remove plaques with a rotating blade device that cuts away the plaques and it is generally used in conjunction with balloon angioplasty or stenting when plaque is exceptionally hard due to calcification. The use of an excimer laser for CVD treatment involves the use of a laser tipped catheter which is used to vaporise the arterial plaque.

Atherectomy and excimer laser treatments are rarely used today, however, balloon angioplasty and stenting are commonly preformed procedures. The use of stents has proven to be more effective, efficient, and less invasive in comparison to other treatments of heart disease. In Ireland, recent studies have found that the use of coronary stents in 1998 was 2.4 times higher than surgical bypass procedures whilst their usage increased by 31% the following year, see Figure 1.3 [9].

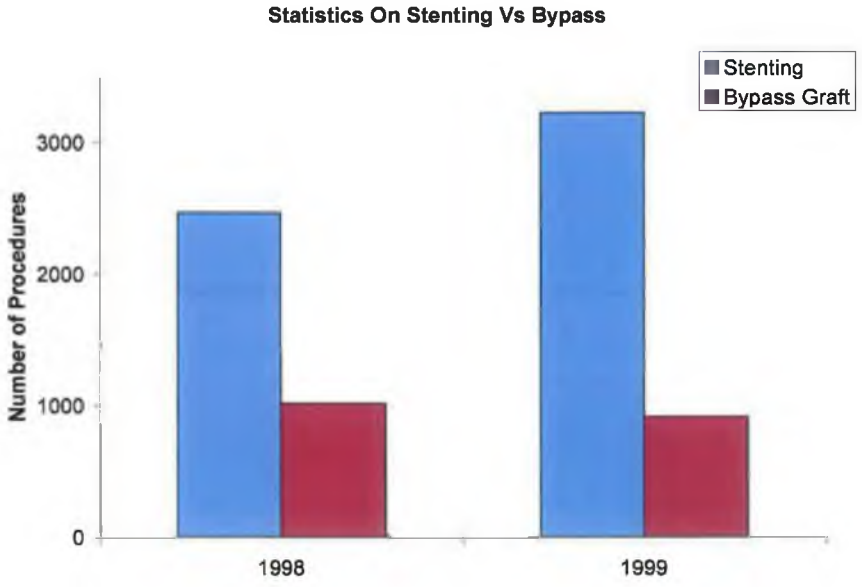

Figure 1.3 Graph of the frequency of the use of coronary stenting and coronary artery bypass grafts in 1998 and 1999, [9].

1.3 Percutaneous Transluminal Coronary Angioplasty

Percutaneous transluminal coronary angioplasty (PTCA) which is also known as plain old balloon angioplasty (POBA) is a widely used catheter-based procedure for the treatment of heart disease. The first PTCA was performed in 1977 by the Swiss physician Andreas Gruntzig, as an alternative form of CABG [8].

PTCA requires a catheter, with a small inflatable balloon on the end, which is positioned within the narrowed section of the affected artery. Inflation of the balloon catheter causes the balloon to push outward compressing the plaque and expanding the surrounding wall of the artery. This results in a wider arterial lumen and hence improved blood flow, see Figure 1.4.

While PTCA is an effective alternative to bypass surgery, there is a risk of early acute closure of the coronary artery and a high rate of reoccurance of the obstruction of blood flow, i.e. restenosis. Restenosis is the renarrowing of the artery lumen induced by elastic recoil, vascular remodelling and excessive growth of neointimal hyperplasia [10]. Several balloon dilation techniques were investigated to minimize the onset of restenosis post PTCA without success [11]. The frequent occurrence of restenosis post angioplasty led to the development of intravascular stents.

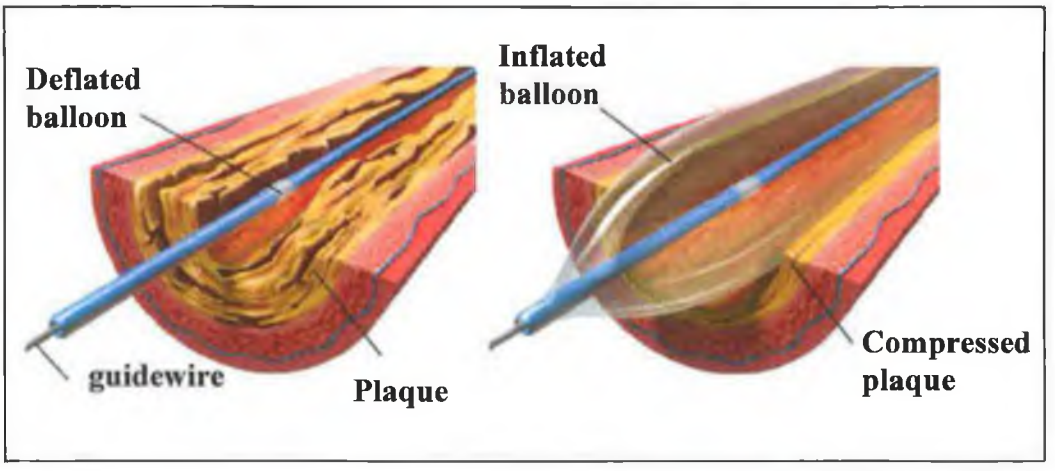

Figure 1.4 Illustration of PTCA procedure [adapted from Heart Centre], [4].

1.4 Intravascular Stenting

An intravascular stent is a small, latticed, expandable wire mesh tube, which is inserted into a blocked artery to restore normal blood flow [4]. Stenting is also a catheter-based and minimally invasive procedure, which was first performed in the mid 1980s and first approved by the FDA in the mid 1990s [10]. It is performed, most often, in conjunction with other catheter-based procedures, such as balloon angioplasty and atherectomy. These adjunct procedures are used to partially reduce the narrowing caused by the plaque prior to stenting, whilst the stent remains in the vessel scaffolding the arterial wall to ensure normal blood flow is maintained in the long-term.

Stenting procedures are most commonly performed via the femoral artery in the groin. However, they can also be delivered via the brachial artery at the elbow or the radial artery in the wrist [12]. A guide catheter is initially inserted into the artery and it is navigated to the location of the blockage. A dye, which acts as a contrast medium, is then injected through the catheter. The dye can be seen using fluoroscopy and provides a visual aid for the interventional cardiologist throughout the procedure [12], see Figure 1.5.

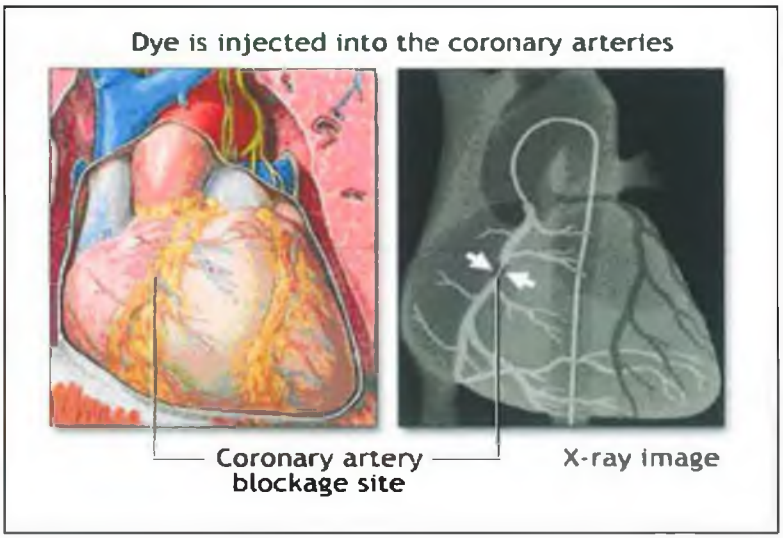

Figure 1.5 Pictorial representation of a flouroscopic image of the heart [adapted from Adam], [13].

The stent is generally expanded by inflation of an angioplasty balloon which plastically deforms the stent structure. The balloon is then deflated and the catheter is removed while the stent remains permanently in the artery, keeping the artery open and hence restoring normal blood flow, see Figure 1.6 [12]. Within one month, the stent becomes embedded in the wall of the artery due to restenotic growth [14].

There are two basic types of stents, balloon expandable stents and self-expanding stents. Balloon expandable stents are most commonly used due to their ability to be precisely positioned. They also have the advantage of allowing expansion to a controlled predetermined diameter.

Self-expanding stents are made from shape memory materials that can recover their predetermined diameter. They are elongated and constrained on a catheter by a rolling membrane sheath and retraction of the sheath at the blockage allows the stent to expand and dilate the vessel [15].

The usage of stents is most commonly known for the treatment of coronary artery disease. However, stents are also used for the treatment of peripheral vascular disease [16], renal vascular hypertension [17], and carotid artery disease [18]. All of these conditions have one aspect in common – blocked arteries. All stents are used to restore blood flow within arteries by scaffolding them open.

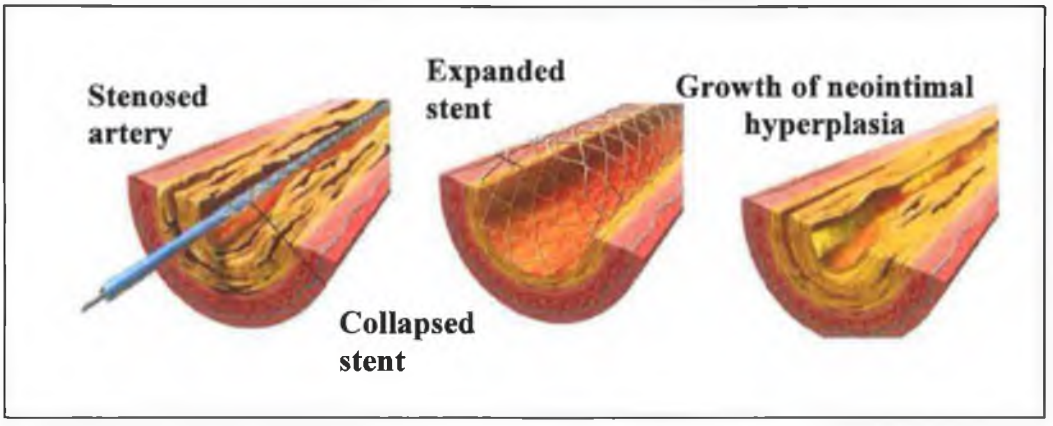

Figure 1.6 Illustration of stenting procedure [adapted from Heart Centre], [4].

All forms of percutaneous coronary interventions cause a certain level of injury to the vessel wall and it is this injury that is thought to be the main cause of restenosis within arteries. The most successful of all the available catheter-based techniques are balloon angioplasty and intravascular stenting. Post–angioplasty restenosis is predominantly due to elastic recoil and vascular remodelling [19]. Comparative studies have shown the benefit of coronary stenting versus balloon angioplasty alone since stenting significantly reduces elastic recoil and vascular remodelling [20]. However, excessive neointimal hyperplasia has been found to occur post-stenting and, as a result, in-stent restenosis also represents the major limitation to stenting procedures. It occurs due to adaptation of the arterial whereby the intima cells begin to proliferate due to the presence of an implanted foreign object. This growth may aggravate depending on the severity of the injury to the arterial wall, thus leading to excessive neointimal hyperplasia [21].

Two main approaches have been adopted that have been successful in reducing in-stent restenosis; (i) optimising the stent design to reduce vascular injury and hence subsequent neointimal hyperplasia, and (ii) using novel stent materials and coatings to inhibit the growth of neointimal hyperplasia through the release of anti-proliferative drugs. It is believed, therefore, that by combining optimal stent design, and both the optimum drug and drug elution method, more effective and successful intravascular stents may be developed [22]. It is therefore vital to address the issue of the exact mechanical stimulus for in-stent restenosis. This information would be invaluable in terms of minimising the occurrence of restenosis since it would enable stent designs to be optimised to lower this stimulus and also to ensure drug delivery to the areas most affected by the stimulus for restenosis. It is generally believed that the stimulus for restenosis is mechanical injury but a measure for the injury has not yet been conclusively determined.

1.5 Clinical and Finite Element Studies of Stents

Numerous clinical studies have been carried out to evaluate the influence of stent design on in-stent restenosis outcome. Hausleiter *et al.* [23] demonstrated that stent design is the strongest predictor of in-stent restenosis. Escaned *et al.* [24],

Hausleiter *et al.* [23] and Hoffmann *et al.* [25] demonstrated that the MultiLink design resulted in the lowest in-stent restenosis rate in comparison to some other commercially available stent designs. A further clinical study, the ISAR-STEREO Trial by Kastrati *et al.* [26] used two variations in the MultiLink stent design to assess the effect of strut thickness on in-stent restenosis outcome. The clinical result indicated the use of a thinner-strut stent is associated with a significant reduction in angiographic and clinical restenosis.

The finite element method is a numerical modelling technique that can be used to provide information on the mechanical behavior of complex structures. It has therefore been used extensively in recent years for research and development into stents as an integral part of the design process. Several numerical modelling simulation studies have been used to address the issue of optimizing stent designs. The majority of these studies have concentrated on analysing the expansion of different stent designs [27, 28, 29] whilst only recently have the stenting simulations included the arterial wall [30, 31, 32]. Complex finite element analyses of this nature, simulating stent expansion within arteries, can be used to preclinically test and evaluate the performance and effectiveness of stents as well as their propensity to cause in-stent restenosis, thereby providing valuable information on the optimum stent design.

Optimisation of stent designs cannot be performed if the mechanical stimulus for restenosis is unknown. It therefore still remains to identify more conclusively the mechanical stimuli for in-stent restenosis in order to know what mechanical variables that need to be minimised to reduce in-stent restenosis. This can be achieved by using numerical modelling techniques to simulate the conditions of previous clinical trials that have clearly identified particular stent designs to have a greater propensity for restenosis than others.

1.6 Objectives of the study

The main objective of this study is to identify the mechanical stimuli for restenosis. The ISAR-STEREO Trial by Kastrati *et al.* [26] examined the clinical restenosis outcome of the ACS RX Multilink and the ACS Multilink RX Duet. These Multilink stents are similar in design but with strut thicknesses of 0.05 mm

and 0.14 mm, respectively. This study focuses on examining the role of strut thickness on restenosis outcome and the hypothesis that a thicker strut stent induces higher stresses on the arterial wall than a thinner strut stent, using the finite element method (FEM). These higher stresses induced in the arterial wall are believed to cause different injury levels to the arterial wall and subsequently influence the variation of restenosis outcome found in the clinical study by Kastrati *et al.* [26].

To achieve this objective, finite element modelling was used to examine the expansion of both stents in various stenosed vessel geometries and the results of these simulations are presented here. The stresses induced within the vascular wall by the stents were estimated for the two different stent designs. The differences in the levels of stresses in the radial, circumferential and longitudinal direction were examined for both stent designs. A comparison to clinical data was used to determine the most likely mechanical stimuli for in-stent restenosis. Overall, this computational study aims to provide valuable information to aid the optimisation of coronary intravascular stent designs.

Chapter 2

LITERATURE REVIEW

2.1 Introduction

In-stent restenosis represents the major limitation for stenting procedures. In-stent restenosis is the renarrowing of the artery lumen within a stent predominantly due to excessive growth of neointimal hyperplasia. Stent design has been found to be a major factor in determining restenosis outcome.

This study focuses on examining the role of strut thickness on the growth of neointimal hyperplasia. It is therefore vital to understand the restenosis process and the progression of this growth that subsequently leads to in-stent restenosis. Finite Element modelling can be used to investigate the influence of stent strut thickness on in-stent restenosis by simulating the biomechanical interaction between a stent and an artery whereby stresses within the arterial vessel wall, caused by the stent struts, are computed and examined. The reliability of the computed results in any finite element study, however, depends upon many parameters; the most essential is the accuracy of the material models for the stent and the artery. It is therefore necessary to establish an appropriate constitutive model for the artery by examining the structure and general characteristics of arterial wall. This chapter therefore reviews the following:-

1. The structure of arterial the wall
2. Constitutive models of the arterial wall
3. The mechanism of restenosis

4. Clinical factors identified to influence the progression of restenosis
5. Finite element studies of stenting procedures

2.2 Structure of the Arterial Wall

Before numerical models of stenting procedures can be carried out, it is necessary to understand the artery into which the stent is expanded. Arteries are blood vessels that supply oxygenated blood to the organs and cells throughout the human body. Coronary arteries are vessels that carry oxygenated blood to the heart. Arteries are made of three distinct layers; the tunica intima, tunica media, and tunica adventitia [33], see Figure 2.1.

The intima consists of a monolayer of endothelial cells (smooth muscle cells) and an underlying thin basal lamina. The basal lamina consists largely of collagen, the adhesion molecules laminin and fibronectin, and some

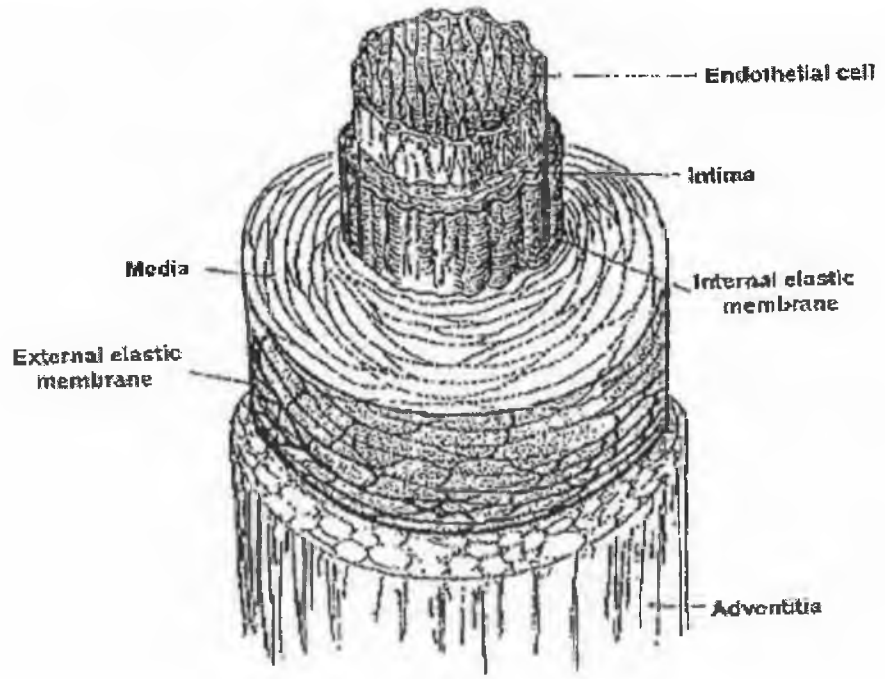

Figure 2.1 Illustration of three layers made up an artery [adapted from [34]].

proteoglycans, where its primary function is to provide a base for the endothelial cells to grow [33]. This layer is crucial since the stent comes into direct contact with the lumen of the arterial wall.

The media consists of beds of smooth muscle cells that are embedded in an extracellular matrix of small amounts of elastic tissue, collagen and proteoglycans. The composition of the arterial wall becomes stiffer as it reaches the outer layer [33]. The ratio of collagen and elastin determines the rigidity of the arterial wall [35]. The internal elastic lamina separates the intima and media, whilst the external elastic lamina separates the media and the adventitia. These elastic laminae allow the transport of water, nutrients, and electrolytes across the wall as well as direct trasmural cell-to-cell communication between the individual layers of the artery [33].

The adventitia consists of a dense network of collagen fibres and elastic tissues. In coronary arteries, the adventitia layer takes up only approximately 10% of the arterial wall. Due to its stiff composition, it is believed to serve as a protective sheath, where it limits acute overdistension of the vessel. Under normal physiological load, the adventitia does not contribute extensively to the mechanical behaviour, it primarily provides tethering to the surrounding connective tissue and provides additional structural support [36].

The size of coronary arteries range from 1.59 mm to 4.15 mm in inner diameter [35] and the thickness of atherosclerotic human coronary arteries have been reported to range from 0.56 mm to 1.25 mm, depending upon the location of the coronary arteries on the surface of the heart [37].

2.3 Constitutive Models of the Arterial Wall

The constitutive model used to describe the arterial wall is very important in finite element analyses to investigate the interaction between a stent and an artery. Many researchers have investigated and experimentally determined the mechanical behaviour of arterial tissue. The increase in studies to characterise the mechanical properties of arterial tissue is due to the advances in intravascular procedures, such as balloon angioplasty and stenting that mechanically deform the

vessel wall. Finite element analysis techniques have been used to preclinically investigate the performance of stents and they require suitable constitutive laws to represent the mechanical behaviour of arterial and plaque tissue, and the stent material.

A constitutive model is the mathematical expression of the relationship between the stress and the strain of a material and it can be established from experimental measurements. The mechanical behaviour of an artery, and hence the constitutive law to represent it, is dependent upon the composition of the artery and it may vary with the type of vessel, disease, age and gender [38, 39] and the deformation mode the sample is subjected to upon testing [40].

Arteries are found to exhibit the following characteristics:-

1. Viscoelasticity

Taking into account the structural constituents of an artery, arterial behaviour is more accurately described as viscoelastic, since arteries have both a solid and fluid component and hence elastic and viscous behaviour. Arteries exhibit hysteresis under cyclic loading, stress relaxation under constant extension and creep under constant load. Hysteresis is observed on loading and unloading curves do not coincide, see Figure 2.2 [47]. When a segment of an artery is tested for a tensile test with cyclic varying strain, a process called preconditioning is depicted whereby the stress response shows the hysteresis loop decreases with succeeding cycle and lead to a steady state after a number of cycles, see Figure 2.2 [47]. The viscoelasticity of arterial tissue is most evident in the tissue's strain-rate dependency, whereby there is a development of additional strains in the arterial tissue over a period of time when subjected to stress. Although arterial tissue is truly viscoelastic, purely elastic models have been used to describe arterial tissue. The elastic models have been used in numerical models whereby the experimental data used to describe the constitutive model was obtained at strain rates typical of that applied in the application of the material model [41].

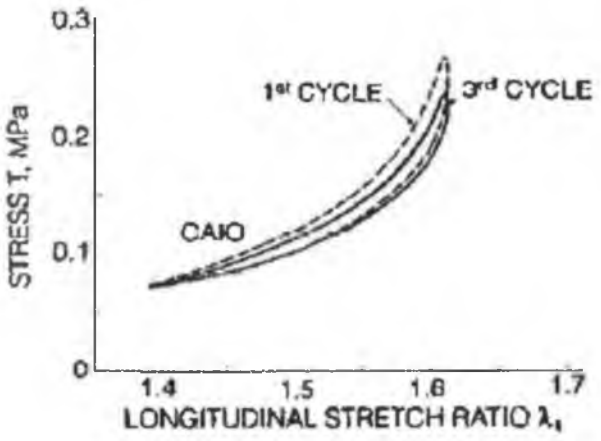

Figure 2.2 Cycle stress response of a dog's carotid artery under preconditioning showing hysteresis loop over a number of cycles [adapted from [47]].

2. Heterogeneous

An artery is composed of endothelial cells, elastin and collagen, and the distribution of these constituents varies from one layer to the other, see Figure 2.1. The varied orientation of these structural constituents determines the mechanical properties of the artery. Many constitutive models used in the literature to describe arterial tissue assume homogeneity for simplification of the constitutive model [40]. The assumption of homogeneity may be justified because the media constitutes the majority of the vessel wall since the adventitia and intima generally constitute only 10% of the vessel wall, and as a result the media bears most of the load [33]. Moreover, the experimental data used to describe constitutive models generally includes the overall mechanical behaviour of the arterial tissue, where uniaxial and equibiaxial data are generally used to describe the model, [40]. Therefore, for the purpose of investigating the stresses and strains induced in the wall of a coronary artery by a stent, the artery properties may be adequately represented by a material model that assumes homogeneity.

3. Incompressibility

Tests on arteries have shown very small changes in volume of the arterial wall over a wide range of deformation. Similar to many other soft tissues the arterial wall is regarded as almost incompressible, where it preserves its volume under load [42].

4. Residual stress

Residual stresses in arteries are the stresses that exists in the arterial wall in the absence of an externally applied load. Residual stress can be characterized by the level of opening angle when a sample segment is radially cut [43]. The inclusion of residual stress into an arterial model was found to result in a more uniform distribution of stress, particularly a decrease in stress at the intimal as opposed to a model without residual stress [40].

5. Anisotropy

Smooth muscle cells are found to be oriented circumferentially in arterial tissue and when they are subjected to an internal pressure, constriction and dilation of the smooth muscle cells alters their orientation. Therefore the arterial wall may be considered anisotropic, where it exhibits different properties in different directions [40]. Holzapfel and Ogden [44] proposed a combination of exponential and polynomial type strain energy functions which include the anisotropic behaviour exhibited by arterial tissue. They have suggested dividing the strain energy function into the addition of the isotropic strain energy function and an anisotropic strain energy function. Although the constitutive model used by Holzapfel successfully captures the anisotropic characteristics of arterial tissue it is unavailable in commercially available software codes and hence complex and highly computationally expensive to implement. In addition, the degree of anisotropy of tissue is highly patient specific and would therefore be most valuable for describing the mechanical properties of arterial tissue from *in vivo* measurements.

For the purpose of preclinically identifying key characteristics of stent designs that affect restenosis outcome, it is proposed that an isotropic model may be sufficient. An isotropic model that includes the main features of arterial tissue such as its non-linear stress stiffening behaviour and its incompressibility could identify the influence of stent design variables on restenosis outcome preclinically.

Many researchers have proposed various constitutive equations, to describe the mechanical behaviour of arterial tissue [40, 44, 45]. The elasticity of an artery is normally quantified in terms of a strain energy density function, W, where the recoverable energy is stored in the material as it deforms. W is defined in terms of suitable strain components and the description of W is used to describe a constitutive equation for the arterial tissue. This is due to the fact that a hyperelastic material is one that, by definition, experiences large deformations that are completely recoverable and has mechanical behaviour that may be defined by its strain energy density function, W, such that differentiating W with respect to a strain component gives the corresponding stress component. For example, where W is described in terms of the Green-Lagrangian strain tensor, E, then each component of the 2nd Piola-Kirchoff stress tensor, S, is given by the differentiation of the strain energy density function, W, with respect to the corresponding component of the Green-Lagrangian strain tensor, E [33]. This may be described by the following equation:-

$$S = \frac{\partial W}{\partial E}$$

Ideally artery wall materials should be represented by a viscoelastic model. Holzapfel *et al.* [42] have proposed a viscoelastic model, describing the strain rate dependent characteristics of the tissue and also including hysteresis. The stress-strain relationship was found to be considerably different at loading and unloading with each stress-strain relationship highly non-linear and unique to each cycle in the process. The strain energy function proposed by Holzapfel *et al.* [42] was decoupled into a viscoelastic and an elastic part. In addition, Holzapfel

et al. [42] divided the artery into two layers, the media and the adventitia, describing each with a unique strain energy density function. The model also included anisotropy through the inclusion of fibre orientations in each layer of the model.

In the most recent computational study of assessing stent design by Holzapfel *et al.* [32], an elastic anisotropic constitutive model is used where the strain energy density function was given by the sum of the isotropic and anisotropic strain energy functions. The material data was taken from an external iliac atherosclerotic artery of a 65 year old women and the model was therefore patient-specific.

The material properties of arterial tissue is known to be dependent upon the composition of the artery and it may vary with the type of vessel, disease, age and gender [37, 38, 39]. It may therefore still be useful to investigate stent design parameters in comparative FE studies using simplified isotropic constitutive material models that are derived based on experimental data from tests on arterial tissue.

Therefore, for the purpose of comparative analyses, the isotropic Mooney-Rivlin model is proposed to limit the complexity of modelling the process of stent expansion within an artery vessel. The main objective of this thesis is to estimate the stresses induced in the arterial wall of stented stenotic vessels by different thickness stent struts, and to relate these stresses to the different restenosis outcomes observed with these different stents. The non-linearity of the stent material and the complex stent geometry alone result in a highly computationally expensive simulations. The key mechanical property of arterial tissue is its stress stiffening behaviour and uniaxial and equibiaxial data are sufficient to adequately represent this behaviour in the main deformation modes that stented arteries experience [46].

The strain energy density function, W, of an isotropic hyperelastic material can be described in polynomial or exponential form. One of the general polynomial forms of the strain energy density function in terms of stretch invariants that has been extensively used to model incompressible isotropic hyperelastic materials is known as the Mooney-Rivlin model and is given by [47]:

$$W(I_1,I_2,I_3,) = \sum_{i,j=0}^{\infty} a_{ij}(I_1-3)^m(I_2-3)^n(I_3-3)^0, a_{000}=0$$

Where a_{ij} are material constants, and m and n are exponents which determine the order of the model. The stretch invariants for the material are defined through the principal stretches ($\lambda_1, \lambda_2, \lambda_3$) of the material as:

$$I_1 = \lambda_1^2 + \lambda_2^2 + \lambda_3^2$$

$$I_2 = \lambda_1^2\lambda_2^2 + \lambda_1^2\lambda_3^2 + \lambda_2^2\lambda_3^2$$

$$I_3 = \lambda_1^2\lambda_2^2\lambda_3^2$$

The Mooney-Rivlin model is widely available in a range of forms in many FE codes. Petrini *et al.* [48] and Lally *et al.* [31] have used forms of the Mooney-Rivlin model in their simulations investigating the interaction between a stent and an artery, where Petrini *et al.* [48] compares the performance of a self-expandable stent with a balloon-expandable stainless steel stent and Lally *et al.* [31] compares the performance of two different stent designs. Both Petrini *et al.* [48] and Lally *et al.* [31] used a third order form of the Mooney-Rivlin model to describe the mechanical behaviour of the artery.

The Mooney-Rivlin model can be used to define a suitable constitutive equation to describe arterial tissue in this study by fitting to published experimental data from uniaxial and equibiaxial tension tests on porcine coronary tissue [41]. Ideally, numerical studies on intravascular stents should use data from fresh human coronary arteries, however, data on human coronary tissue is very difficult to obtain. Recently, van Andel et al. [37] carried out a comparative study of the inflation response of a limited number of human and porcine arteries. The study found that the porcine arteries have three times greater elasticity than the human arteries. However, the published test data cannot easily be used to define the constitutive model parameters within the available material model in Marc/Mentat (MscSoftware, Santa Ana, CA, USA). In addition, another study

has shown that the porcine coronary artery has very similar mechanical properties to the human coronary artery [49].

The main goal of FE studies on stenting procedures is to understand the effects of stent deployment on the arterial wall. These numerical studies are highly concerned with the large deformation of the arterial wall caused by the stents structure. Some studies, including recent studies, have modelled the artery using a simple linear-elastic model [50, 51, 52]. Others have used isotropic hyperlastic constitutive models based on uniaxial data [48, 53]. It is proposed that the use of the experimental data describing the main deformation modes that arterial tissues physiologically experience, namely uniaxial and biaxial tension, is the best way to describe an isotropic material which can represent the properties of arterial tissue. This data is available in the literature for porcine coronary arteries [41]. The uniaxial and equibiaxial data are found sufficient to represent the key feature of the non-linear stress-stiffening behaviour of the arterial tissue.

Atherosclerotic vessels are also composed of stenotic plaque which may also be described by a hyperelastic constitutive model and used to represent the plaque tissue in numerical models. A suitable constitutive model for plaque can be described by fitting to published data on the stress-strain behaviour of human atherosclerotic plaque. Experimental data from uniaxial tension tests on human aortic atherosclerotic plaques has been published by Loree *et al.* [54]. To the authors knowledge no other uniaxial tensile test data on human atherosclerotic plaques have been published and no data on the biaxial tensile behaviour of human atherosclerotic plaques could be found in the literature.

2.4 Mechanism of Restenosis

Restenosis is the reoccurance of a stenosis within a vessel after an intravascular procedure. Reduction of restenosis is the main advantage of stenting compared with conventional PTCA. Balloon angioplasty is less successful compared to stenting due to elastic wall recoil and vascular remodelling, which results in early lumen loss [19]. Stenting was introduced to act as a permanent scaffold following PTCA and thereby prevent negative remodelling and elastic recoil of the arterial wall.

Comparative studies between stenting and angioplasty have shown that stenting had a higher rate of procedural success than angioplasty. One study shows a larger immediate increase in the diameter of the vessel lumen (1.72 mm vs. 1.23 mm, $P<0.001$), and a larger luminal diameter immediately after the procedure (2.49 mm vs. 1.99 mm, $P<0.001$) and a lower rate of binary restenosis (31.6% vs. 42.1%, $P=0.046$) than vessels treated with balloon angioplasty [20]. BENESTENT and GISSOC trials show the benefit of coronary stenting versus balloon angioplasty, where the results reported the effectiveness of stenting in treating stenosed coronary arteries. The results of these studies demonstrate the suitability of stents to achieve large lumen cross-sectional areas and their ability to prevent negative vascular remodelling whilst scaffolding the vessel open [55, 56, 57].

The factors which cause restenosis after balloon angioplasty are acute vessel recoil, thrombus formation, chronic constrictive remodelling and neointimal growth [58]. In-stent restenosis occurs due to adaptation of the arterial wall to the presence of an implanted foreign object and it is predominantly due to growth of neointimal hyperplasia [59, 60]. All of these studies have identified smooth muscle cell hyperplasia as the major component of in-stent restenosis [61].

The mechanism of in-stent restenosis is important in understanding the stimuli for the disease. Many researchers have observed and identified the main steps leading to the formation of in-stent restenosis as follows, see Figure 2.3:-

1. Initial reaction to the foreign body leading to thrombosis.
2. This growth of thrombosis leads to an inflammatory reaction of the arterial wall.
3. Inflammation is followed by proliferation of intimal cells. This phase is found more prominent after a stenting procedure compared with balloon angioplasty, where the stent is permanently fixed as it scaffolds the arterial wall.
4. Finally remodelling of the artery wall occurs due to the abundant growth of smooth muscle cells.

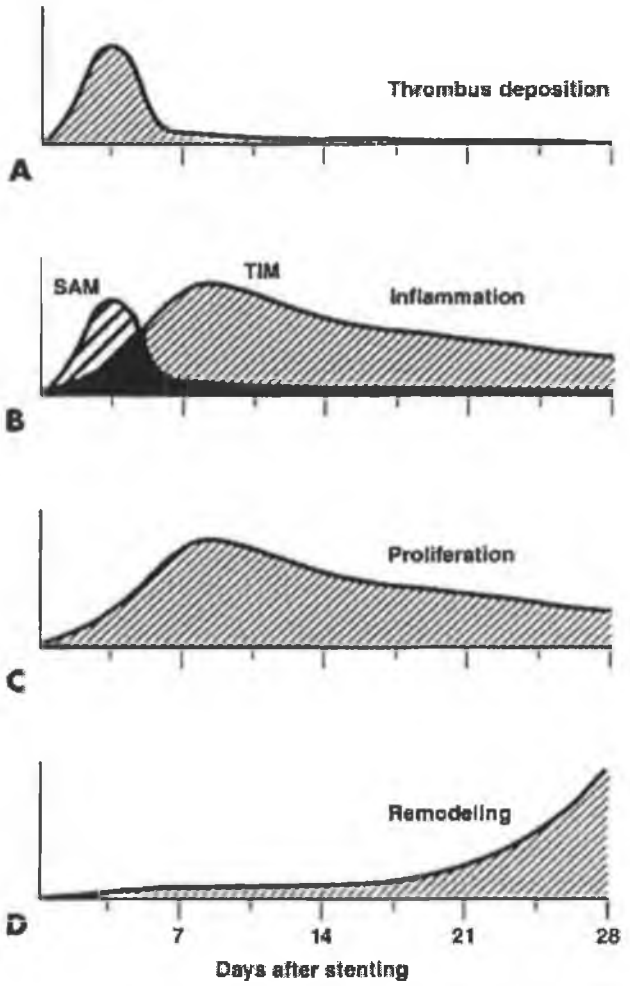

Figure 2.3 The four phases of vascular repair after stenting, leading to the formation of in-stent restenosis [14].

2.4.1 Thrombosis

Thrombus formation begins at the site of injury caused by the stent struts. The thrombotic phase usually takes place within 1-3 days after the intervention [14, 59]. As the stent struts are expanded to scaffold open the arterial wall, the stent struts may penetrate and lacerate the arterial wall. This is defined as the acute arterial injury to the arterial wall that initiates the initial healing process.

Thrombosis is the formation of a blood clot, a sealing mechanism to restore normal blood flow when injury is induced in the vessel wall. The formation of a thrombus is governed by the severity of damage to the arterial wall and can obstruct blood flow [62].

2.4.2 Inflammation

The thrombus at arterial injury sites develops an inflammatory reaction where leukocytes make their way to the tightly stretched internal elastic membrane of the artery. This process occurs approximately 3-7 days after the intervention and results in a layer of inflammatory cells at the thrombotic sites at and between the stent struts [14].

2.4.3 Neointimal proliferation

Proliferation is the third phase of vascular response to stenting. Intimal cells begin to proliferate and simultaneously the inflammatory cells migrate from the vessel surface to the neointima. This process begins approximately 7 days after the stent implantation and may continue for many months [14]. At this stage the thrombus and inflammatory cells are replaced by neointimal cells that progressively proliferate toward the injured media. This leads to the activation of smooth muscle cells (SMC) in the media. The activation of the smooth muscle cells results in both SMC proliferation and SMC migration into the intima. Simultaneously large amounts of extracellular matrix are produced by the SMCs. This growth response to the arterial injury leads to the development of neointimal hyperplasia or the thickening of the intima. As the growth of the neointimal hyperplasia progresses, it results in a narrowed lumen, thus blocking the flow of the blood to the heart muscle, see Figure 2.4 [21, 63, 64, 65].

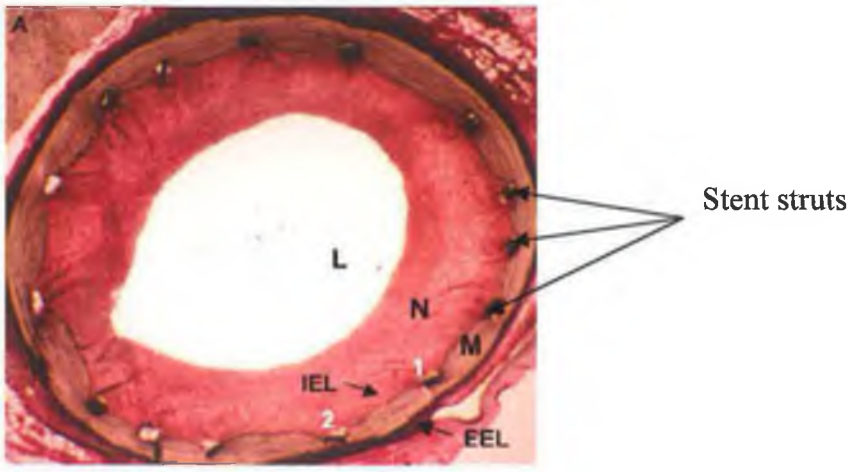

Figure 2.4 An illustration of response to injury from stent strut expansion in normal porcine coronary artery after 28 days. L=lumen; N=neointima; IEL/EEL=internal/external elastic lamina [adapted from Lowe *et al.*, [65]].

2.4.4 Vascular remodelling

The last phase in the response to vascular injury is the vascular remodelling. In response to the neointimal hyperplasia growth, geometric remodelling occurs and causes the artery to contract [14]. The artery is dynamic and responsive and it adapts to the high strain imposed by the stent. It fights against the resulting strain of the arterial wall due to neointimal hyperplasia by increasing levels of collagen and stiffening the vessel wall. However, in the case of a stented vessel, the high radial strength of stent prevents vascular remodelling after stenting and it has therefore been found to be an almost insignificant contributor to in-stent restenosis [66].

The growth of neointimal hyperplasia has been found to be the main limitation in the long-term success of intravascular stenting procedures. Vascular injury caused by the stent structure is the major determinant of the growth of neointimal hyperplasia [67]. Drug eluting stents have emerged in the recent years, where the drug inhibits SMCs proliferation [68]. With or without drug elution,

stent design has been extensively reported to play a vital role in determining restenosis [69].

2.5 Clinical Trials on Intravascular Stents Examining Restenosis Outcome

Cellular response is the key to the development and progression of in-stent restenosis. It is still as yet unknown the exact feature of a stenting procedure that stimulates cell proliferation. Some researchers have considered the influence of the altered fluid flow around the stent and hypothesised that it may govern the development of neointimal proliferation [70]. Some other studies concluded that the material of the stent and/or stent coating played an important role in governing this proliferation [71]. However, a large number of studies have demonstrated that stent design is the major key factor in determining restenosis outcome [22, 69, 72]. These studies on stent design have also investigated the influence of the mechanism of expansion, the strut thickness, the metal-to-artery ratio, the cross-sectional area and the length of the stent structure have on restenosis outcome.

2.5.1 Influence of stent design on restenosis outcome

There are two basic designs of stent; (i) self-expanding and (ii) balloon-expandable stents. Self-expanding stents are made from shape memory materials that can recover their predetermined diameter when placed at the site of treatment [15]. They are elongated and constrained in a catheter by a rolling membrane sheath. Retraction of the sheath results in stent self-expansion. The most common self-expanding stent is the Wallstent (Schneider), see Figure 2.5, which has a multiple wire braid structure and is commonly made from a cobalt alloy [73]. The main advantage of the Wallstent is its flexibility. It is considered one of the most desirable features in a coronary stent where it eases deployment through tortuous vessels and consequently results in a less traumatised vessel when subjected to bending [74]. Self-expanding stents, such as the Wallstent, have an advantage in terms of luminal gain since their inherent expanding force

enables them to continue to expand after implantation [24]. Despite the Wallstent's advantage of flexibility and higher luminal gain, assessment of its clinical outcome has shown that this design is inferior in the long-term where it caused the highest restenosis rate of 49% in comparison to balloon expandable stents [24]. The high luminal gain and the large metal surface area of this stent design led to a greater growth of neointima. As discussed above, many studies have identified smooth muscle cell hyperplasia as the major component of in-stent restenosis. It can be concluded that high luminal gain can serve as a disadvantage where it challenges the original belief that "bigger is better" [75]. However, recent studies show promising results by combining the use of intracoronary beta radiation with the Wallstent, whereby the beta radiation reduced neointimal proliferation and thus maintained a wider lumen diameter [76].

Balloon expandable stents are commonly made from stainless steel materials. They are expanded by a balloon and plastically deformed to a desired diameter. These are most commonly used because they can be precisely positioned and have the advantage of being able to accurately achieve a predetermined diameter. There are two major designs of balloon expandable stent; coil stent designs and slotted tube stent designs. The former is fabricated out of a continuous single strand of wire formed into a repeating pattern while the latter is made of a stainless steel tube by laser machining the tube into the desired pattern [73]. The most common coil stent is the Gianturco-Roubin (Cook), see Figure 2.5, which has a coiled structure and a continuous spine that serves as longitudinal support, and prevents separation of the coils. This coil like design has a very flexible structure and is therefore often favoured for complex bifurcation lesions [10]. However, clinical studies have reported restenosis rates of 43% [77], 46% [24], and 57% [10] for the Gianturco-Roubin stent. These studies have demonstrated that the coil stent design has less initial gain and significantly large luminal loss during follow-up. A high level of recoil contributed largely to the large luminal loss found in these studies. Carrozza *et al.* [78] have demonstrated that the Gianturco-Roubin stent recoiled 30% of its initial gain cross sectional area. The coil stent designs have shown poor radial strength and allow tissue prolapse between the widely spaced wire elements [24]. In

addition, neointimal proliferation also contributed largely to the long-term luminal loss.

The earliest commercially available stent design was a slotted tube stent made from a stainless steel tube called the Palmaz-Schatz stent (Johnson & Johnson), see Figure 2.5, [73]. The Palmaz-Schatz stent has been found to have lower recoil (15%) when compared to the Gianturco-Roubin stent [78]. It has been proposed that this lower recoil that subsequently lead to lower luminal loss as recorded in the clinical study by Escaned *et al.*, [24]. The Palmaz-Schatz stent structure provides good surface coverage of a stented lesion and subsequently provides good scaffolding against the collapsing force of the arterial wall. Clinical studies have reported 98% of procedural success with the Palmaz-Shatz stent [10] with restenosis rates of 20% reported by Escaned *et al.* [24] and 36.8% by Hausleiter *et al.* [23]. The slightly higher restenosis rate reported by Hausleiter *et al.* [23] was expected as the stents were implanted in small coronary arteries. These restenosis rates are consistent with the findings of Colombo and Tobis [10] where the restenosis rate associated with the Palmaz-Schatz stents were reported to be 19% in large vessels and 30% for small vessels. Stankovic *et al.* [79] have also reported a significant reduction in angiographic restenosis for the same group of stents used in large vessels compared with those used in small vessels.

The early slotted tubular stent design became the basic structure of the modern stent designs. Studies showed that flexibility is a critical requirement of a stent [10]. During deployment, the stent may be subjected to bending at certain areas and therefore flexibility is essential to ease deployment through tortuous vessels to the target area. Advances in manufacturing methods have enabled more flexible geometries to be generated in recent years. The emergence of laser machining has also created diversity in stent designs [73]. Recent generation of tubular stents can be classified into slotted tube and modular stent designs [69]. The recent generation of slotted tube stent design has a closed cell structure, a common example is the NIR stent (Medinol/Boston Scientific), see Figure 2.5, whilst a modular stent design has an open cell structure, a common example being the MultiLink stents (Guidant), see Figure 2.5. Escaned *et al.* [24] examined both of these afore mentioned stent designs in a clinical study and found them to have similar scaffolding properties, similar radial strength and similar total metal area.

This clinical study also compared the restenosis rate for multicellular, slotted tube, coil and self-expandable stent designs. The MultiLink and NIR stents were in the multicellular design group and these stents were found to have the lowest restenosis rate of 10% in comparison to the other stents.

Carrozza *et al.* [78] reported similar percentage diameter recoils for these multicellular stents, with 9.6% observed in the MultiLink stent and 10.4% in the NIR stent. Costa *et al.* [80] carried out a comparison study between the MultiLink stent and NIR stent. They reported that the Multilink stent resulted in a slightly higher degree of neointimal formation at 6 months of 46 mm^3 whilst the NIR stent resulted in 39.9 mm^3 of neointimal formation. This was expected as the length of the MlinkLink stent was greater than the NIR stent and stent length has been reported as one of the factors affecting neointimal proliferation [23]. Hoffmann *et al.* [25] reported the intimal hyperplasia thickness caused by the MultiLink stent and the NIR stent to be 0.20 mm and 0.31 mm respectively, while the Palmaz-Schatz caused 0.26 mm thickness of intimal hyperplasia. The same pattern neointimal formation was observed in a clinical study by Hausleiter *et al.* [23] whereby the restenosis rate was reported to be 29.6% in the MultiLink, 36.8% in the Palmaz-Schatz and 44.3% in the NIR stent.

These recent stent designs addressed more difficult and challenging tasks such as achieving flexibility without compromising radial strength and lesion coverage. The development of newer stent designs generally revolves around varying the multi-ring design such as varying the connection between the rings. There has been a vast growth of commercially available endovascular stents in recent years [72]. It is clear that stent design plays a major role in determining restenosis outcome. Taylor *et al.*, [81] studied the stent-artery interactions of four different stent designs; the BX stent, MultiLink stent, Radius Nitinol stent and Palmaz-Schatz stent, see Figure 2.5. There was a significant difference between the vascular response of each of these stent designs, as shown in Figure 2.6.

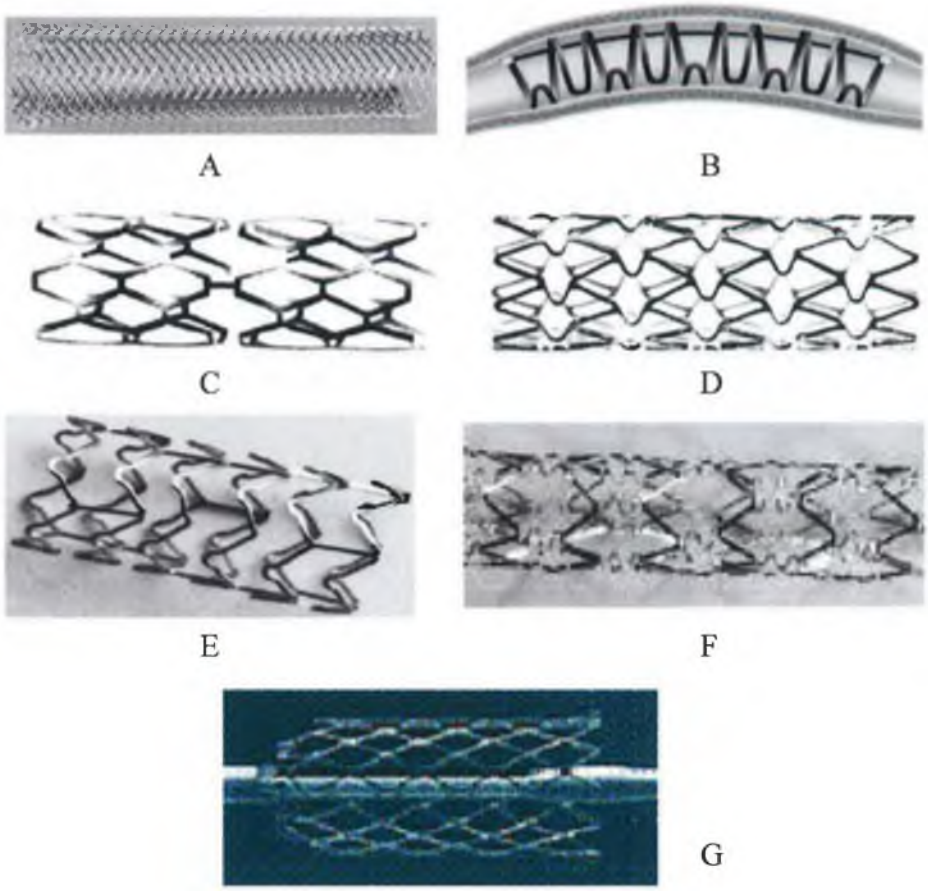

Figure 2.5 Illustration of selected stent designs: (A) self-expanding stent, Wallstent (Schneider), (B) coil stent, Gianturco-Roubin stent (Cook), (C) slotted tube stent, Palmaz-Schatz stent (Johnson & Johnson), (D) closed cell structure, NIR stent (Medinol/Boston Scientific), (E) open cell structure, MultiLink stent (Guidant), (F) BX stent (Cordis) and (G) Radius Nitinol (Scimed), [adapted from [10, 73]].

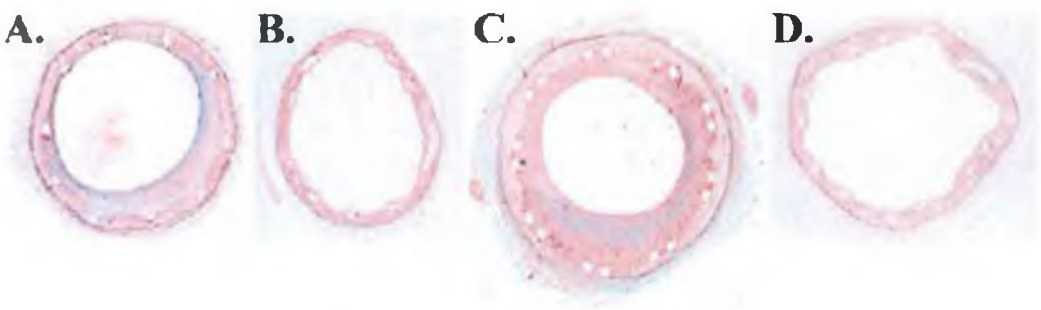

Figure 2.6 Representative Movat pentachrome-stained sections from the four stent designs: (A) BX stent, (B) Multilink, (C) Radius Nitinol, and (D) Palmaz-Schatz, [adapted from Taylor *et al.*, [81]].

Following studies of *in vitro* and *in vivo* testing, animal studies, clinical evaluation and clinical application over the years, the ideal stent design is characterised to compose the following critical requirements [10]:-

1. Good flexibility – to navigate through tortuous vessel
2. Adequate radiopacity – to aid visual visibility through stenting procedure for accurate manipulation and positioning
3. Low recoil – to maintain the desired resulting lumen diameter, without compromising lesion coverage.
4. Sufficient radial strength – to withstand the collapsing of the arterial vessel and to promote adequate scaffolding ability
5. A low profile – to have minimal wall thickness and metallic surface area as they were found to contribute widely to thrombosis formation and neointimal proliferation.
6. Good biocompatibility – to ensure low adverse reaction of the stent material when implanted inside the human body

2.5.2 Influence of stent material on restenosis outcome

Clinical studies have shown the superiority of one stent design over another. Clinical trials have evolved to examine the specific characteristics of a stent that cause the differences in the level of restenosis outcome. Stent coating has been identified as one of the predictors of restenosis outcome. Endovascular stents are frequently made of stainless steel [72]. It is durable and has a relatively good radiopacity. However, the thinner the struts of a stainless steel stent, the lower the level of radiopacity [82]. Therefore, some gold-coated stents were made available for the purpose of increasing radiopacity. Gold has a low melting point and high malleability, which leaves it ideal to work with [82]. Although gold-coated stents have a high radiopacity, they have relatively poor biocompatibility in comparison to stainless steel stents [23, 25, 82]. These clinical studies by Edelman *et al.* [82], Hausleiter *et al.* [23], and Hoffmann *et al.* [25] examined the restenosis outcome

of gold coated stents versus stainless steel stents and demonstrated that gold-coated stents trigger significantly more intimal proliferation.

2.5.3 Influence of strut thickness on restenosis outcome

Randomised clinical studies [23, 26, 79, 83] have demonstrated that strut thickness affects the long-term clinical outcomes. Stankovic *et al.* [79] also evaluated the effect of stent strut thickness of different stent types (slotted tube and ring design) on angiographic restenosis rates. The stents were divided into 2 groups of thin-strut (<0.1 mm) and thick-strut (>/=0.1 mm). The clinical study was divided according to the coronary vessel sizes (small (<2.8 mm) and large (>/=2.8 mm)) and lesion lengths (short lesion (<15 mm) and long lesion (>/=15mm)). The clinical result indicated that there is a significant reduction in angiographic restenosis with the implantation of a thin-strut stent.

Kastrati *et al.* [26] investigated the effect of strut thickness on restenosis outcome with similar stent designs. They randomly assigned a total of 651 patients in ISAR-STEREO Trial to receive one of two commercially available stents of similar design but with different strut thickness. The thinner strut stent used was the ACS RX MultiLink (Guidant) with a strut thickness of 0.05 mm and the ACS MultiLink RS Duet (Guidant) with a strut thickness of 0.14 mm. The clinical result indicated that the use of a thinner strut stent was associated with a significant reduction of angiographic restenosis (15% in the thin-strut group and 25.8% in the thick-strut group) and clinical restenosis (8.6% among the thin-strut patients and 13.8% in the thick-strut group). Angiographic restenosis is the percentage of cases where the diameter stenosis is greater than 50% found during angiographic evaluation and the clinical restenosis is the percentage of cases that required reintervention because of restenosis-induced ischemia. This result is consistent with the findings by Hausleiter *et al.* [23] where the thinner strut stent of the MultiLink was associated with a lower restenosis rate of 29.6% as compared to 34.2% restenosis rate with the thicker strut MultiLink Duet stent.

The ISAR-STEREO-2 Trial by Pache *et al.* [83] was carried out after the ISAR-STEREO Trial, which concluded that for two stents with similar design, the

risk for restenosis is dependent on the strut thickness. The ISAR-STREREO-2 Trial assessed the impact of stent strut thickness of different stent designs on restenosis outcome. A total of 611 patients were randomly assigned to receive either the thin-strut ACS RX MultiLink stent (Guidant) (strut thickness 0.05 mm, interconnected ring design) or the thick-strut BX Velocity stent (Cordis Corp.) (strut thickness 0.14 mm, closed cell design). The clinical result indicated that the use of thinner struts is associated with a significant reduction of angiographic restenosis (17.9% in the thin-strut group and 31.4% in the thick-strut group) and clinical restenosis (12.3% of the thin-strut group and 21.9% of the thick-strut group), after intervention.

Clinical studies have assessed the performance of commercially available intravascular stents with examination of the restenosis outcome set as a measure of success of the intravascular stents. It is clear that stent design is a key factor determining restenosis outcome.

2.6 Finite Element Studies of Stenting Procedures

Implantation of balloon expandable coronary stents in a human artery to treat coronary artery disease is a complicated process. The behaviour of the stent expansion during stent deployment in an artery is complicated and difficult to model using the finite element method. Despite a number of software tools available, published works on the behaviour of stent expansion using computer simulations are limited and the current knowledge is mostly based on the results of clinical trials. Stent deployment involves the interaction of a balloon, stent and artery and therefore some researchers have investigated balloon and stent interaction [50, 84]. Most of FE studies, however, have investigated free stent expansion whereby the stent is expanded without any interaction with a balloon or an artery [27, 28, 29, 48, 85]. Some recent studies have investigated the stent and artery interaction [31, 32, 48, 52, 86, 87].

Dumoulin and Cochelin [27] simulated a balloon-expandable stent that had a similar geometrical design to the Palmaz Schatz stent by using the commercial code ABAQUS. The expansion of the stent structure and its

mechanical properties were investigated. Stent expansion was characterised by radial recoil, longitudinal recoil and foreshortening for different final diameters of stent expansion. Stress-strain fields in the stent were examined. It was found that the major equivalent plastic strains were localised in the corners while the major stresses were located in the middle of the stent cells' junctions. The sensitivity of the critical pressure to geometric imperfections was also studied and the fatigue life was tested. The results showed that the P308 Palmaz stent studied was insensitive to geometric imperfections and that the stent could withstand an indefinite number of cardiac cycles. The main limitation of this study was the analysis of the stent behaviour by only analysing one unit of the stent structure. The external force applied to compress the expanded stent structure was also based on an assumption and may have had a significant effect on the findings of this study.

Migliavaca *et al.* [29] investigated the mechanical behaviour of several coronary stents using the finite element method. The effects of different geometrical parameters such as the thickness and the metal-to-artery surface ratio were evaluated in terms of radial recoil, longitudinal recoil, foreshortening and dogboning. Three models were analysed, a typical diamond-shaped Palmaz Schatz stent, a stent resembling a MultiLink Tetra stent (Guidant, Indianopolis, IN, USA) and a stent resembling a Carbostent (Sorin Biomedica, Saluggia, Italy). The stents were assumed to be made of 316L stainless steel. The inelastic constitutive response was described through a Von Mises-Hill plasticity model with isotropic hardening. A large deformation analysis was performed using the finite element commercial code ABAQUS. The results of the simulation showed the influence of the stent geometry on the mechanical behaviour of the stent. A stent with a low metal-to-artery surface ratio was shown to have a higher radial and longitudinal recoil, but lower dogboning. The stent strut thickness was found to influence the stents' performance in terms of foreshortening, longitudinal recoil and dogboning. The von Mises stress distribution along the stent in the loaded configuration showed that stresses were concentrated in the area of the connection between slots, where the plastic hinges allowed the stent to expand. Again, the geometries of the stent structures were based on some assumptions and the influence of the arterial wall was ignored.

A recent study of stent free expansion by McGarry *et al.* [85] incorporated a microscale deformation mechanism into the computational models of stent expansion. Another recent study by this research group has shown that the stress-strain behaviour of stent struts is size dependent and as a result it has been suggested that certain areas of thin struts could experience local failure which would not be described if macroscale stress strain curves were used to describe the material behaviour [88]. The finite element analyses of the stent expansion found non-uniform and localised deformation occurred in the structure due to the material inhomogenity and the discontinuity of crystal lattice orientation within the microstructure. The stent geometry used was based on the NIR stent, represented by a two-dimensional model of a single unit structure. With such a microscale representation of the stent, it would be extremely difficult to investigate the behaviour of the entire stent structure and the influence of the arterial wall.

Chua *et al.* [28] carried out a finite element simulation of free expansion of a balloon-expandable stent that has a similar geometrical design to the Palmaz Schatz stent. Later, Chua *et al.* [84] incorporated the influence of a balloon into their analyses. In the most recent study by Chua *et al.* [52] the deformation characteristics of the stent were investigated as a stent was expanded inside an artery. These analyses were performed using ANSYS (version 5.5) as a pre- and post-processor and LS-DYNA for solution. They reported the von Mises stresses in the stent structure and the distribution of the von Mises stress in the vessel wall. Some limitations of the analyses include the geometry of the stent structure, which was scaled up, and the use of 304 stainless steel material properties as opposed to 316L. In addition, the non-linear material of the artery was represented by a simple linear-elastic model. These assumptions and simplifications in the material model would affect stent expansion and the resulting stress distribution in the arterial wall.

Recent studies of stent expansion simulation studies have included the artery and plaque in the analyses. Petrini et al. [30, 48, 86] have reported numerous computational studies examining the expansion of metallic stents and the expansion of a metallic stent in a stenotic coronary artery by using the finite element method. The numerical analyses were performed using the commercial

code ABAQUS (Hibbit Karlsson & Sorenses, Inc., Pawtucket, RI, USA). Each simulation consisted of three parts: the artery, the artherosclerotic plaque and the stent. The simulation consisted of a stent model resembling the Palmaz Schatz stent, and the material was assumed to be made of 316L stainless steel. The 316L stainless steel stents was described using the von Mises-Hill plasticity model with kinematic hardening from the ABAQUS material library. The Young's Modulus of the 316L was 193 GPa, the Poisson ratio was 0.3 and the yield stress was 205 MPa. The material of the arterial wall and the plaque were modelled as non-linear, isotropic hyperelastic materials using a third order Mooney-Rivlin model obtained from experimental data. The effects of the expansion of the stent were analysed in terms of contact pressures, stresses and radial displacements. The simulation results showed that the stresses were concentrated in the contact areas of the plaque with the stent. They also reported that the pressure required to expand the stent increases with the stiffness of the plaque. Therefore the amount of pressure required is dependent upon the material properties of the plaque.

Petrini *et al.* [48] also evaluated the effect of different materials, comparing a 316L stainless steel stent with a self-expandable Shape Memory Alloy (SMA) stent (Nickel-Titanium alloy). The simulations consisted of a stent model resembling the Palmaz Schatz stent. SMAs have the unique ability to recover their original shape (superelastic effect) when mechanically deformed to a much greater extent than conventional metals. The comparison of the two analyses showed that the stainless steel stent induced a 50% higher magnitude of von Mises stress at the maximum expansion compared with the SMA stent. The lower stiffness of the SMA, however, resulted in the stent having a lower ability to expand and to contrast the vessel elastic recoil.

Petrini *et al.* [30] continued their numerical analyses to analyse the behaviour of new generation stents. Two different stent models were simulated resembling the Cordis BX-Velocity (CV) (Johnson & Johnson) and the Carbostent Sirius (SC) (Sorin Biomedica) coronary stents. Both models consisted of similar tubular-like rings and the rings were connected with different bridging links. The stents were made of 316L stainless steel and modelled using a von Mises-Hill plasticity model with isotropic hardening. The meshes were generated by GAMBIT commercial code (Fluent Inc., Lebanon, NH, USA) and large

deformation analyse was performed using the ABAQUS commercial code. A comparison of the numerical simulations indicated that the links of the stent model resembling the Cordis BX-Velocity showed a greater capability to deform independently from the rings during bending. The stresses were found to be concentrated in the links and increase in a continuous way as the material plastically deformed, while the rings remained unstressed. This is due to the way the link members are connected to the ring structure. In the stent model resembling the Carbostent Sirius stent, the stresses developed both in the links and in the segments of the rings connected to the links. The Carbostent Sirius stent structure was found to be stiffer than the Cordis BX-Velocity stent.

Recently, Lally *et al.* [31] investigated the mechanical behaviour of two stent designs, NIR stent and S7 stent, on the biomechanical interaction between the stents and the artery during stenting procedure. These analyses were performed using Marc/Mentat (MscSoftware, Santa Ana, CA, USA). A third order Mooney-Rivlin model was used to model the atherosclerotic coronary vessel geometry for the artery, incorporating arterial properties from uniaxial and equibiaxial tensile test of human femoral arterial tissue and calcified plaque tissue properties from uniaxial tensile test on cellular human calcified plaque. The examination of the arterial wall stresses and the computed amount of volume stress in the stented arteries by the NIR and the S7 indicated that the more flexible S7 stent design would cause lower stresses than the NIR stent design. This result was found to correlate with the findings of clinical studies, whereby the S7 has been reported to be less likely to cause restenosis than the NIR. The main limitations of this study were the idealised geometrical representation of the stenosed coronary artery and the fact that the stents were modelled in their expanded shape, whereby the process of stent expansion was not modelled.

Holzapfel *et al.* [32] evaluated the difference in the mechanical environment within the arterial wall by a vessel stented with three different stent designs; the Multi-Link-Tetra stent, the NIROYAL Elite stent and the InFlow-Gold-Flex stent. The computational models included a complex stenosed arterial vessel geometry obtained from high resolution magnetic resonance images (hrMRI) of a human iliac stenotic artery. An anisotropic constitutive model was used to represent the arterial tissue properties. They examined the performance of

three different stent designs in term of luminal gain, intimal pressure concentration and the circumferential stress changes within the arterial wall caused by the stent. General observation found that as luminal gain increased, the intimal pressure concentration and the stresses within the vessel rapidly increased. The Multi-Link-Tetra stent was found to be the least likely to cause restenosis. It was found to cause half the magnitude of stress induced within the arterial wall by the InFlow-Gold-Flex stent when the Multi-Link-Tetra stent gained 90% of the luminal gain of the InFlow-Gold-Flex stent. This analysis is probably the most complete to-date since it includes the anisotropy of the tissue and the realistic vessel geometry. However, the more simplistic representation of the arterial tissue and artery geometry in other studies have also successfully identified key characteristics of stents that may influence restenosis outcome.

2.7 Conclusion

It may be concluded that stent design is the key determinant in the propensity of stents to cause restenosis. Stent design is responsible for the different levels of vascular damage within stented vessels leading to the growth of neointimal hyperplasia and restenosis. Clinical studies have demonstrated that different stent designs cause different levels of restenosis. Researchers have carried out FE studies in an attempt to understand the process of stenting procedures by simulating the expansion of stents and their interaction with arterial vessels by simulating their expansion inside stenotic coronary artery models. Most of FEM studies focused on the expansion characteristics of stents after deployment in free expansion, without the influence of the stenotic coronary artery. The results focused on the influence of the stent geometry on the stent expansion behaviour. In simulations of the free expansion of stents, the absence of the external force on the stent structure caused by the arterial wall structure presents a major limitation of these studies. Whilst these studies have concentrated on the geometrical characteristics of specific stent designs, the resulting geometrical results, such as the structure recoil, from these free expansion simulations are likely to be different with the influence of an arterial vessel. However, there are limited FEM studies incorporating the influence of stenotic coronary artery due to the

complexity of modelling the procedure. Analyses that have incorporated the arterial wall have generally examined the contact pressures and stresses within the vessel induced by the stent and the radial displacements within the artery. The stress concentrations within the stented vessels have generally been interpreted as a measure for vascular injury.

This study focuses on determining the amount of vascular injury caused by different stent designs. The ISAR-STEREO clinical Trial [26] indicated that the use of a thinner-strut stent is associated with a significant reduction of angiographic and clinical restenosis than the thicker-strut stents. Therefore it is hypothesised that the thicker-strut stents induces higher stresses on the arterial wall and that these high stresses may be responsible for the injury stimuli for growth of neointimal hyperplasia. The stresses induced in the arterial wall will therefore be determined for the different stent designs and a comparison to clinical data will be used to determine more conclusively the mechanical stimulus for in-stent restenosis.

Chapter 3

MATERIALS AND METHOD

3.1 Introduction

The purpose of this study is to identify the mechanical stimuli for in-stent restenosis. This may be achieved by investigating the mechanical cause of the difference in restenosis outcome by thinner and thicker strut stents following the ISAR-STEREO clinical trial. Finite element models of these stents were developed and the stents were deployed in various stenosed vessel geometries in order to achieve this objective. The stents were expanded and deployed within the arteries to scaffold open stenosed arteries, in line with that which was carried out in the clinical trial.

To generate these numerical simulations, the finite element method requires a number of inputs; the geometry of the stents and the various stenosed coronary arterial vessels, the material properties of the stents, the plaque and the artery, and the appropriate application of loading and boundary conditions. The finite element models of the stents were developed in ANSYS (Canonsburg, PA, USA), a finite element software package. The properties of 316L stainless steel were assigned to the stents' material. The material behaviour of the artery was obtained from available published data on porcine coronary arterial tissue. The material model for the plaque was obtained from available published data on hypocellular human atherosclerotic plaques. The finite element analyses were carried out to compare the stresses induced within the stented artery vessels by

these stents, and hence used to determine the level of vascular injury caused to the artery by different strut thickness stents.

3.2 Modelling of Stent Geometry

In finite element simulations, it is extremely important to realistically model the problem. To realistically represent stent deployment, full three-dimensional models of the stents had to be developed. The models were generated and meshed using ANSYS and the elements, nodes and their connectivities were transferred into Marc/Mentat (MscSoftware, Santa Ana, CA, USA) for solving.

A number of finite element packages have been used for modelling the deployment of intravascular stents, such as ABAQUS [27, 29, 30, 48, 86], ANSYS/LS-DYNA [28, 52, 84] and Marc/Mentat [31]. Marc/Mentat was chosen for solving the analyses in the current project because of its capability of handling highly non-linear and large deformation material behaviour. The non-linear regression routine, available in Marc/Mentat, was used to obtain the hyperelastic constitutive model that best fit the uniaxial and equibiaxial published data and was found to be effective in obtaining a stable material. It has a robust contact algorithm that is suitable for defining the contact between the stent, plaque and artery. Marc/Mentat has mesh adaptivity capability which is highly advantageous for the contact analyses used in this study since it enables automatic mesh refinement of the arterial element, as contact occurs between the stent and the surface of the artery. This mesh refinement was needed for accurate stress analysis of the stenosed artery and this function was found effective in minimising penetration, thus obtaining convergence. Cyclic symmetry is another option available in Marc/Mentat which was used in these analyses. Circumferential symmetry was found in the stent's design and the cyclic symmetry capability in Marc/Mentat allowed one third in the circumferential direction to be modelled as apposed to the full stent. The number of elements used for the analyses was therefore minimised and hence the computational time and resources required were reduced.

The stent geometries in the finite element models were based on the stents used in the ISAR STEREO Trial [26]. They were the ACS RX MultiLink and the ACS MultiLink RX Duet. Both stents are manufactured by the same company, namely Guidant/Advanced Cardiovascular Systems. Both stents have an interconnected-ring design and different strut thickness. These stents have similar design with a strut width of 0.1 mm. The strut thickness of the ACS RX MultiLink ($Mlink_{thin}$) is 0.05 mm and the strut thickness of the ACS MultiLink RX Duet ($Mlink_{thick}$) is 0.14 mm. They have a square cross-sectional area.

Full three-dimensional models of the stents were developed to determine the expansion characteristics of the stents after stent deployment. The main measurements of the stents were extrapolated from the handbook of coronary stents [89]. Both stents are available in a range of lengths, whilst the length of the stents investigated in this study was 7.2 mm. For this length, the ACS MultiLink RX Duet stent consists of six rings in the longitudinal direction with six crowns in each ring, see Figure 3.1. The rings are connected to one another at three different evenly spaced locations and these locations are offset from one another along the length of the stent as shown in Figure 3.1. For both of the finite element models of the stents, all the parameters, such as the length and width were kept constant and the only variation between the two designs was the thickness of the stent struts. A strut thickness of 0.05 mm was assigned to the model of the ACS RX MultiLink ($Mlink_{thin}$) whilst a strut thickness of 0.14 mm was assigned to the ACS MultiLink RX Duet ($Mlink_{thick}$). Both stents were simulated with an inner radius of 0.72 mm and length of 7.2 mm with a corresponding outer radius of 0.77 mm for the $Mlink_{thin}$ and 0.86 mm for the $Mlink_{thick}$, see Figure 3.2.

The stent does not show symmetry in the longitudinal direction however, symmetry is observed in the circumferential direction. Due to the circumferential symmetry, only one third in the circumferential direction was modelled with the full length in the longitudinal direction. The stent geometry was initially modelled in three-dimensional Cartesian coordinate system, representing the stent in an opened-out, planar configuration. To generate the planar geometry of the stents, line profiles that represented the skeleton of the stent were created and a square area was subsequently extruded through the lines profiles to generate the planar geometry of the stent volume, see Figure 3.3.

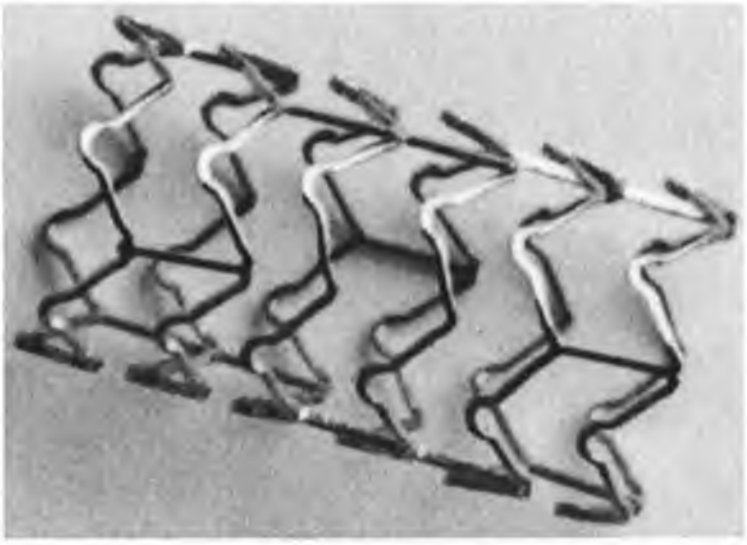

Figure 3.1 Expanded ACS MultiLink RX Duet [adapted from [90].

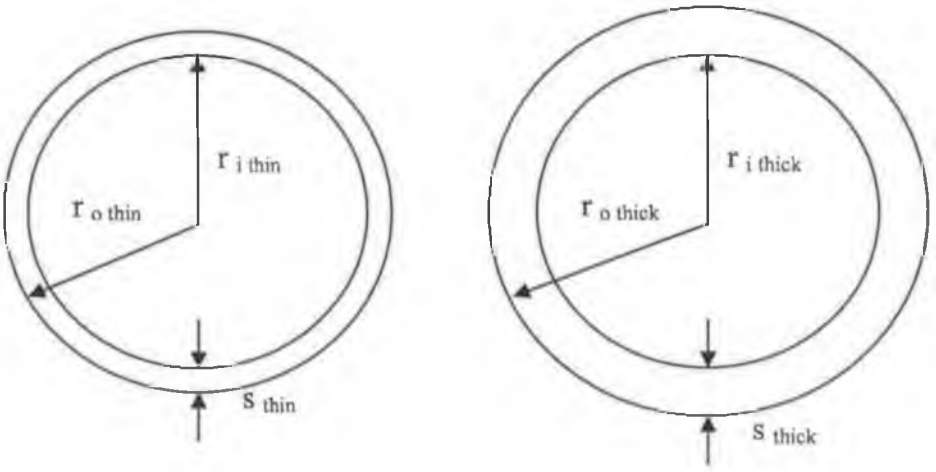

$r_{i\ thin} = 0.72$ mm
$r_{o\ thin} = 0.77$ mm
thickness (s_{thin}) = 0.05 mm

$r_{i\ thick} = 0.72$ mm
$r_{o\ thick} = 0.86$ mm
thickness (s_{thick}) = 0.14 mm

Figure 3.2 Schematic illustrating the radial dimensions of the $Mlink_{thin}$ and $Mlink_{thick}$ models.

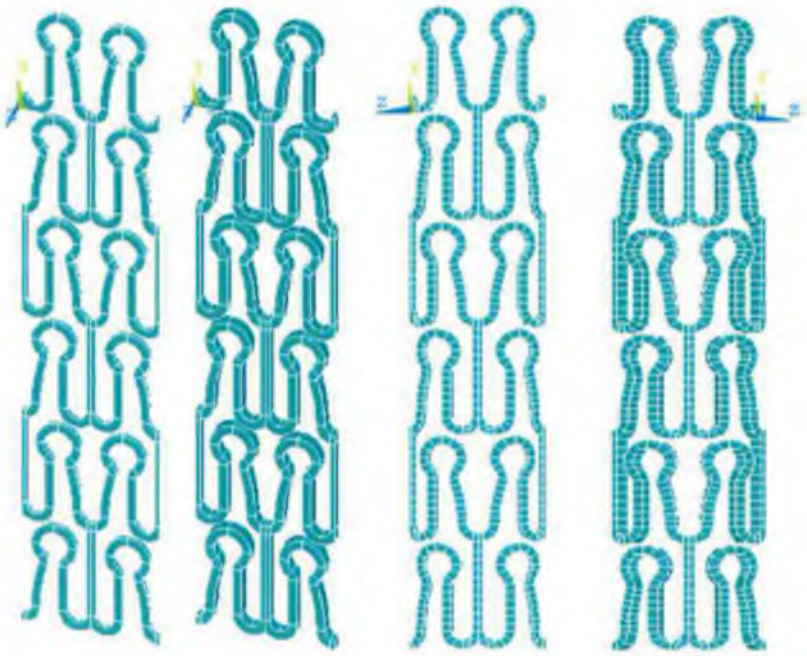

Figure 3.3 Volumes of (a) $Mlink_{thin}$ and (b) $Mlink_{thick}$ in the Cartesian coordinate system and the meshed model of (c) $Mlink_{thin}$ and (d) $Mlink_{thick}$.

The volumes of $Mlink_{thin}$ and $Mlink_{thick}$ were discretised by means of eight-noded isoparametric, three-dimensional brick elements. The models were meshed with one element through the thickness, see Figure 3.3. Both stents were meshed with a total of 532 elements with corresponding 2010 total number of nodes. The elements were checked for their shape to ensure that no distorted elements were generated. Contact analysis for Marc/Mentat requires a finer mesh on the most deformable body of the contact bodies, i.e. the stenosed artery in this case. Therefore this mesh density of the stent was chosen to minimise the number of elements and was found reasonable. A finer mesh of the stent structure would lead to a finer mesh density of the artery and much greater heavy computational time and resources.

The nodal coordinates of the meshed model were transferred from a Cartesian coordinate system into a cylindrical coordinate system, using a procedure reported by Lally *et al.* [31], whereby the planar configuration was wrapped to represent the cylindrical structure of the stents.

The elements, nodes and their connectivity were then transferred into the finite element code MSC Marc Mentat and large deformation analyses were solved to simulate the expansion of the stents. Although ANSYS was used to model the stents' geometries, it was found that it was not suitable for solving the analyses which included contact between the stent, plaque and artery and the use of hyperelastic material models to define the plaque and the arterial wall.

Four case studies were carried out for each of the stent designs to investigate the influence of strut thickness on stent deployment. The influence of variations in strut thickness on the stresses that were induced within arteries during and after stent deployment by the stents' struts were also investigated. The four case studies carried out were as follows:-

I. Case study 1:

   Free expansion of $Mlink_{thin}$ and $Mlink_{thick}$. This study investigated the performance of the stents in the absence of an artery.

II. Case study 2:

   Expansion of $Mlink_{thin}$ and $Mlink_{thick}$ inside a straight stenotic vessel geometry with arterial material properties. The same initial expanded lumen diameter, $Ø_I$, where $Ø_{I\ thin} = Ø_{I\ thick}$ was achieved for both stents. $Ø_I$ is achieved when pressure is applied, see Figure 3.4.

III. Case study 3:

   Expansion of $Mlink_{thin}$ and $Mlink_{thick}$ inside a straight stenotic vessel geometry with arterial material properties as in Case study 2. However, the same final expanded lumen diameter, $Ø_F$, where $Ø_{F\ thin} = Ø_{F\ thick}$ was achieved for both stents in this case. $Ø_F$ is achieved when pressure is completely removed, see Figure 3.4.

IV. Case study 4:

   Expansion of $Mlink_{thin}$ and $Mlink_{thick}$ inside a localised stenotic artery vessel geometry with plaque and arterial material properties assigned to the two

components of the arterial wall. The same initial expanded lumen diameter, $Ø_I$, where $Ø_{I\,thin} = Ø_{I\,thick}$ was achieved for both stents.

The output geometric quantities and calculated parameters of interest during the analyses are summarised in Table 3.1. These values were taken from the stents' structures for the unexpanded stents' configurations, at loading and on removal of the expansion pressure at unloading during stent deployment for all four case studies.

- *Stent before expansion*

  R_{orig} = original radius

  L_{orig} = original length

- *Stent after loading*

  $R_{load\ proximal}$ = radius of stent at the proximal end of stent

  $R_{load\ distal}$ = radius of stent at the distal end of stent

  $R_{load\ central}$ = radius of stent at the centre of stent

  L_{load} = length at the end of loading

- *Stent after unloading*

  $R_{unload\ proximal}$ = radius of stent at the proximal end of stent

  $R_{unload\ distal}$ = radius of stent at the distal end of stent

  $R_{unload\ central}$ = radius of stent at the centre of stent

  L_{unload} = length at the end of unloading

- *Calculated parameters*

$$\text{Proximal radial recoil} = \frac{R_{load\ proximal} - R_{unload\ proximal}}{R_{load\ proximal}}$$

$$\text{Central radial recoil} = \frac{R_{load\ central} - R_{unload\ central}}{R_{load\ central}}$$

$$\text{Distal radial recoil} = \frac{R_{\text{load distal}} - R_{\text{unload distal}}}{R_{\text{load distal}}}$$

$$\text{Longitudinal recoil} = \frac{L_{\text{load}} - L_{\text{unload}}}{L_{\text{load}}}$$

$$\text{Foreshortening} = \frac{L_{\text{orig}} - L_{\text{load}}}{L_{\text{orig}}}$$

$$\text{Dogboning} = \frac{R_{\text{load distal}} - R_{\text{load central}}}{R_{\text{load distal}}}$$

Table 3.1 List of geometric data taken following the expansion of $Mlink_{thin}$ and $Mlink_{thick}$ for all four case studies.

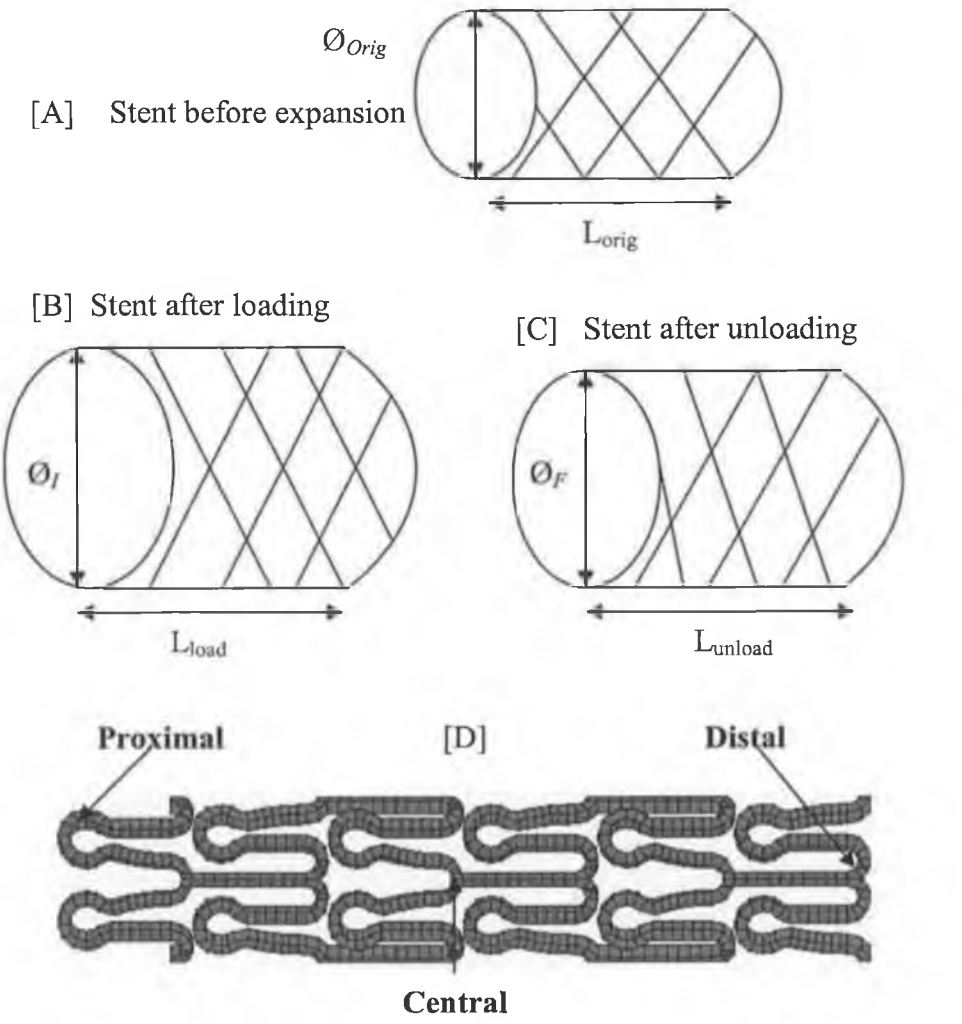

Figure 3.4 Schematic illustrating the stent's expansion at (A) stent before expansion, (B) stent at loading when pressure is applied and (C) stent at unloading when pressure is removed and (D) illustrates the division of interest.

The von Mises stress, σ, and the equivalent plastic strain, $\dot{\varepsilon}_{eqv}$, were evaluated for the expanded stent structures. These quantities are defined as follows:-

$$\sigma = \frac{[(\sigma_1 - \sigma_2)^2 + (\sigma_2 - \sigma_3)^2 + (\sigma_3 - \sigma_1)^2]^{1/2}}{\sqrt{2}}$$

where, $\sigma_1, \sigma_2, \sigma_3$ are the principal stresses.

$$\dot{\varepsilon}_{eqv} = \int_0 \sqrt{\frac{2}{3}\dot{\varepsilon}^{pl} : \dot{\varepsilon}^{pl}}\, dt$$

where, $\dot{\varepsilon}^{pl}$ is the plastic strain rate tensor.

3.2.1 Case study 1:

Free expansion of $Mlink_{thin}$ and $Mlink_{thick}$.

Stent deployment involves expansion of the stent by the application of an internal pressure (loading), and removal of the internal pressure (unloading). Initially in this study, the stents were subjected to free expansion to investigate their expansion under loading without the influence of the artery, see Figure 3.5. A uniform, linearly increasing radial pressure (P) was applied as a surface load to the internal surface of the stent until a radius of 3 mm was achieved in the central region of the stent.

The pressure required to expand $Mlink_{thin}$ was 0.437 MPa and the pressure required to expand $Mlink_{thick}$ was 1.3 MPa, see Figure 3.6. The pressure was ramped for a time step size of 0.01. This was an iteration process whereby the static analyses involve the application of pressure to achieve the desired stent's expansion. The pressure was unloaded by half the time it took to load it. Too high of a time step size results in too much pressure being applied in one increment over time and this may cause too much deformation resulting in non-convergence of the solution.

Cyclic symmetry boundary conditions were imposed on the nodes of the stent in the circumferential plane of symmetry. The top and bottom ends of the stent were free from any constraints. Two nodes in the centre of the stent were constrained in the circumferential direction to prevent rigid body rotation of the stent.

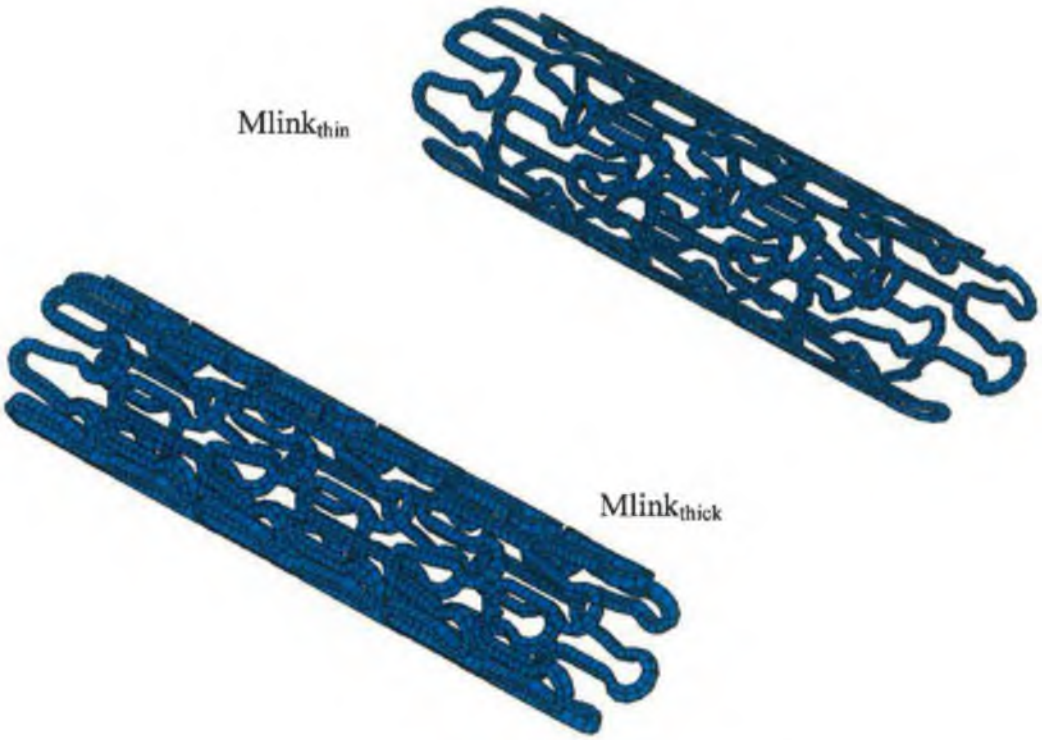

Figure 3.5 Finite element meshes of unexpanded Mlink$_{thin}$ and Mlink$_{thick}$, used for case study 1.

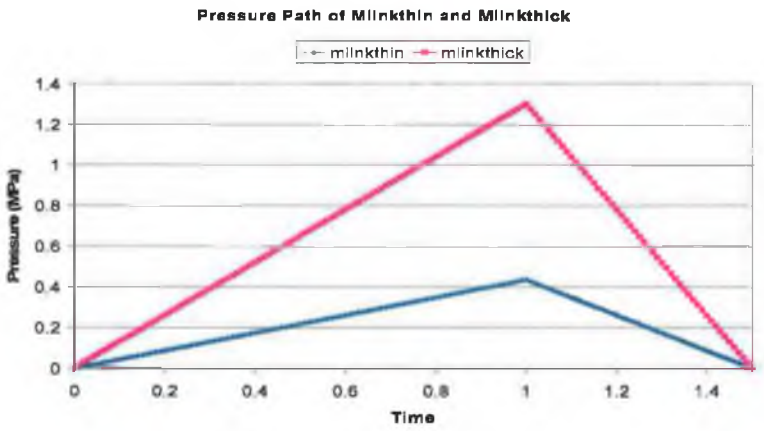

Figure 3.6 Plot of pressure path of Mlink$_{thin}$ and Mlink$_{thick}$.

3.2.2 Case study 2 and case study 3: Expansion of $Mlink_{thin}$ and $Mlink_{thick}$ inside various stenosed coronary artery vessels.

Three-dimensional simulations of stent deployment within various stenosed vessel geometries were developed to determine more realistically the expansion of $Mlink_{thin}$ and $Mlink_{thick}$ and to quantify the stresses induced within stented stenotic coronary arteries by $Mlink_{thin}$ and $Mlink_{thick}$.

For case study 2 and case study 3, the same finite element models were simulated, with the only difference being the amount of pressure applied. For case study 2, 8.2 MPa was applied to expand $Mlink_{thin}$ and 10.5 MPa was applied to expand $Mlink_{thick}$, to achieve the same initial vessel lumen diameter. For case study 3, the pressure required to expand $Mlink_{thin}$ and $Mlink_{thick}$ were 8.2 MPa and 2.2 MPa respectively, to achieve the same final vessel lumen diameter. The pressure was applied as a uniform, linearly increasing surface load and was applied to the internal surface of the stent. The pressure was removed linearly in half the time of loading, to the pressure of 13.3 kPa, which corresponds to mean blood pressure of 100 mmHg.

A full model of the stent was expanded inside a stenotic straight vessel and it was found to be highly computationally expensive. The results were analysed and it was found that the movement in the midplane was minimal, see Appendix A. Therefore to save computational time and resources, the full model were divided into two half models; a proximal half and a distal half of the stented vessels and each half was analysed separately and compared for each stent design.

As a result of the necessity to divide the model in two, four simulations had to be carried out to complete case study 2 and case study 3, see Figure 3.6. Each simulation model composed of two bodies, the stent and the stenotic coronary artery. The geometrical models for the two stent designs remained the same. The stenotic coronary artery was modelled as a straight vessel geometry of internal radius of 1 mm and thickness of 0.8 mm, see Figure 3.7. The thickness of atherosclerotic human coronary arteries range from 0.56 mm to 1.25 mm, depending upon the location of the arteries on the surface of the heart [37]. For

this reason, a thickness of 0.8 mm was chosen to represent the stenosed coronary artery. Arterial properties were assigned to the stenosed vessel. Due to cyclic symmetry, only one-third of the artery and stent were represented in the model. Five elements were assigned through the thickness of the vessel, thirty elements were assigned in the circumferential length and forty-eight elements were assigned in the longitudinal length. There were 7200 elements in total for the stenotic coronary artery.

In addition, adaptive meshing was used to ensure minimal penetration occurred as the stent came into contact with the stenotic artery as the edge of an element of one body would penetrate the other body if the meshing was not sufficiently fine to prevent penetration. Penetration during stent deployment simulations can be a significant problem since the relatively thin struts of the stents contact the artery in very localised areas and have to support the whole arterial structure. Local mesh adaptivity was assigned to the elements where the stent came into contact with the stenotic artery, i.e. the inner layer of the artery wall. As a result, these associated elements were subdivided by two in all three coordinate directions resulting in a substantial refinement of the mesh and hence an improvement in the accuracy of the solution.

When adaptive meshing occurs, to ensure compatibility, the new nodes created are internally tied to the neighbouring nodes. For example, to ensure compatibility node E is effectively tied to node A and node B, and node F is effectively ties to node B and C, see Figure 3.8. This occurs internally and does not conflict with other use-defined ties or contact. These new nodes are automatically inherent the same boundary conditions as the neighbouring nodes tying the new generated nodes. In the case of the new nodes generated on the exterior of a contact body are automatically treated as potential contact nodes and they are checked to determine if they are in contact.

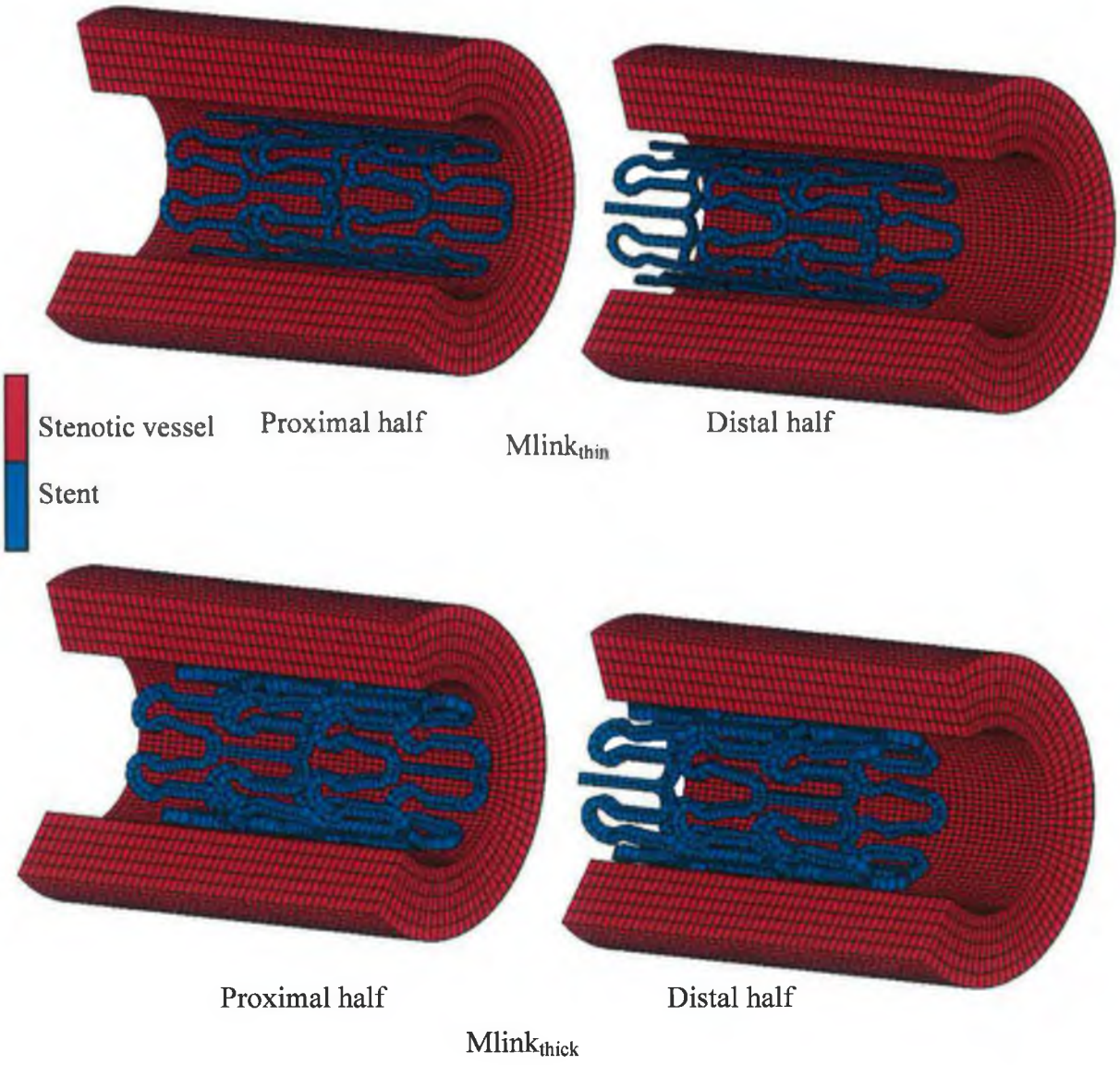

Figure 3.7 Finite element mesh of unexpanded Mlink$_{thin}$ and Mlink$_{thick}$ inside a stenotic coronary artery, with an inner radius of 1 mm and outer radius of 1.8 mm, used for case study 2 and case study 3.

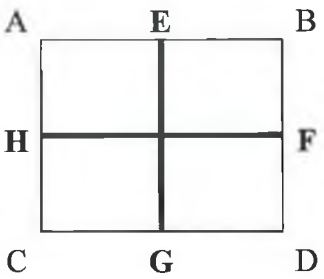

Figure 3.8 Illustration of discontinuities created as local mesh adaptivity occurs.

3.2.3 Case study 4:

Expansion of $Mlink_{thin}$ and $Mlink_{thick}$ inside localised stenotic coronary artery vessels.

For case study 4, two simulations were carried out to expand the distal half of $Mlink_{thin}$ and $Mlink_{thick}$ inside a localised stenotic coronary artery vessel, see Figure 3.9. The pressure used to expand $Mlink_{thin}$ was 41 MPa and 45.7 MPa for $Mlink_{thick}$, to achieve the same initial lumen diameter. The pressure was applied as a uniform, linearly increasing surface load on the internal surface of the stent. The pressure was removed linearly in half the time of loading, to the pressure up to 13.3 kPa, which corresponds to mean blood pressure of 100 mmHg.

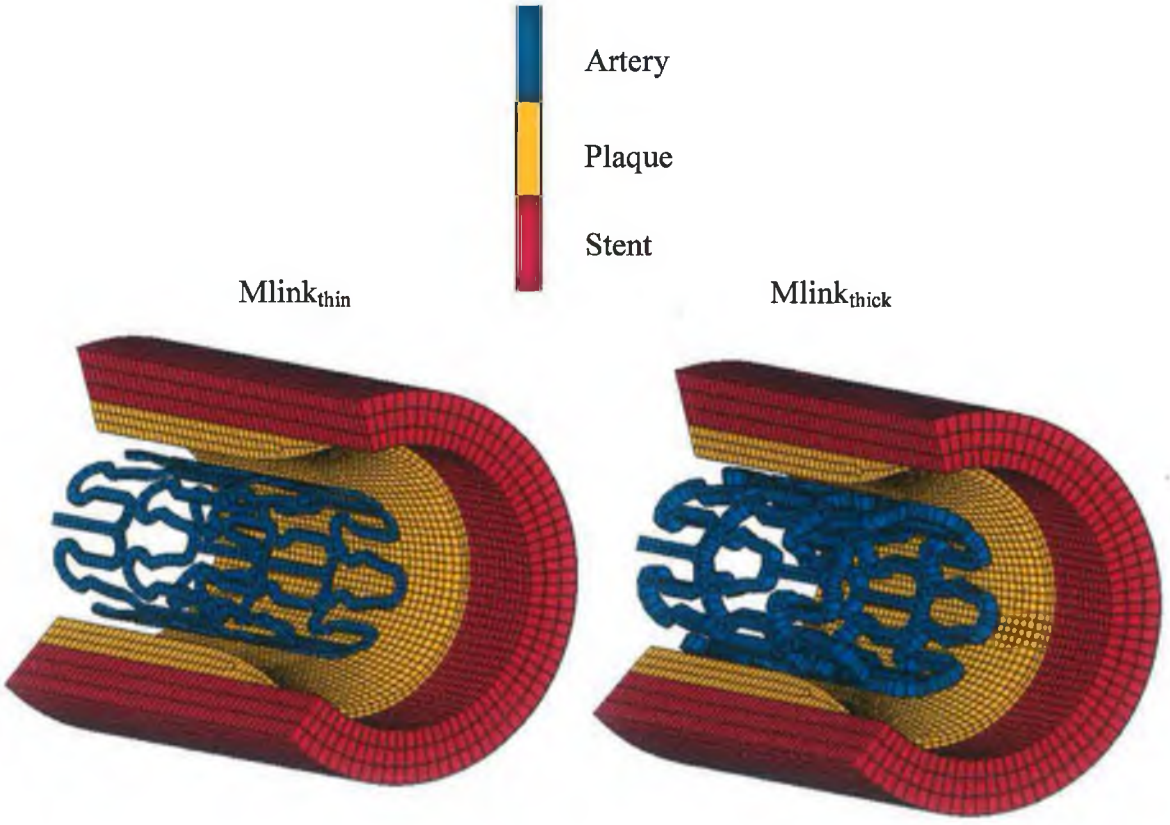

Figure 3.9 Finite element mesh of unexpanded $Mlink_{thin}$ and $Mlink_{thick}$ inside a localised stenotic vessel, with an inner radius of 1 mm and outer radius of 1.8, used for case study 4.

The vessel incorporated arterial and plaque properties. The stenosed coronary artery was modelled as a vessel with a localised stenosis. This was represented by a localised crescent-shaped axisymmetric stenosis with an internal radius of 1 mm and outer radius of 1.8 mm. Six elements were assigned through the thickness of the artery, thirty elements were assigned in the circumferential length and forty-eight elements were assigned in the longitudinal length. The healthy arterial tissue of the artery was meshed with 4320 elements, whilst the plaque was meshed with 3270 elements. In total the localised stenotic coronary artery vessel were discretised by 7590 elements, see Figure 3.9.

For this case study, adaptive meshing was again applied to the inner layer of the artery to allow element refinement upon contact with the stent during stent deployment.

For case study 2, 3 and 4, the element type used for the stenotic coronary artery was a full integration, three-dimensional eight-node isoparametric arbitrary hexahedral element (Type 7 in Marc/Mentat). Cyclic symmetry boundary conditions were imposed on the nodes of the stent and stenotic coronary artery in the circumferential plane of symmetry. This cyclic symmetry condition enables the nodes on the two cyclically symmetrical faces to be coupled or tied. All nodes of the stent were constrained in the longitudinal direction along the central plane of the stent to represent the half symmetry condition. These nodes were the nodes that would have connected to the other half of the model. Both ends of the stenotic artery were constrained in the longitudinal direction to represent the longitudinal tethering. One node on the outer surface of the stenotic artery was constrained in the circumferential direction to prevent rigid body rotations.

In cases 2, 3 and 4, surface to surface frictionless contact was assigned between the stent and the stenotic artery. Using this procedure, the motion of the contact bodies are tracked, and when contact occurs direct constraints are placed on the motion using boundary conditions – both kinematic constraints on transformed degrees of freedom and nodal forces. Deformable-deformable contact was also used to describe the contact between the stent and the stenotic artery. The contacting surfaces of both contact bodies were represented as analytical NURB surfaces. The description of the contact bodies using NURB surfaces enables recalculation of these surfaces as the stent and artery deform and

as a result this technique represents the deployment procedure more accurately than the default discrete technique where the boundary of the contacted body is described by the finite elements that the body is made up. This can cause problems due to the fact that the normals of the body are not continuous for a curved boundary. As a result the analytical NURB surfaces technique leads to a better convergence.

3.3 Stent Material: 316L Stainless Steel

The ACS RX MultiLink and the ACS MultiLink RX Duet stents are made of 316L stainless steel [89]. 316L stainless steel is a common material used for stents and its bulk properties are well known.

However, an experimental study was carried out by Murphy *et al.* [88] to investigate the mechanical behaviour of 316L stainless steel stent struts to determine the influence of strut size on the material's behaviour. During stent deployment, the stent must undergo plastic deformation to ensure that it remains in its expanded configuration and can therefore scaffold open the artery. Upon deployment, stents may undergo as much as 20%-30% plastic strain. The study by Murphy *et al.* [88] demonstrated that a size dependent stress-strain relationship must be used to describe the tensile behaviour of the 316L stainless steel for the size scale of coronary stent struts particularly as the breaking strength of 316L stainless steel is clearly size dependant, see Figure 3.10. The stress-strain relationship of 316L stainless steel for $Mlink_{thin}$ (strut thickness of 0.05 mm) and $Mlink_{thick}$ (strut thickness of 0.14 mm) in the finite element models in this study may therefore be described by the mechanical behaviour of the struts tested by Murphy *et al.* [88] as shown in Figure 3.10.

The material was described as an isotropic material with the linear elastic region of the curve defined through the material values for 316L stainless steel; Young's Modulus of 196 GPa, Poisson's Ratio of 0.3.

When the stress reaches the yield stress, the material no longer exhibits elastic behaviour and the stress-strain behaviour becomes non-linear. A piecewise linear function was used to represent this non-linearity through a von Mises

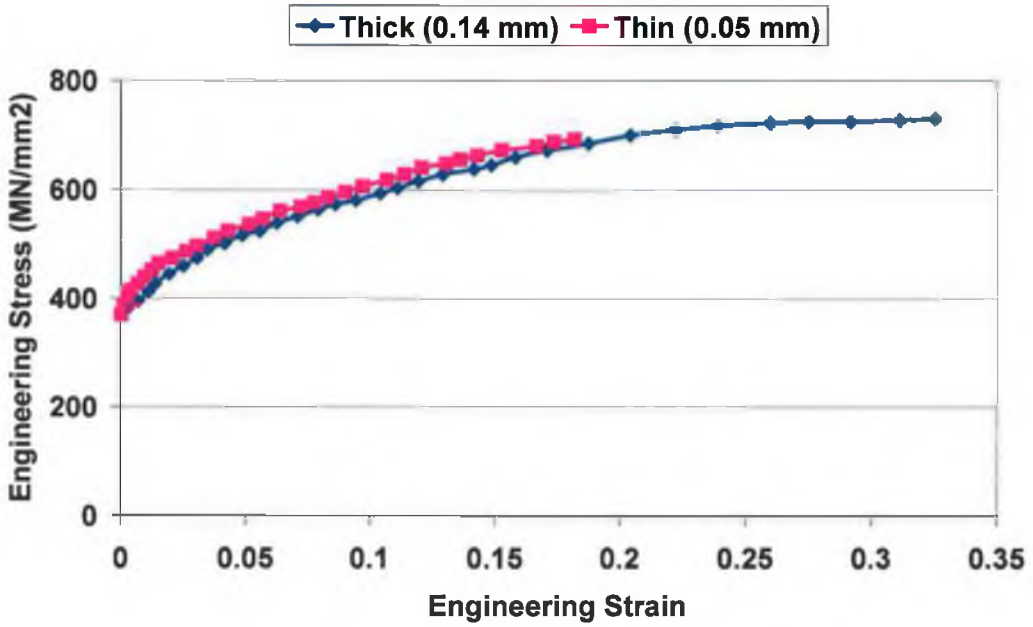

Figure 3.10 Plot of stress-strain relationship of 316L stainless steel for $Mlink_{thin}$ (0.05 mm) and $Mlink_{thick}$ (0.14 mm), [adapted from Murphy *et al.* [88]].

plasticity model with isotropic hardening. In a uniaxial test, the workhardening slope is defined as the slope of the stress-plastic strain curve. The workhardening slope relates the incremental stress to incremental plastic strain in the inelastic region and dictates the conditions of subsequent yielding. The Von Mises yield criterion ensures that yield occurs when the equivalent stress equals the yield stress initially defined. The uniaxial stress-plastic strain curves of 316L stainless steel for the two strut thickness stents were represented by a piecewise linear function, as described by the curves shown in Figure 3.10.

The yield stress and the workhardening data input into the finite element code had to be compatible with the procedure used in the analysis. In Marc Mentat, when LARGE DISPLACEMENT, UPDATE, FINITE parameters or PLASTICITY are used, the yield stress must be defined in terms of Cauchy stress, and the workhardening data with respect to logarithmic plastic strains.

The LARGE DISPLACEMENT option was used for this large deformation non-linear analysis. A LARGE STRAIN UPDATED LAGRANGE

formulation was used whereby the element quantities were evaluated with respect to the current updated deformed configuration. The FINITE parameter was allowing the effects of the change in metric due to large inelastic deformation to be included. This resulted in a different stiffness of the structure as well as in a modified calculation of stresses and inelastic strains.

In analyzing the mechanical performance of the stents, the material behaviour is of critical importance in acquiring accurate simulated studies. Once the stent is delivered to the site of lesion, it is plastically expanded. The plastically deformed structure remains as it supports the arterial wall. It is therefore essential to accurately model the plastic region of the stress-strain response of the material after the yield stress is reached. Validation tests were carried out to ensure accurate simulations of the material behaviour of 316L stainless steel. This was achieved by simulating a uniaxial test of a rectangular 316L specimen and the results of the simulation confirmed that the stress-strain behaviour of the material in the finite element models was the same as that represented in Figure 3.10.

3.4 Artery Material: Porcine Coronary Artery

A second order Mooney-Rivlin hyperelastic constitutive equation was used to represent the non-linear stress-strain relationship of the arterial wall. A Mooney-Rivlin hyperelastic material is defined by a strain energy density function, W given in Eq. (1). The hyperelastic constitutive equation was determined by fitting to available published data from uniaxial and equibiaxial tension tests of porcine coronary tissue [41].

A non-linear regression routine, available in Marc/Mentat, was used to obtain the hyperelastic constitutive model that best fit the uniaxial and equibiaxial data. The least-squares error was minimised during data fitting, and in this case was based on absolute error defined as follows:-

$$\text{Absolute error} = \sum_i [data\ measured(i) - data\ calculated(i)]^2$$

The uniaxial and biaxial data fits were checked for positive definiteness and the least squares fit yielded a strain energy density function describing the stress-strain curves shown in Figure 3.11. The regression routine fitted both the uniaxial and biaxial data simultaneously that led to the slight deviation in the stress-strain curves. This was found as a good fit comparatively with other models, with the lowest error value of 0.487657 associated with this fit. A Signiorini model (second order model) was found to best fit to the data as given by the following hyperelastic constitutive equation:

$$W = 708.416\,(I_1 - 3) - 620.042\,(I_2 - 3) + 2827.33\,(I_1 - 3)^2 \qquad \text{(kPa)}$$

where W is the strain energy density function of the material and I_1 and I_2 are the strain invariants. The second order model was found to best fit the chosen uniaxial and biaxial datas despite the third order model that was used by Lally *et al.* [41]. The resulting hyperelastic constitutive equation is specific to the stress-strain curves from a specific sample.

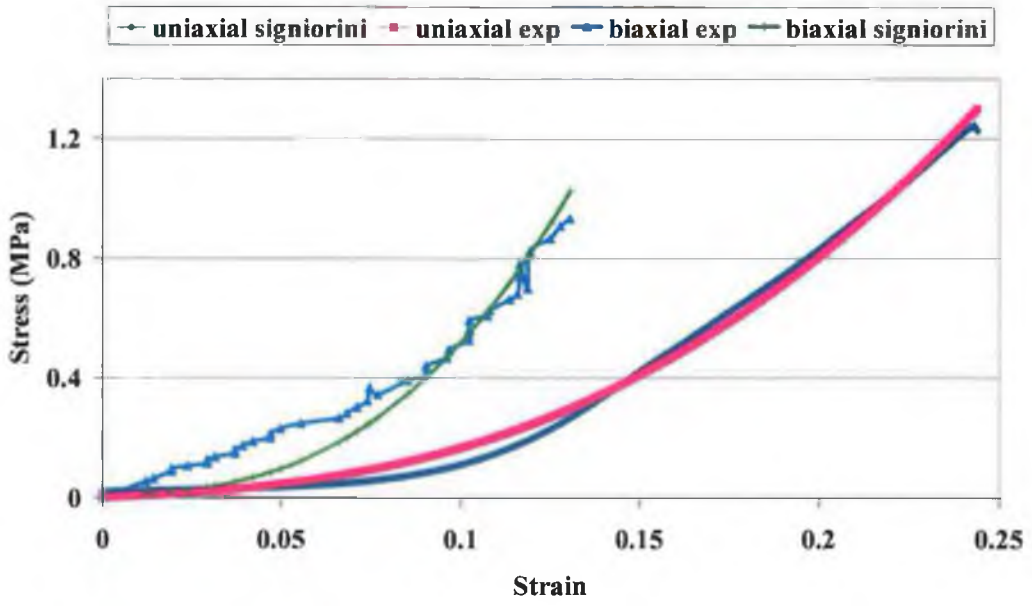

Figure 3.11 Plot of stress-strain uniaxial and biaxial data for porcine coronary tissue [41].

3.5 Plaque Material:
Hypocellular Human Atherosclerotic Plaques

A third order Mooney-Rivlin hyperelastic constitutive equation was used to represent the non-linear stress-strain relationship of human atherosclerotic plaque. The hyperelastic constitutive equation was determined by fitting to available published data on uniaxial tensile tests carried out on human atherosclerotic plaques [54].

Again, using the non-linear regression routine in Marc/Mentat, the model that best fit the uniaxial data was determined. The least-squares error was minimised during data fitting, and in this case was based on relative error defined as follows:-

$$\text{Relative error} = \sum_i [1 - \frac{data\ measured(i)}{data\ calculated(i)}]^2$$

The uniaxial data fit was checked to ensure that it yielded curves that were positive definite and that were a best fit to the data with a low error value. A third order deformation model was found to best fit to the data and the hyperelastic constitutive equation is given by:

$$W = -677.134\ (I_1 - 3) + 977.734\ (I_2 - 3) - 296180\ (I_1 - 3)^2 + 326979\ (I_1 - 3)(I_2 - 3) + 148343\ (I_1 - 3)^3 \quad \text{(kPa)}$$

where W is the strain energy density function of the material and I_1 and I_2 are the strain invariants. The uniaxial and biaxial behaviour described by this strain energy density function are shown in Figure 3.12. The fit to the data was achieved with an error value of 0.123461.

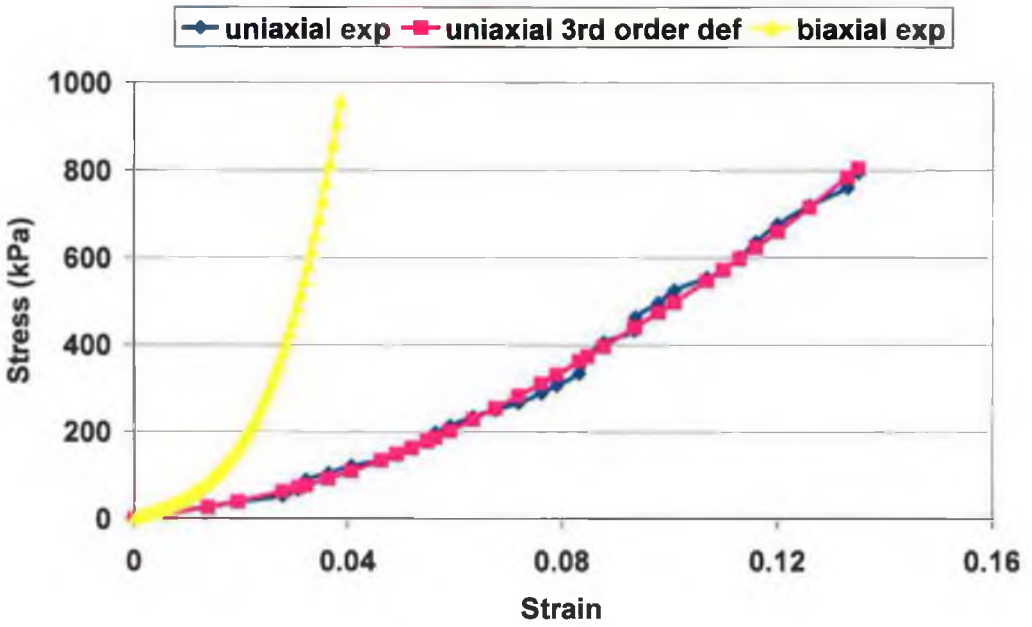

Figure 3.12 Plot of stress-strain uniaxial and biaxial data for hypocellular human atherosclerotic plaque.

3.6 Summary

This chapter has detailed all of the methods used in this study to investigate the performance of different strut thickness stents using the finite element method. The numerical models outlined enable the influence of stent design to be analysed in terms of the expansion characteristics of the stent. The models also include the important property that the vessel wall is non-linearly elastic and they may therefore be used to investigate the loading that different stents impose on different arterial geometries during their expansion. In this way, the models enable the stresses induced in stented arteries to be estimated and a greater insight into the mechanical stimuli for restenosis to be gained.

Chapter 4

RESULTS

4.1 Introduction

The following chapter outlines all of the results obtained for the four case studies examined during this thesis to investigate the influence of stent strut thickness on stent expansion and vessel wall stresses. Both stents, $Mlink_{thin}$ and $Mlink_{thick}$, were subjected to free expansion and later to expansion inside two different vessel geometries. The vessel wall stresses were examined where stents were expanded to achieve the same initial expanded lumen diameter, $Ø_I$ and also for cases where the stents were expanded to the same final expanded lumen diameter, $Ø_F$. The stresses induced within the vessels were studied for all of the load cases and for both stents.

4.2 Case Study 1: Free Expansion of $Mlink_{thin}$ and $Mlink_{thick}$

$Mlink_{thin}$ and $Mlink_{thick}$ were expanded to achieve an outer diameter of 3 mm, which corresponds to a typical diameter of a coronary artery, see Figure 4.1. The pressure required to expand $Mlink_{thin}$ was 0.437 MPa and the pressure required to expand $Mlink_{thick}$ was 1.3 MPa.

The radial expansion distribution was found to be similar for both $Mlink_{thin}$ and $Mlink_{thick}$. The radial displacement distribution throughout both

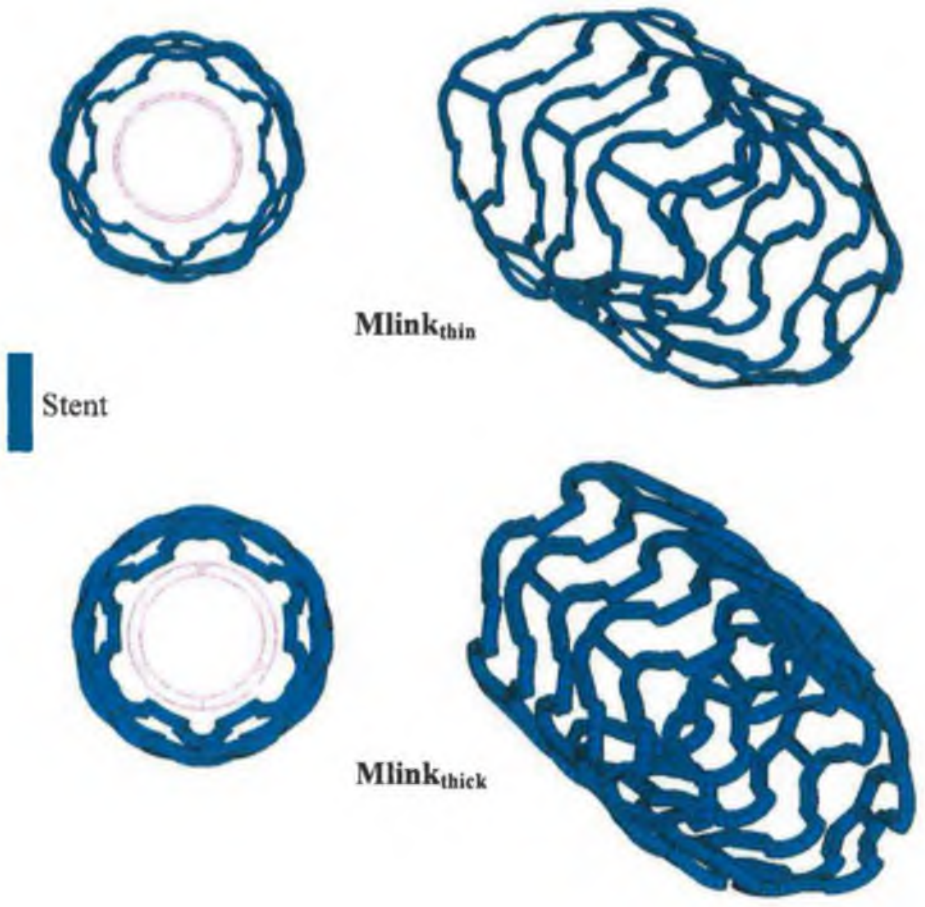

Figure 4.1 Deformed geometry of $Mlink_{thin}$ and $Mlink_{thick}$ under free expansion, achieving an initial outer diameter of 3 mm.

models was found to be highly non-uniform with the lowest radial displacement observed at the proximal end of the stents' structures, see Figure 4.2.

Radial displacement measurements were obtained at key geometrical markers along the lengths of both stents in order to allow direct comparison of their radial expansion, see Figure 4.3 and Table 4.1. The proximal end experienced the least radial displacement, followed by distal end 2, whilst the central region and distal end 1 were found to undergo similarly high radial displacements, see Figure 4.4.

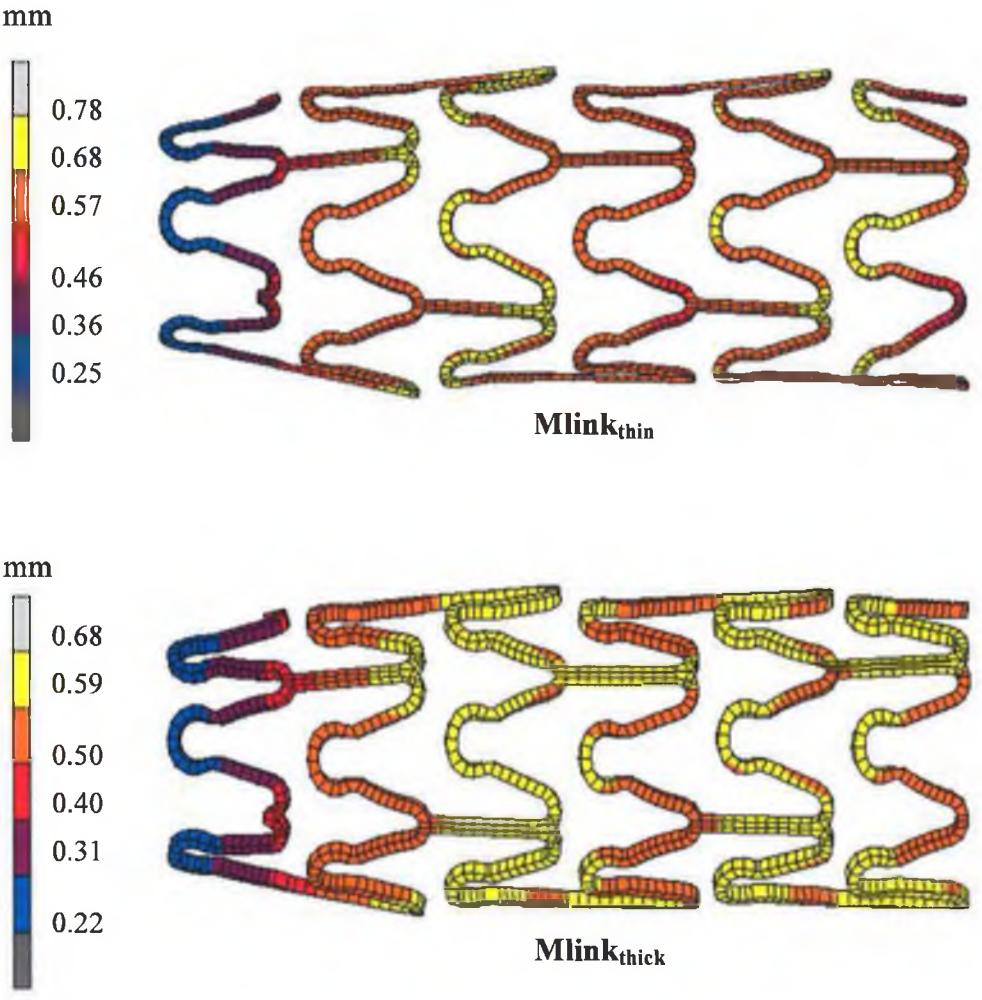

Figure 4.2 Radial displacement distribution throughout the stent structure of $Mlink_{thin}$ and $Mlink_{thick}$, subjected to free expansion, achieving an initial outer diameter of 3 mm.

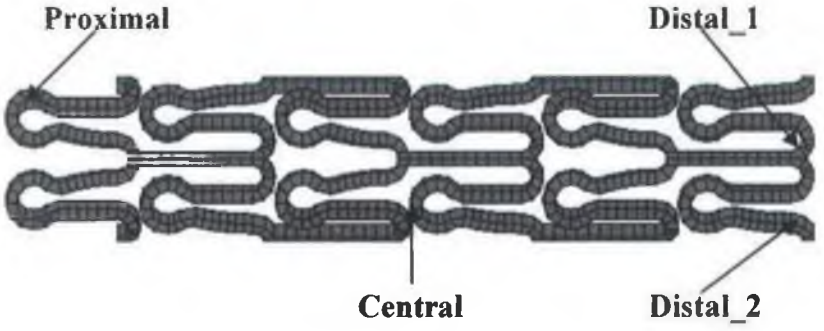

Figure 4.3 The proximal, central and distal points of interest.

	Mlink$_{thin}$	**Mlink$_{thick}$**
▪ *Stent before expansion*	(mm)	(mm)
R_{orig}	0.77	0.86
L_{orig}	7.2	7.2
▪ *Stent after loading*		
$R_{load\ proximal}$	1.06	1.1
$R_{load\ central}$	1.43	1.48
$R_{load\ distal\_1}$	1.42	1.47
$R_{load\ distal\_2}$	1.23	1.37
L_{load}	7.31	7.35
▪ *Stent after unloading*		
$R_{unload\ proximal}$	0.99	1.05
$R_{unload\ central}$	1.36	1.43
$R_{unload\ distal\_1}$	1.38	1.42
$R_{unload\ distal\_2}$	1.18	1.33
L_{unkoad}	7.29	7.33
▪ *Calculated parameters*	(%)	(%)
Longitudinal recoil	0.3	0.3
Foreshortening	-1.5	-2.1
Dogboning $_{proximal}$	-34.9	-34.5
Dogboning $_{distal\_1}$	-0.7	-0.7
Dogboning $_{distal\_2}$	-16.3	-8.0

Table 4.1 Geometric data of Mlink$_{thin}$ and Mlink$_{thick}$ through loading and unloading, subjected to free expansion, achieving an initial outer diameter of 3 mm.

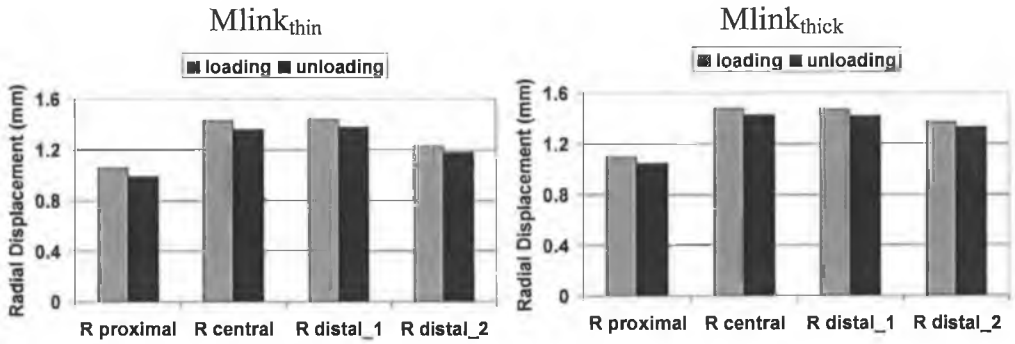

Figure 4.4 Radial displacement of Mlink$_{thin}$ and Mlink$_{thick}$ through loading and unloading, subjected to free expansion, achieving an initial outer diameter of 3 mm.

The radial percentage recoil for the proximal end was found to be 25% higher than the central and distal end for both stents. However, the radial percentage recoil was found to be consistently higher throughout the Mlink$_{thin}$ stent structure compared with the Mlink$_{thick}$, see Figure 4.5.

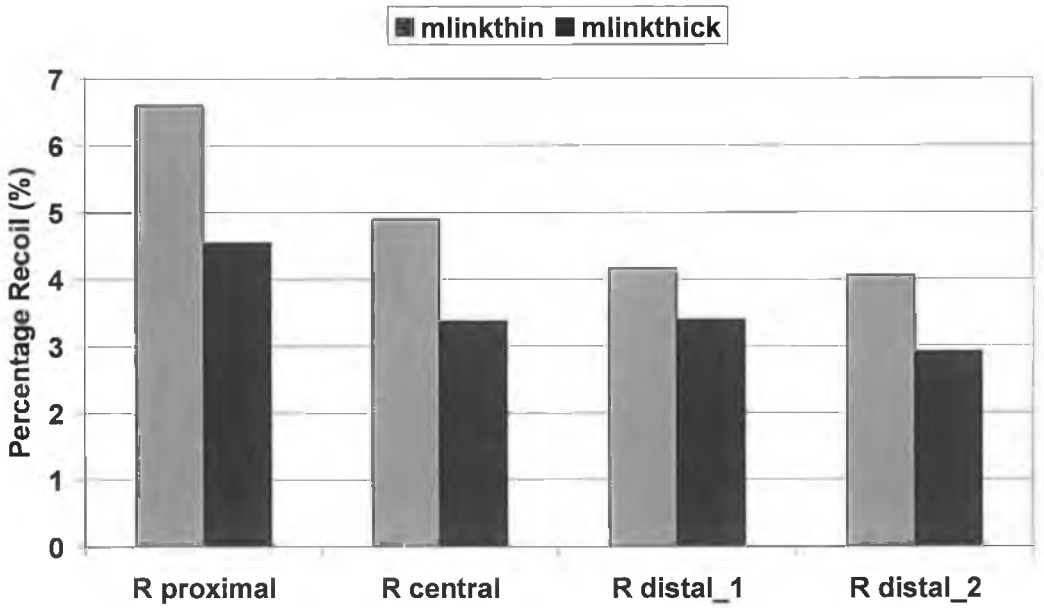

Figure 4.5 Comparison of percentage radial recoil of Mlink$_{thin}$ and Mlink$_{thick}$, subjected to free expansion, achieving an initial outer diameter of 3 mm.

During loading the stent structure may shorten giving rise to stent foreshortening. Negative foreshortening values were found for free expansion of the stents which indicated that the length of the stent structure elongated during loading.

Shortening of the stent structure can also occur during unloading of the stents, which gives a measure of the longitudinal recoil of the stents. No significant longitudinal recoil was observed during the free expansion of either the $Mlink_{thin}$ or $Mlink_{thick}$ stent structures, see Table 4.1.

Dogboning has been observed in stents during expansion, whereby the ends of the stents radially expand to a larger extent than the central portion of the stents. Dogboning was not observed in the $Mlink_{thin}$ or $Mlink_{thick}$ during free expansion, in fact, a high degree of radial retraction was observed at the proximal ends of both stents, see Table 4.1.

On examination of the von Mises stress contours within the stent structures, it can be seen that the highest stresses are concentrated in the area of the arcs. The arcs appear to act as plastic hinges allowing the stent structure to expand, see Figure 4.6. The maximum von Mises stresses in both stents are concentrated in the arcs and where the arcs connect to the longitudinal struts of the stent. The maximum von Mises stress magnitude for $Mlink_{thin}$ was found to be 604.4 MPa and for $Mlink_{thick}$ was found to be 596.9 MPa. The analysis also shows that the longitudinal struts of the stents experience low stresses during expansion, see Figure 4.6.

The resulting contours of Total Equivalent Plastic strain throughout the expanded structure of $Mlink_{thin}$ and $Mlink_{thick}$, were taken at the end of loading. High plastic strains are evident on the arcs of the stent structure and the maximum Total Equivalent Plastic strain was found to be 0.0924 for $Mlink_{thin}$ and 0.0997 for $Mlink_{thick}$, see Figure 4.7.

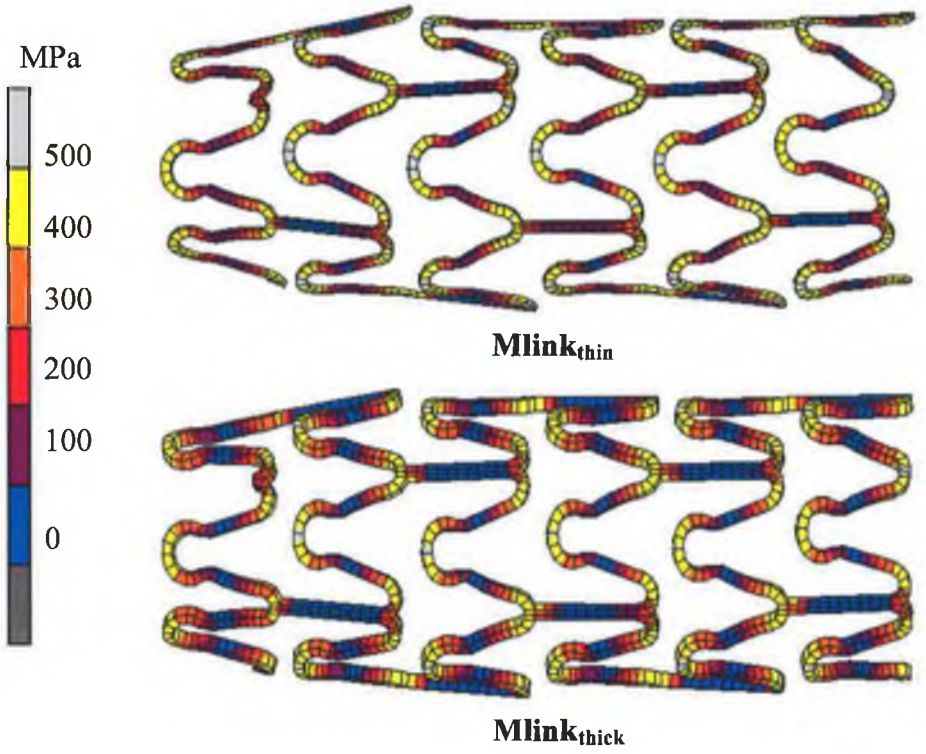

Figure 4.6 The resulting von Mises stress contours throughout the structures of $Mlink_{thin}$ and $Mlink_{thick}$, subjected to free expansion.

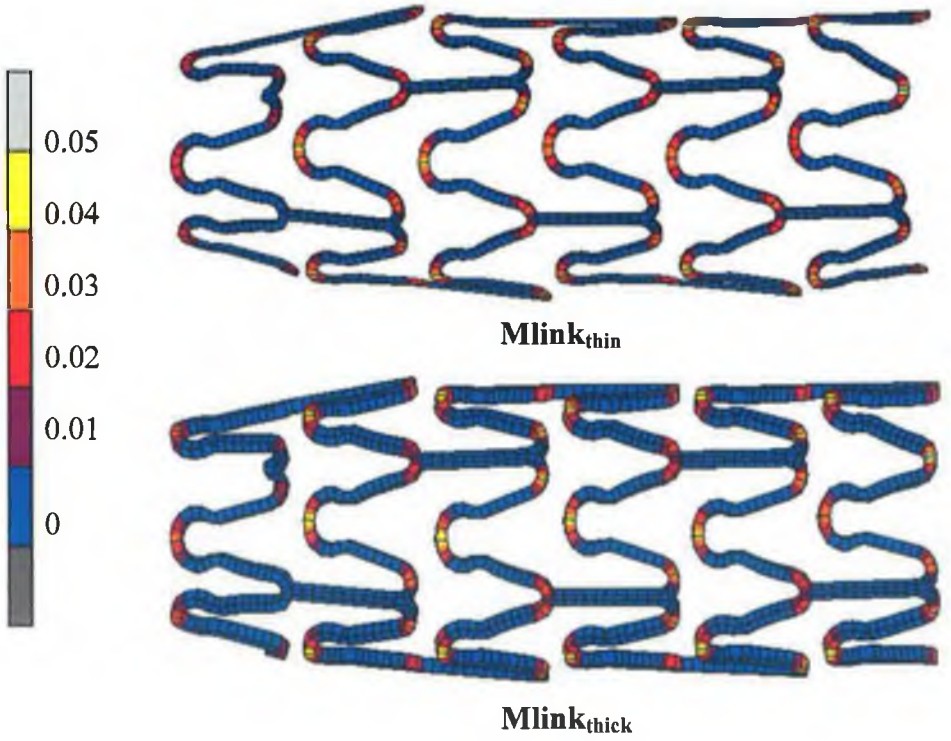

Figure 4.7 The resulting Total Equivalent Plastic strain contours throughout the structures of $Mlink_{thin}$ and $Mlink_{thick}$, subjected to free expansion.

4.3 Case Study 2:

Expansion of $Mlink_{thin}$ and $Mlink_{thick}$ inside a stenotic coronary artery achieving the same initial expanded lumen diameter

Four simulations were carried out, expanding the proximal and distal halves of $Mlink_{thin}$ and $Mlink_{thick}$ inside a stenotic coronary artery, represented as an idealised cylindrical vessel. $Mlink_{thin}$ and $Mlink_{thick}$ were expanded to achieve the same initial expanded lumen diameter (internal diameter of vessel), $\emptyset_I$ = 3 mm, see Figure 4.8. The pressures required to expand $Mlink_{thin}$ and $Mlink_{thick}$ were 8.2 MPa and 10.5 MPa, respectively. The same pressure was applied for both the proximal and distal halves of each structure.

The radial displacement throughout both structures of $Mlink_{thin}$ and $Mlink_{thick}$ was found to be highly non-uniform. The lowest values of radial displacement were observed at the proximal and distal ends of the stent structures, see Figure 4.9.

Radial displacements were measured at key locations on both the proximal and distal half of each stent, see Figure 4.10, in order to compute the structural characteristics of the stents through the loading and unloading process of the stents' expansion, see Table 4.2.

It can be seen that both stents, $Mlink_{thin}$ and $Mlink_{thick}$ have the same pattern of radial displacement distribution. The radial displacement was found to be in increasing order, as follows: the least radial displacement in the proximal end, followed by the distal end and then the central region of the distal half. The highest radial displacement was found in the central region of the proximal half of the stent structure, see Figure 4.11. Foreshortening was found to be low in magnitude and similar for both $Mlink_{thin}$ and $Mlink_{thick}$, but in contrast to free expansion, the stents did foreshorten to some degree, see Table 4.2.

Upon unloading, longitudinal recoil was found to be low in both stent structures, however, the fact that the values are negative indicates that the stents undergo elongation on unloading, unlike in free expansion. Radial retraction of

the stents was observed at the ends of the stents when compared with the radial diameter of the central portion of the stent structures. This 'negative dogboning' was found to be more prominent on the proximal half of the stents structures.

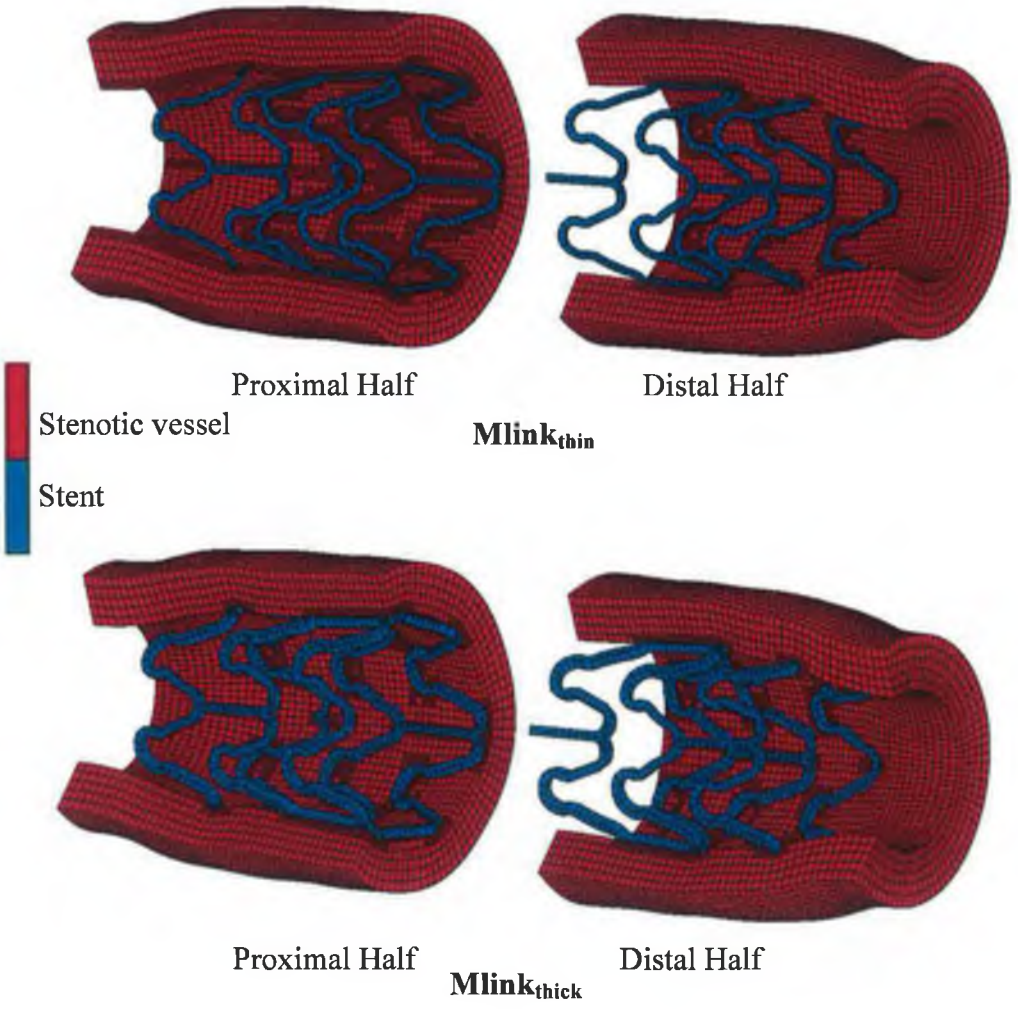

Figure 4.8 Deformed geometry of the proximal and distal halves of Mlink$_{thin}$ and Mlink$_{thick}$, scaffolding a stenotic vessel with thickness of 0.8 mm, achieving the same initial vessel lumen diameter of $\emptyset_I = 3$ mm.

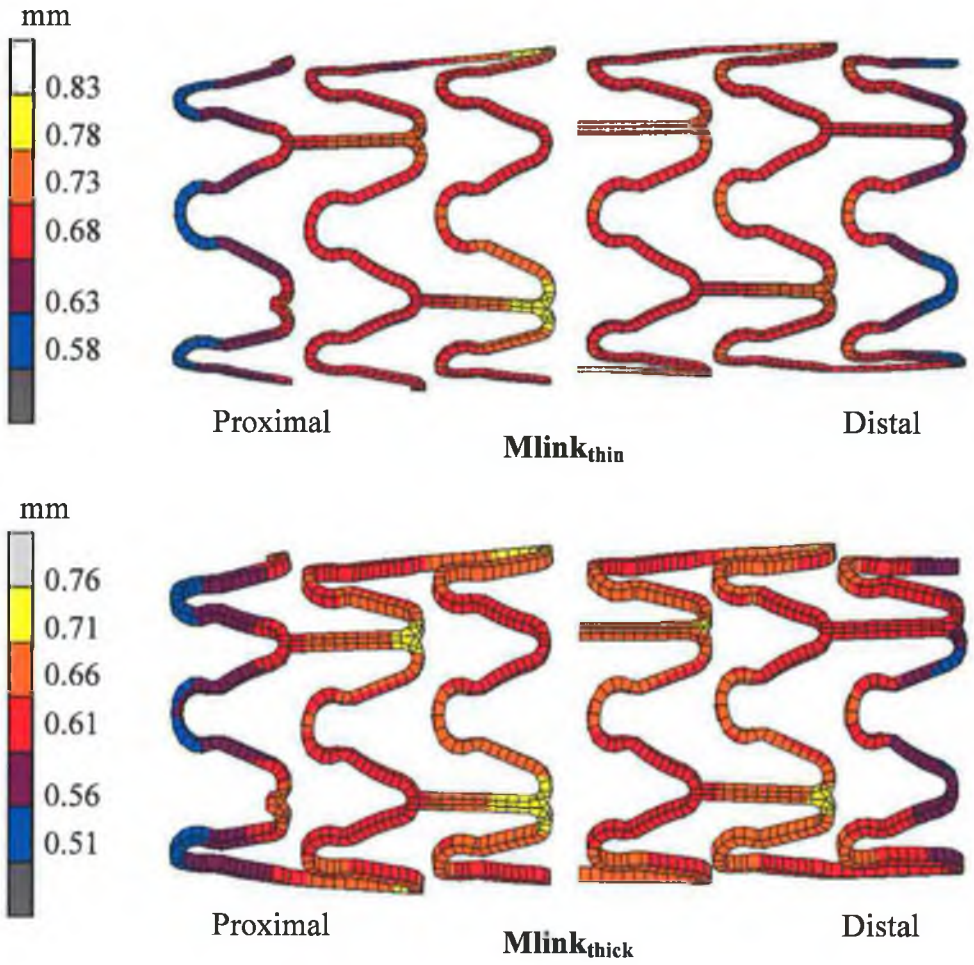

Figure 4.9 Radial displacement distribution throughout the stents' structure of $Mlink_{thin}$ and $Mlink_{thick}$, under the influence of a stenotic vessel, achieving the same initial vessel lumen diameter of $Ø_I$ = 3 mm.

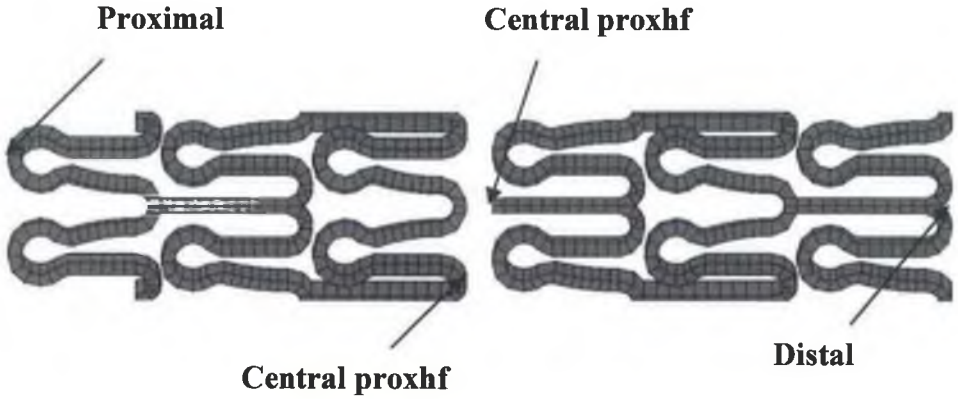

Figure 4.10 The proximal, central and distal points of interest.

	Mlink$_{thin}$	**Mlink$_{thick}$**
▪ *Stent before expansion*	(mm)	(mm)
R_{orig}	0.77	0.86
L_{orig}	3.6	3.6
▪ *Stent after loading*		
$R_{load\ proximal}$	1.39	1.42
$R_{load\ central\ proxhf}$	1.6	1.62
$R_{load\ central\ dishf}$	1.5	1.56
$R_{load\ distal}$	1.45	1.48
$L_{load\ proxhf}$	3.39	3.44
$L_{load\ dishf}$	3.41	3.43
▪ *Stent after unloading*		
$R_{unload\ proximal}$	1.12	1.19
$R_{unload\ central\ proxhf}$	1.19	1.29
$R_{unload\ central\ dishf}$	1.16	1.27
$R_{unload\ distal}$	1.13	1.21
$L_{unload\ proxhf}$	3.5	3.51
$L_{unload\ dishf}$	3.51	3.49
▪ *Calculated parameters*	(%)	(%)
Longitudinal $_{proxhf}$ recoil	-3.2	-2.0
Longitudinal $_{dishf}$ recoil	-2.9	-1.7
Foreshortening $_{proxhf}$	6.8	4.4
Foreshortening $_{dishf}$	5.3	4.7
Dogboning $_{proxhf}$	-15.1	-14.1
Dogboning $_{dishf}$	-3.4	-5.4

Table 4.2 Geometric data of Mlink$_{thin}$ and Mlink$_{thick}$ through loading and unloading, under the influence of stenotic vessel of 0.8mm thickness, achieving the same initial vessel lumen diameter of $\emptyset_I = 3$ mm.

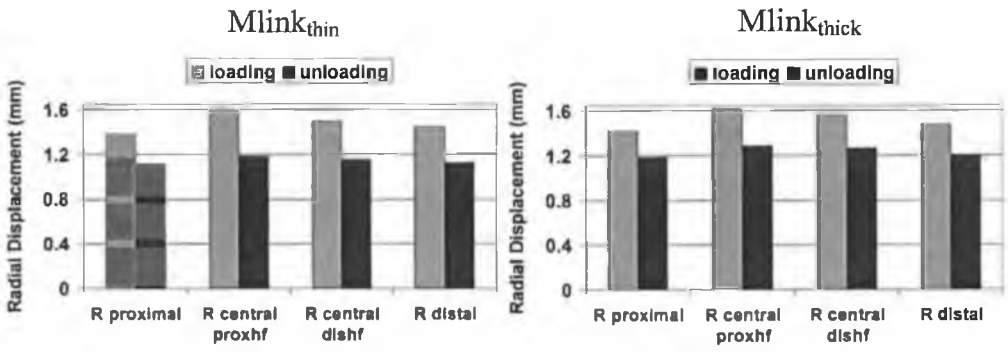

Figure 4.11 Radial displacement of Mlink$_{thin}$ and Mlink$_{thick}$ through loading and unloading, under the influence of stenotic vessel, achieving the same initial vessel lumen diameter of $\emptyset_I = 3$ mm.

Radial recoil throughout the Mlink$_{thick}$ structure was found to be less than the Mlink$_{thin}$, see Figure 4.12. The percentage of radial recoil was observed to follow the same pattern as the radial displacement with the least recoil found in the proximal end, followed by the distal end and the central region of the distal half, and finally, the greatest recoil was observed in the central region of the proximal half.

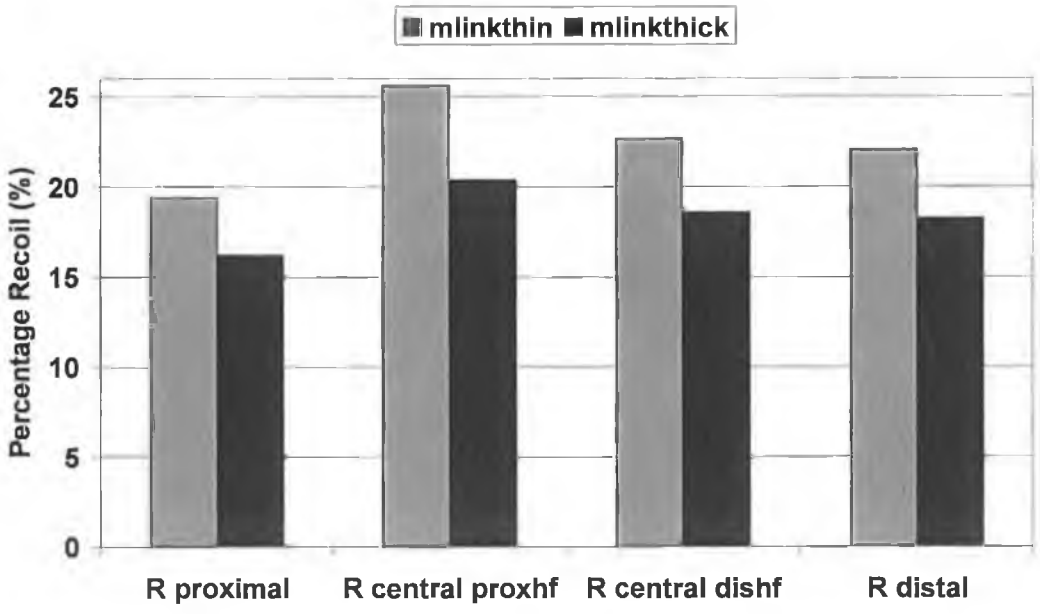

Figure 4.12 Comparison of percentage radial recoil of Mlink$_{thin}$ and Mlink$_{thick}$, subjected to free expansion, achieving the same initial vessel lumen diameter of $\emptyset_I = 3$ mm.

The resulting von Mises stress contours show similar stress distribution patterns as observed during free stent expansion whereby the highest stresses are along the arcs of the stent structure, see Figure 4.13. The maximum von Mises stress magnitude for $Mlink_{thin}$ was found to be 603.1 MPa and 675.1, and for $Mlink_{thick}$ was found to be 575.1 MPa and 658.7, for the proximal and distal halves respectively.

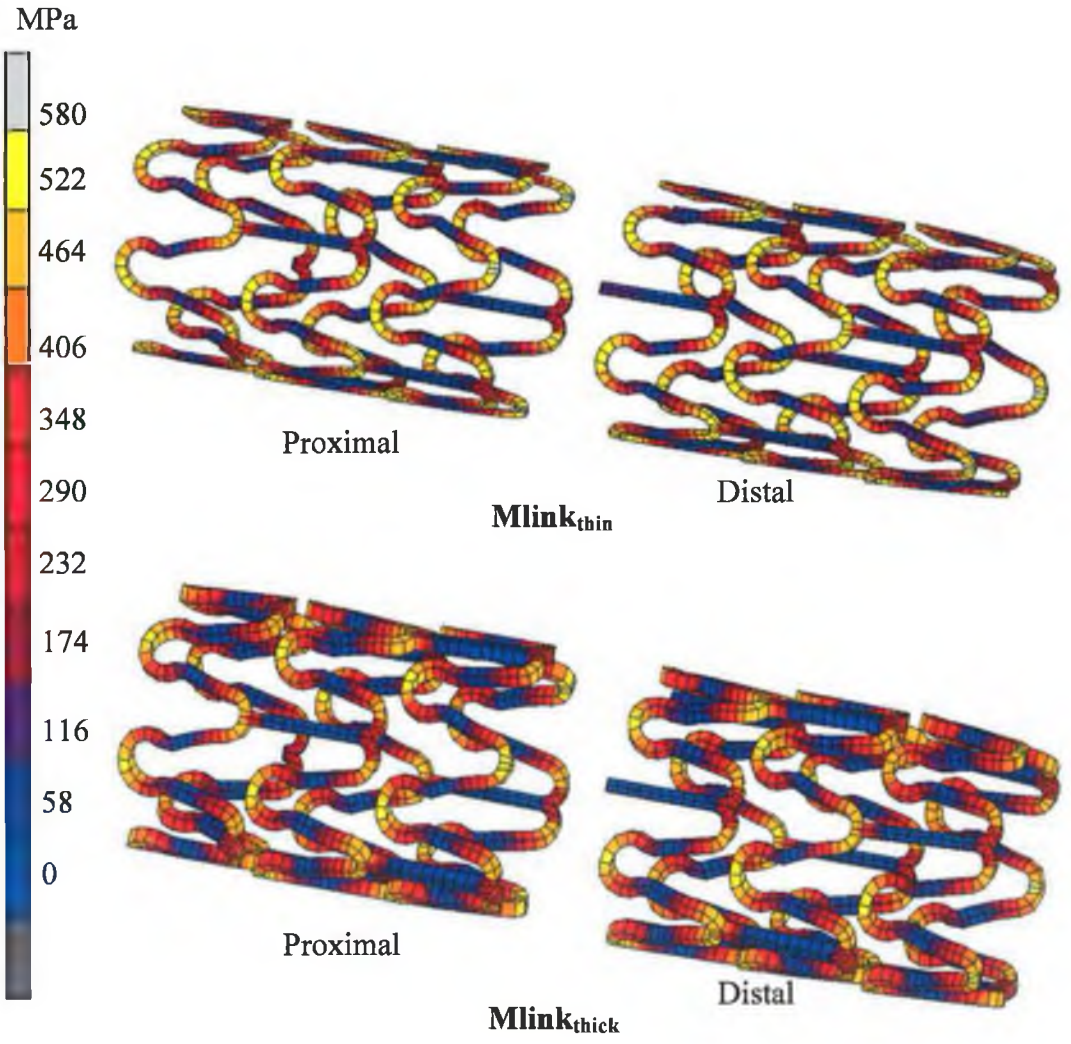

Figure 4.13 The resulting von Mises Stress contours throughout the structure of $Mlink_{thin}$ and $Mlink_{thick}$, under the influence of stenotic vessel of 0.8 mm thickness, achieving the same initial vessel lumen diameter of $Ø_I = 3$ mm.

Subsequently the resulting Total Equivalent Plastic strain throughout $Mlink_{thin}$ and $Mlink_{thick}$ structures showed the same pattern of distribution, see Figure 4.14, whereby high plastic strains are observed on the arcs of the stent structure. The maximum Total Equivalent Plastic strains were found to be 0.094 and 0.142 for the proximal and distal half of $Mlink_{thin}$, respectively, and 0.086 and 0.144 for the proximal and distal half of $Mlink_{thick}$, respectively.

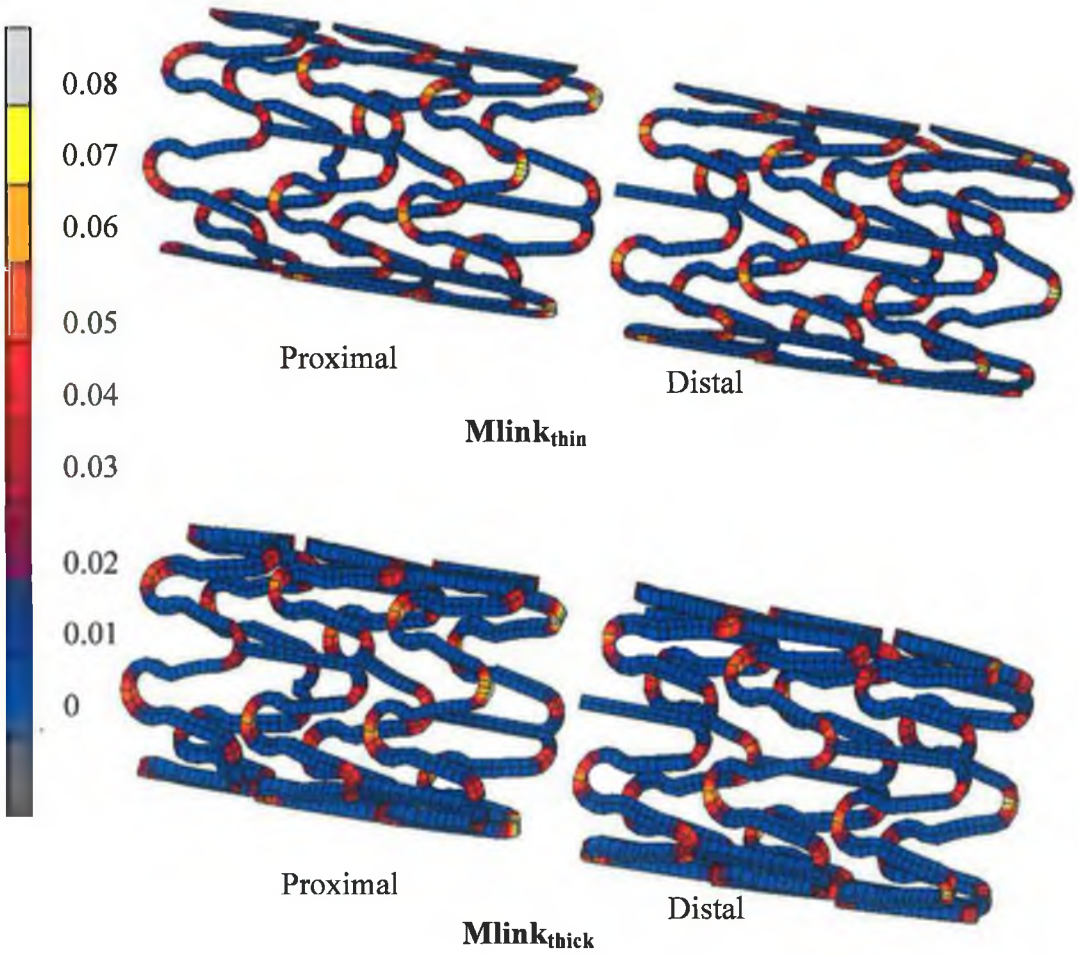

Figure 4.14 The resulting Total Equivalent Plastic Strain contours throughout the structure of $Mlink_{thin}$ and $Mlink_{thick}$, under the influence of stenotic vessel of 0.8 mm thickness, achieving the same initial vessel lumen diameter of $\emptyset_I = 3$ mm.

4.3.1 Stress Analysis of the Stented Vessels

It is of interest to note that both stresses induced in the artery on loading and unloading may contribute to restenosis. The stresses on loading will act as a stimulus for acute damage whilst the stresses on unloading will remain in the artery long-term and may be related to long-term damage.

I. Stresses after stent loading; Stimulus for acute damage

The $Mlink_{thin}$ and $Mlink_{thick}$ were expanded to achieve the same initial lumen diameter of $Ø_I$ = 3 mm. The stresses generated with the vessel wall on loading were examined to determine the degree of acute damage as it reached the initial lumen diameter of $Ø_I$ = 3 mm.

The stresses in the vessels were examined in the circumferential direction, radial direction and the longitudinal direction. It was observed that tensile stresses were induced within the stented vessel in the circumferential direction, see Figure 4.15, and compressive stresses in the radial direction, see Figure 4.16, while in the longitudinal direction, both tensile and compressive stresses were induced within the stented vessel, see Figure 4.17. It is clear that the vessel stented with $Mlink_{thick}$ has considerably more tissue stressed at high levels than the vessel stented with $Mlink_{thick}$.

For initial loading, the volume of tissue stressed to various levels was computed for specific stress values in the circumferential, radial and longitudinal directions within the stented stenotic vessels, see Figure 4.18 and Figure 4.19. The highest magnitude of stress induced within the stented stenotic vessels was found to be the tensile circumferential stress, where some tissue was stressed above 6 MPa. The lowest stresses observed were the longitudinal compressive stresses, where less than 5% volume of tissue was stressed at above 40 kPa. The volumes of tissue stressed by the compressive stresses in the radial and longitudinal direction were found to be similar in the vessels stented by the $Mlink_{thin}$ and $Mlink_{thick}$. Different volumes of tissue were subjected to elevated tensile stresses in the circumferential and longitudinal directions in the vessels stented with the two different stents, see Figure 4.18 and Figure 4.19

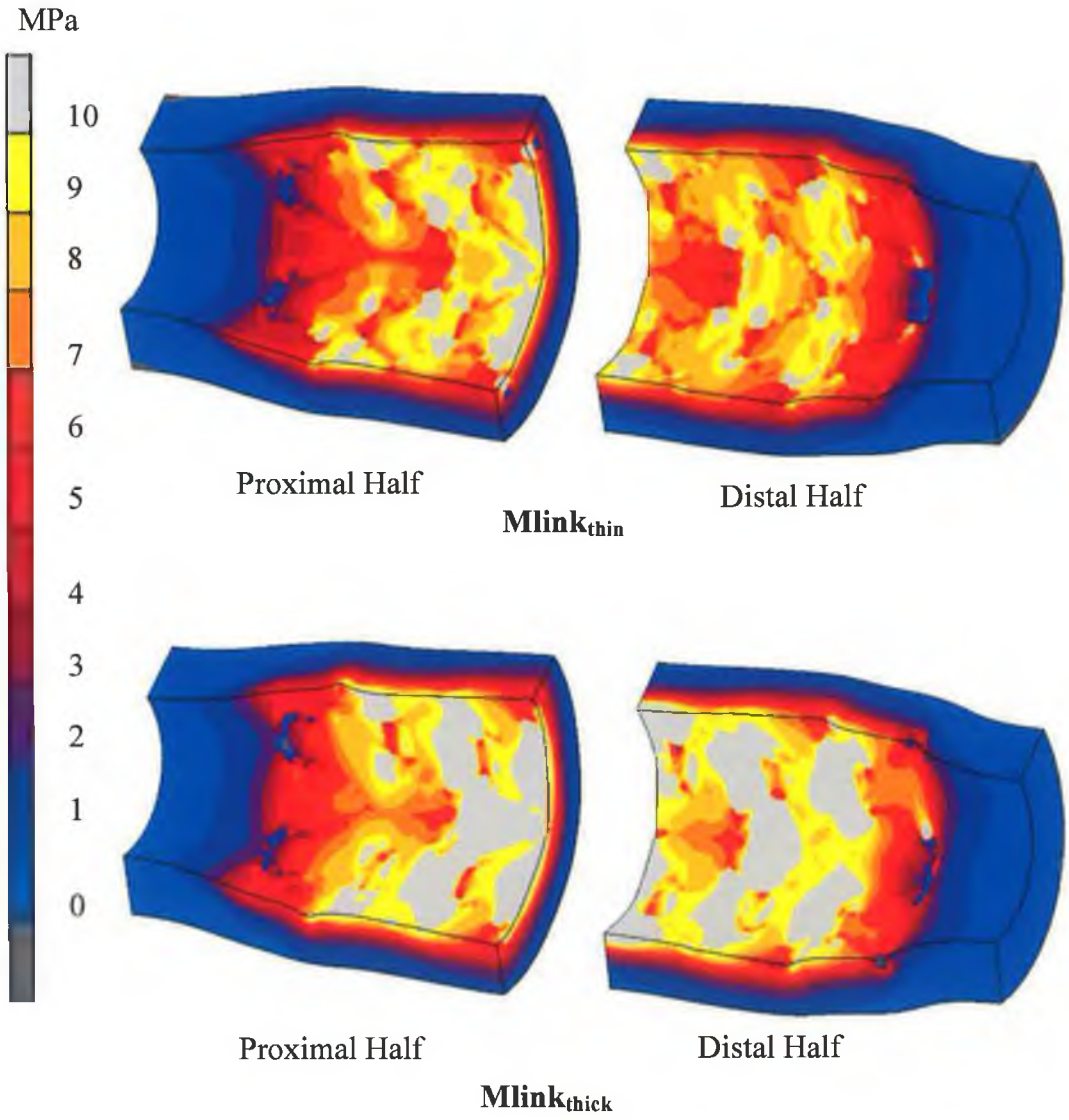

Figure 4.15 Tensile circumferential stresses induced in the arterial wall stented by $Mlink_{thin}$ and $Mlink_{thick}$, at loading, achieving the same initial vessel lumen diameter of $Ø_I$ = 3 mm.

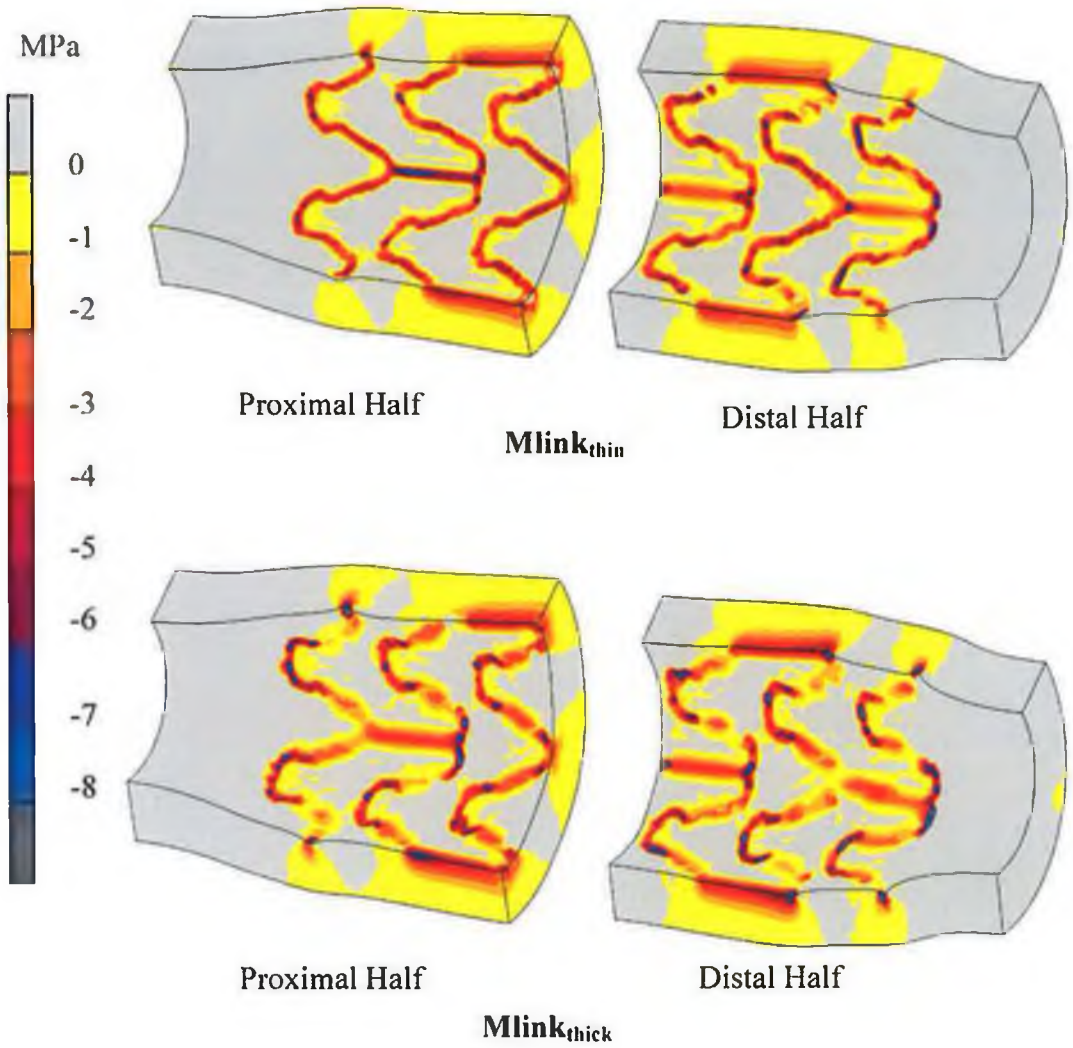

Figure 4.16 Compressive radial stresses induced in the arterial wall stented by $Mlink_{thin}$ and $Mlink_{thick}$, at loading, achieving the same initial vessel lumen diameter of $\emptyset_l = 3$ mm.

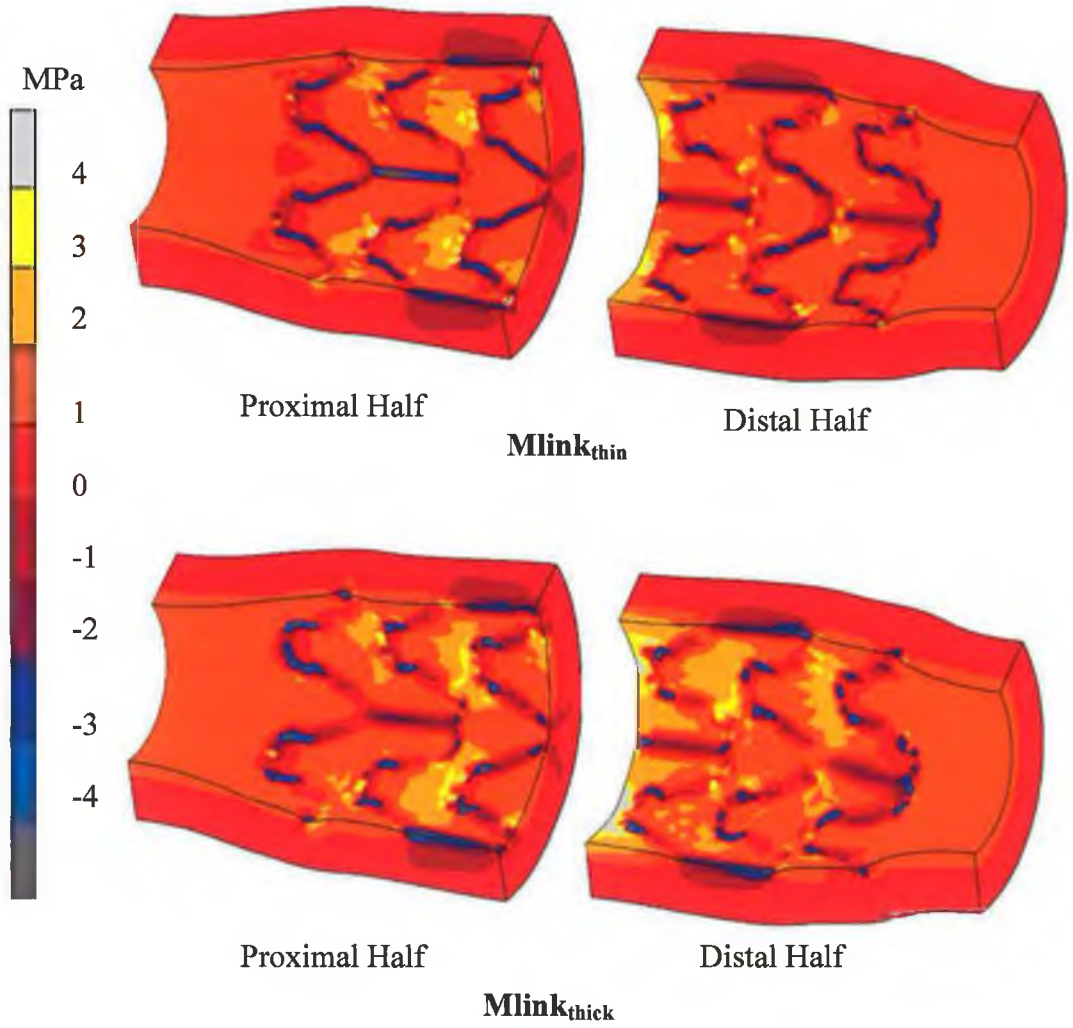

Figure 4.17 Tensile and compressive longitudinal stresses induced in the arterial wall stented by $Mlink_{thin}$ and $Mlink_{thick}$, at loading, achieving the same initial vessel lumen diameter of $\emptyset_I = 3$ **mm**.

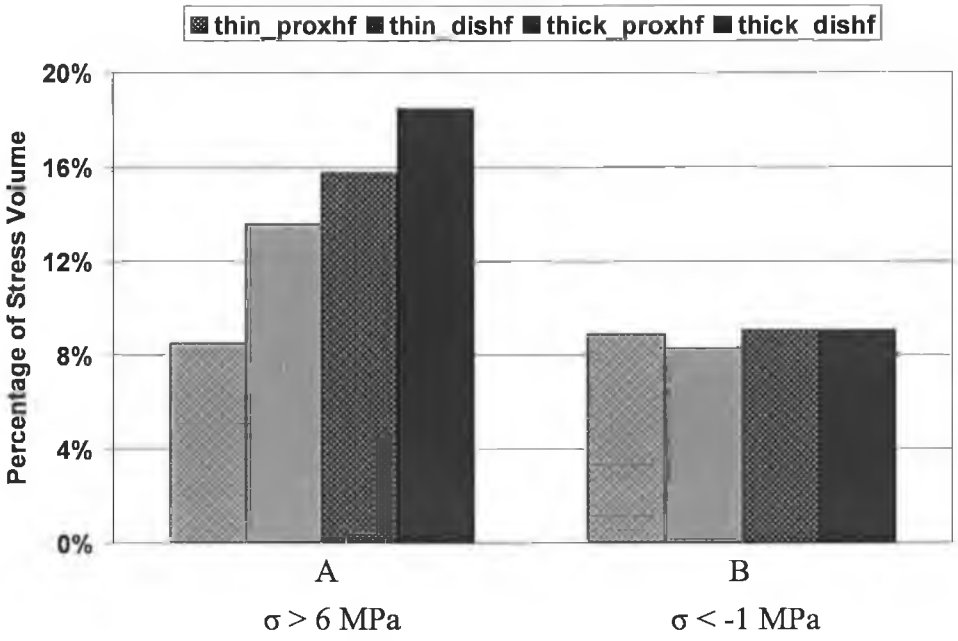

Figure 4.18 The percentage stress volumes by the tensile circumferential stress (A) and radial compressive stress (B), within the stented vessel by $Mlink_{thin}$ and $Mlink_{thick}$,, at loading, achieving the same initial vessel lumen diameter of $Ø_I = 3$ mm.

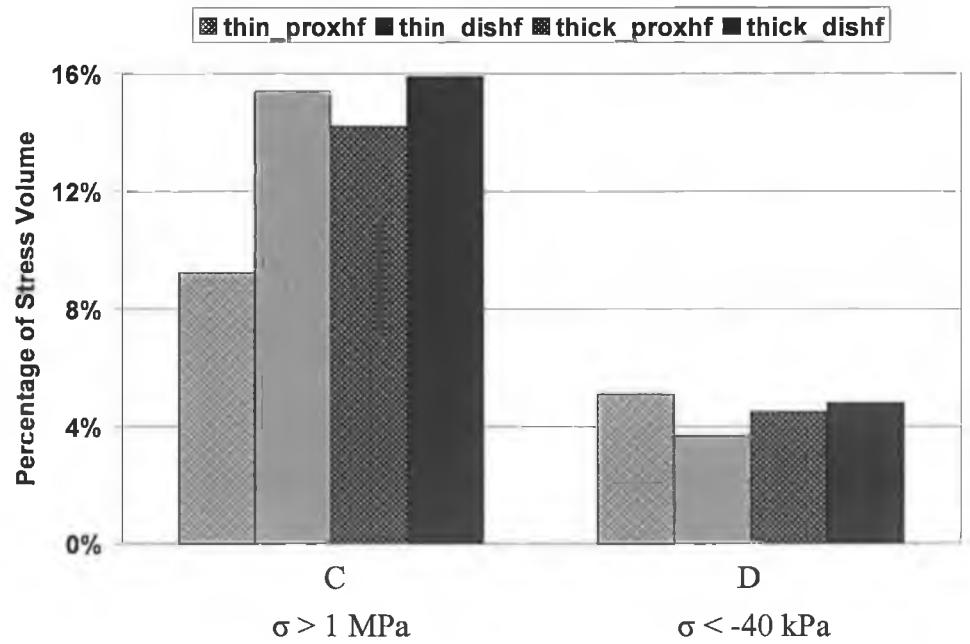

Figure 4.19 The percentage stress volumes by the tensile longitudinal stress (C) and longitudinal compressive stress (D), within the stented vessel by $Mlink_{thin}$ and $Mlink_{thick}$, at loading, achieving the same initial vessel lumen diameter of $Ø_I = 3$ mm.

II. Stresses after stent unloading; Stimulus for long-term damage

The pressure was removed from the stent once the 3 mm diameter lumen was achieved. The resulting final arterial lumen diameter, $\emptyset_F$, was found to be different for vessels stented with $Mlink_{thin}$ and $Mlink_{thick}$. The proximal half model stented with $Mlink_{thin}$ produced a final lumen diameter of $\emptyset_F$ = 2.38 mm and the distal half produced $\emptyset_F$ = 2.32 mm. The proximal half model stented with $Mlink_{thick}$ produced a final lumen diameter of $\emptyset_F$ = 2.58 mm and the distal half produced $\emptyset_F$ = 2.54 mm. These variations in the final lumen diameter were as a result of the difference in the radial recoil of both stent structures, where $Mlink_{thin}$ was found to have higher recoil than $Mlink_{thick}$.

The stresses in the vessels were examined in the circumferential direction, see Figure 4.20, radial direction, see Figure 4.21, and the longitudinal direction, see Figure 4.22, and similar stress patterns were observed in the stented vessels as those observed on loading . A decrease in stresses in all direction was found in the stented stenotic vessels.

As the pressure was completely removed, leaving the stents scaffolding open the arterial wall, the volume of tissue stressed to various levels was computed for specific stress values in the circumferential, radial and longitudinal directions within the stented stenotic vessels, see Figure 4.23 and Figure 4.24. The tensile circumferential stresses were found to be the highest magnitude of stress induced within the stented stenotic vessels, where some tissue was stressed above 0.5 MPa. Similar to loading, the longitudinal compressive stress was found to be the least magnitude of stress induced in the stented vessels with less than 5% stress volumes above 40 kPa. Significant differences in volumes of tissue stressed at high levels were observed in the vessels stented with the $Mlink_{thin}$ and $Mlink_{thick}$, see Figure 4.23 and Figure 4.24.

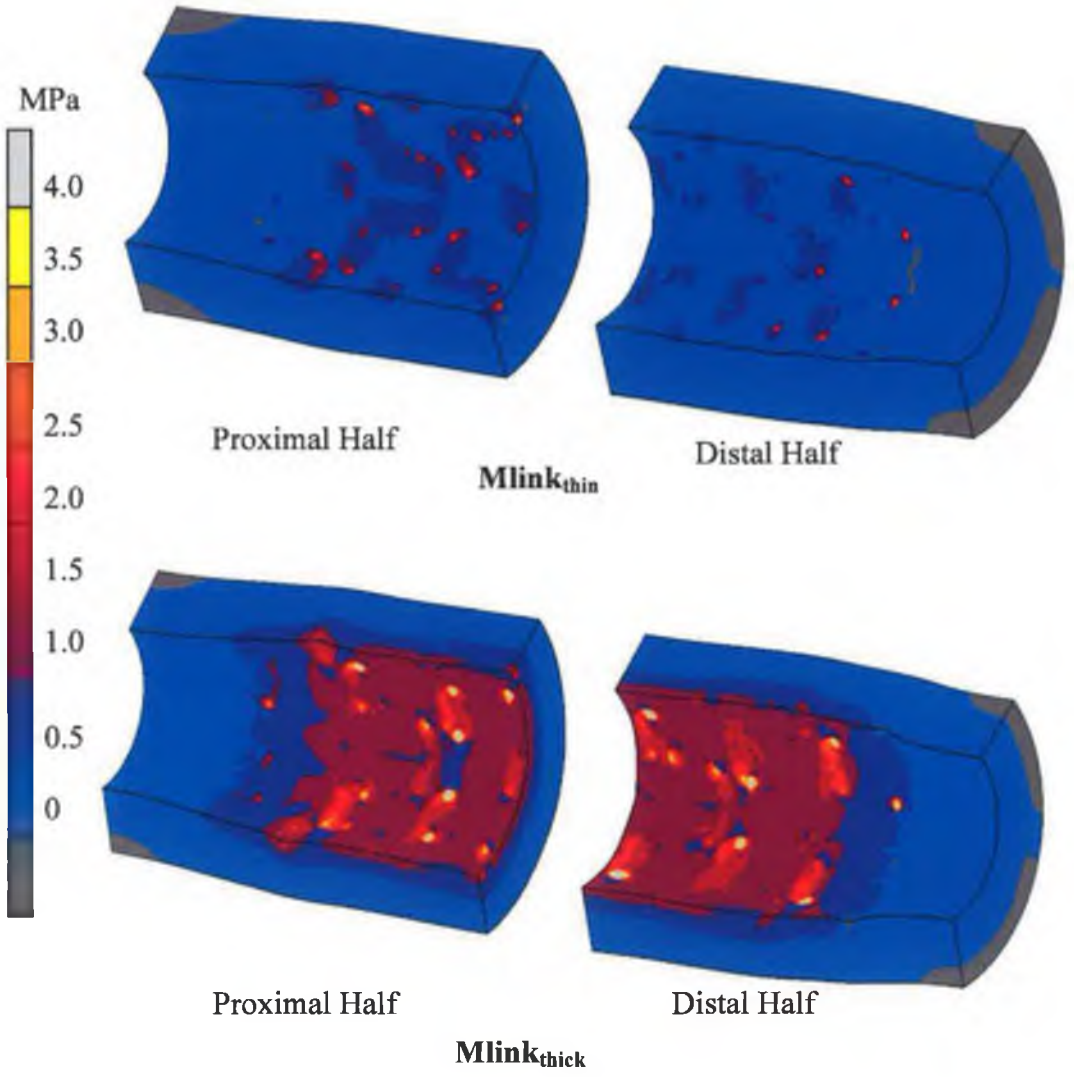

Figure 4.20 Tensile circumferential stresses induced in the arterial wall stented by Mlink$_{thin}$ and Mlink$_{thick}$, at unloading, resulting in different final lumen diameter.

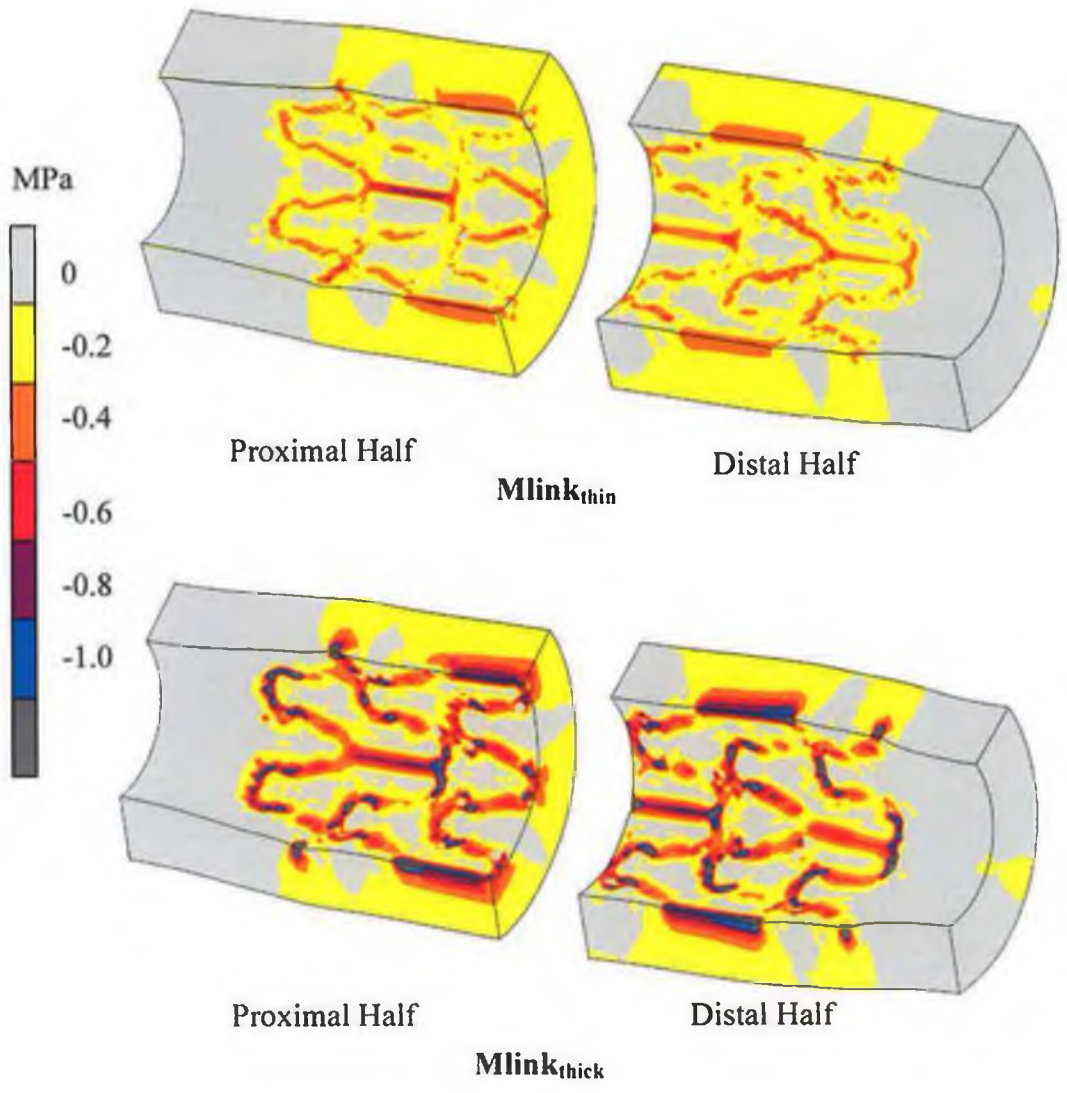

Figure 4.21 Compressive radial stresses induced in the arterial wall stented by $Mlink_{thin}$ and $Mlink_{thick}$, at unloading, resulting in different final lumen diameter.

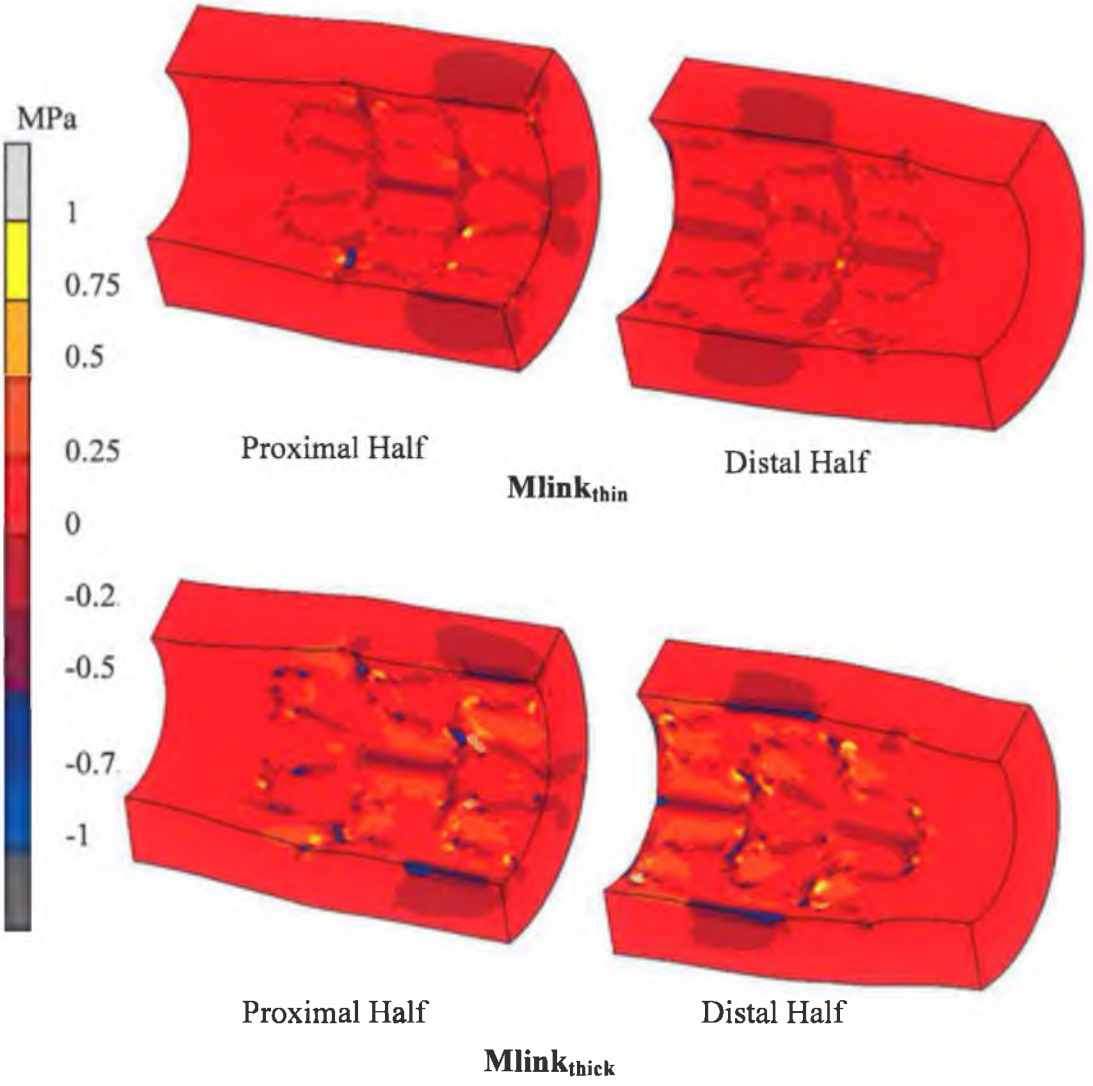

Figure 4.22 Tensile and compressive longitudinal stresses induced in the arterial wall stented by $Mlink_{thin}$ and $Mlink_{thick}$, at unloading, resulting in different final lumen diameter.

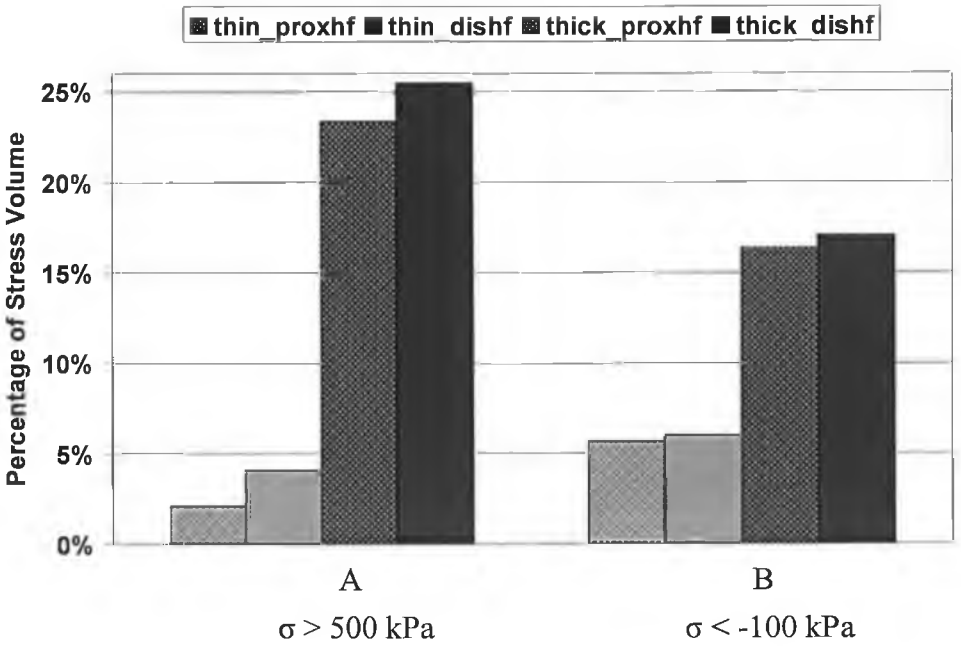

Figure 4.23 The percentage stress volumes by the tensile circumferential stress (A) and radial compressive stress (B), within the stented vessel by $Mlink_{thin}$ and $Mlink_{thick}$, at unloading, resulting in different final lumen diameter.

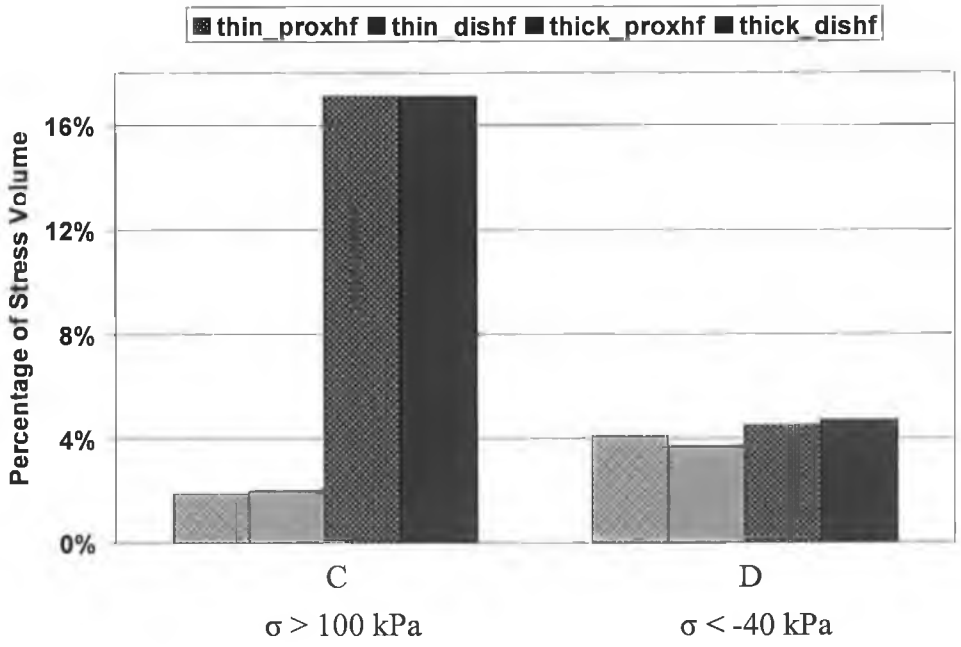

Figure 4.24 The percentage stress volumes by the tensile longitudinal stress (C) and longitudinal compressive stress (D), within the stented vessel by $Mlink_{thin}$ and $Mlink_{thick}$, at loading, resulting in different final lumen diameter.

4.4 Case Study 3:

Expansion of $Mlink_{thin}$ and $Mlink_{thick}$ inside a stenotic coronary artery achieving the same final expanded lumen diameter

Four simulations were carried out, expanding the proximal and distal halves of $Mlink_{thin}$ and $Mlink_{thick}$ inside a stenotic coronary artery, represented as an idealised cylindrical vessel. For this case study, $Mlink_{thin}$ and $Mlink_{thick}$ were expanded and allowed to recoil to achieve the same final expanded lumen diameter of $Ø_F$ = 2.28 mm, see Figure 4.25. The pressures required to expand $Mlink_{thin}$ and $Mlink_{thick}$ were 8.2 MPa and 2.2 MPa respectively. The same pressure was applied for both the proximal half and distal half of each structure.

The radial expansion throughout both models was found to be highly non-uniform. The lowest values of radial displacement were observed at the proximal and distal ends of the stent structures, see Figure 4.26.

Radial displacement were measured at key locations on both the proximal and distal half of each stent, see Figure 4.10, in order to compute the structural characteristics of the stents through the loading and unloading process of the stents' expansion, see Table 4.3.

A similar pattern of radial displacement distribution to case study 2 was observed, and the pattern was similar for both the $Mlink_{thin}$ and $Mlink_{thick}$. The least radial displacement was found in the proximal end, followed by the distal end and then the central region of the distal half. The highest radial displacement was found in the central region of the proximal half of the stent structure, see Figure 4.27. For this case study, $Mlink_{thin}$ was found to have greater radial displacement at loading, where $Ø_{I\ thin}$ = 3 mm and $Ø_{I\ thick}$ = 2.48 mm, to achieve similar final vessel lumen diameter, $Ø_F$ = 2.28 mm.

Upon loading, foreshortening was observed to be low in magnitude, however, in contrast to case study 2, $Mlink_{thin}$ foreshortens to a larger degree than the $Mlink_{thick}$, see Table 4.3. Again, the 'negative dogboning' was found more

prominent in the proximal region of the stent structures, however, the $Mlink_{thick}$ showed this to a lesser extent.

Upon unloading, elongation occurred in both stents structures, which gave rise to the negative values for longitudinal recoil. A greater degree of longitudinal recoil was observed in the $Mlink_{thin}$ than the $Mlink_{thick}$ and the magnitude of the longitudinal recoil in $Mlink_{thick}$ was found to be very low in this case, see Table 4.3.

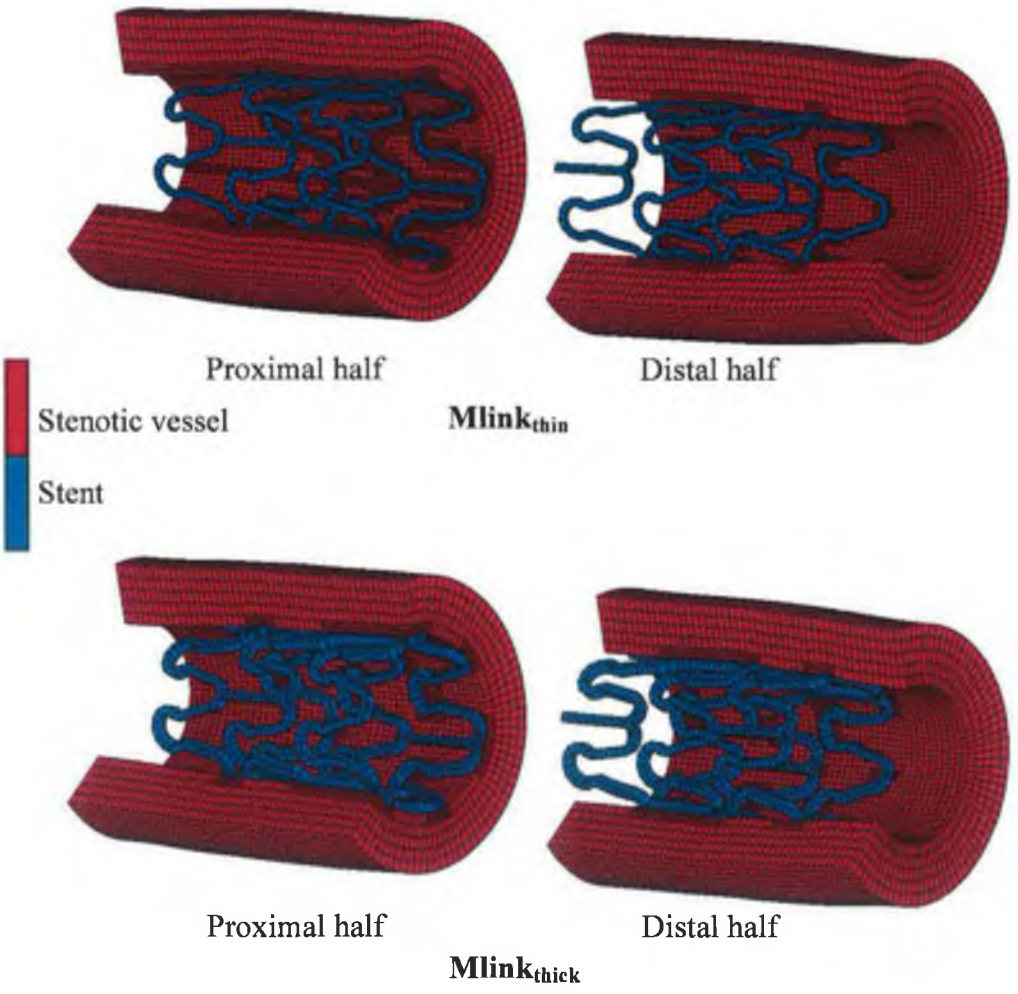

Figure 4.25 Deformed geometry of proximal and distal half of $Mlink_{thin}$ and $Mlink_{thick}$, scaffolding a stenotic vessel, thickness of 0.8 mm, achieving the same final vessel lumen diameter of $Ø_F$ = 2.28 mm.

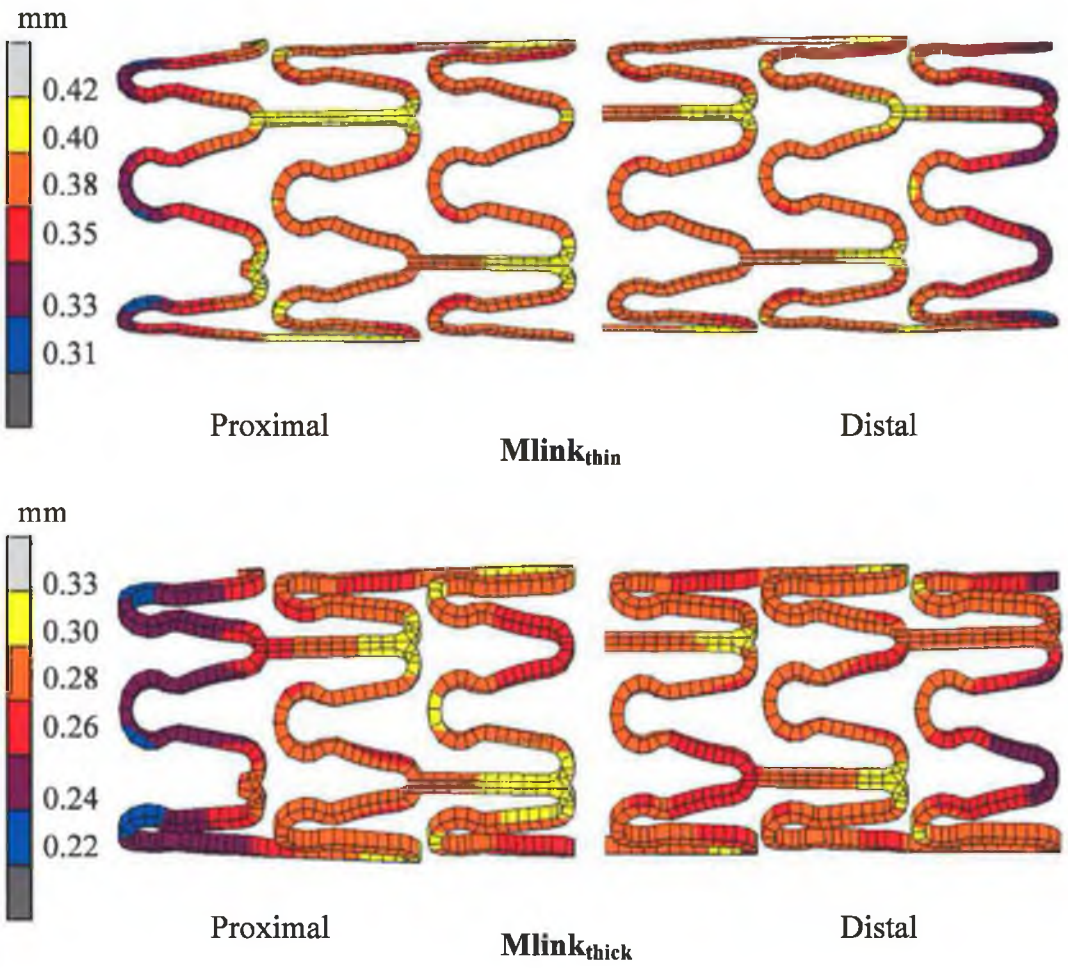

Figure 4.26 Radial displacement distribution throughout the stents' structure of $Mlink_{thin}$ and $Mlink_{thick}$, under the influence of a stenotic vessel, achieving the same final vessel lumen diameter.

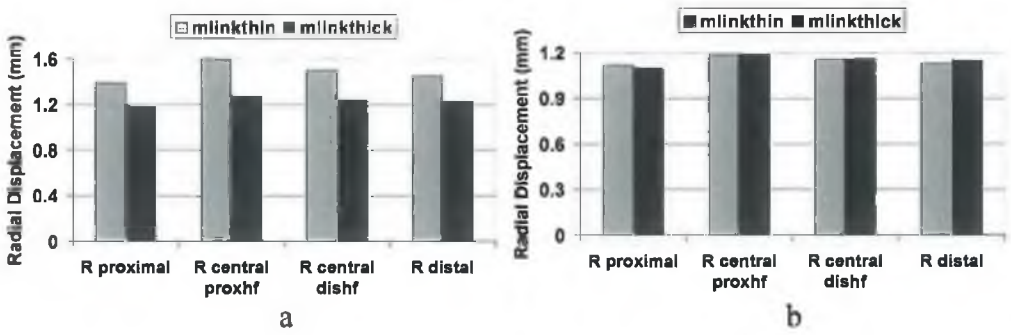

Figure 4.27 Radial displacement of $Mlink_{thin}$ and $Mlink_{thick}$ through (a) loading and (b) unloading, under the influence of a stenotic vessel, achieving the same final vessel lumen diameter.

	$\mathbf{Mlink_{thin}}$	$\mathbf{Mlink_{thick}}$
▪ *Stent before expansion*	(mm)	(mm)
R_{orig}	0.77	0.86
L_{orig}	3.6	3.6
▪ *Stent after loading*		
$R_{load\ proximal}$	1.39	1.18
$R_{load\ central\ proxhf}$	1.6	1.27
$R_{load\ central\ dishf}$	1.5	1.24
$R_{load\ distal}$	1.45	1.23
$L_{load\ proxhf}$	3.39	3.54
$L_{load\ dishf}$	3.41	3.53
▪ *Stent after unloading*		
$R_{unload\ proximal}$	1.12	1.1
$R_{unload\ central\ proxhf}$	1.19	1.19
$R_{unload\ central\ dishf}$	1.16	1.16
$R_{unload\ distal}$	1.13	1.15
$L_{unload\ proxhf}$	3.5	3.55
$L_{unload\ dishf}$	3.51	3.55
▪ *Calculated parameters*	(%)	(%)
Longitudinal $_{proxhf}$ recoil	-3.2	-0.3
Longitudinal $_{dishf}$ recoil	-2.9	-0.6
Foreshortening $_{proxhf}$	5.8	1.7
Foreshortening $_{dishf}$	5.3	1.9
Dogboning $_{proxhf}$	-15.1	-7.6
Dogboning $_{dishf}$	-3.4	-0.8

Table 4.3 Geometric data of $Mlink_{thin}$ and $Mlink_{thick}$ through loading and unloading, under the influence of stenotic vessel of 0.8mm thickness, achieving the same final vessel lumen diameter.

Radial recoil throughout the $Mlink_{thick}$ structure was found to be less than the $Mlink_{thin}$, see Figure 4.28. In fact, the radial recoil of $Mlink_{thin}$ was found to be three times greater than the $Mlink_{thick}$. $Mlink_{thin}$ shows the highest radial recoil at the region where it experienced the highest radial displacement.

The resulting Von Mises stress contours show similar stress distribution patterns as observed in previous case studies, whereby the highest stresses are along the arcs of the stent structure, see Figure 4.29. The maximum Von Mises stress magnitude for $Mlink_{thin}$ was found to be 603.1 MPa and 675.1, and for $Mlink_{thick}$ was found to be 493.2 MPa and 559.5 for proximal and distal halves respectively.

The resulting Total Equivalent Plastic strain throughout $Mlink_{thin}$ and $Mlink_{thick}$, structures showed the same pattern of distribution, see Figure 4.30, whereby high plastic strains are observed on the arcs of the stent structure. The maximum Total Equivalent Plastic strain was found to be 0.094 and 0.142 for the proximal and distal half of $Mlink_{thin}$ respectively, and 0.037 and 0.072 for the proximal and distal half of $Mlink_{thick}$ respectively.

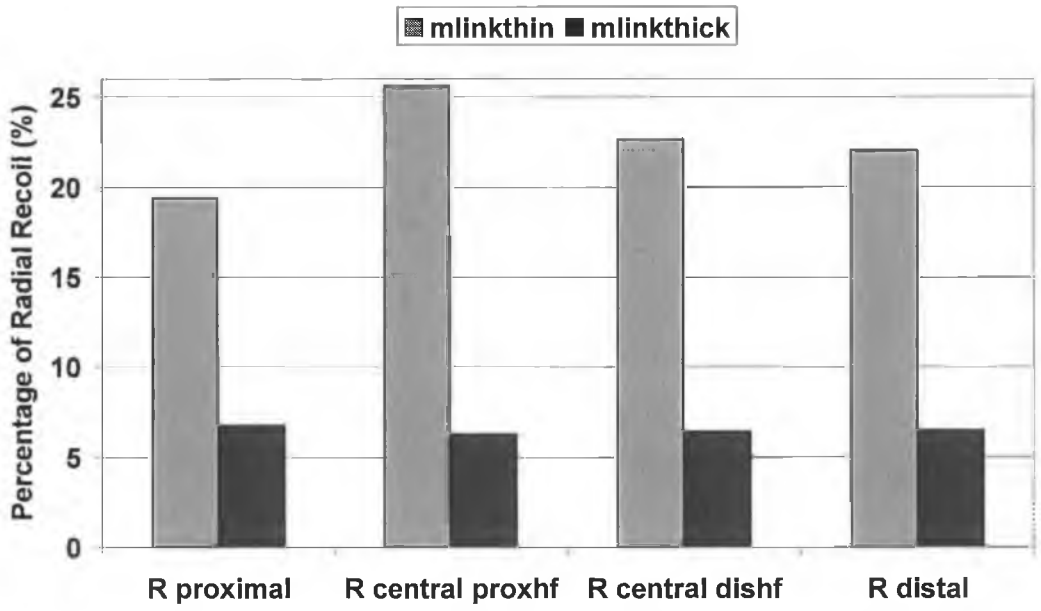

Figure 4.28 Comparison of percentage radial recoil of $Mlink_{thin}$ and $Mlink_{thick}$, subjected to free expansion, achieving the same final vessel lumen diameter.

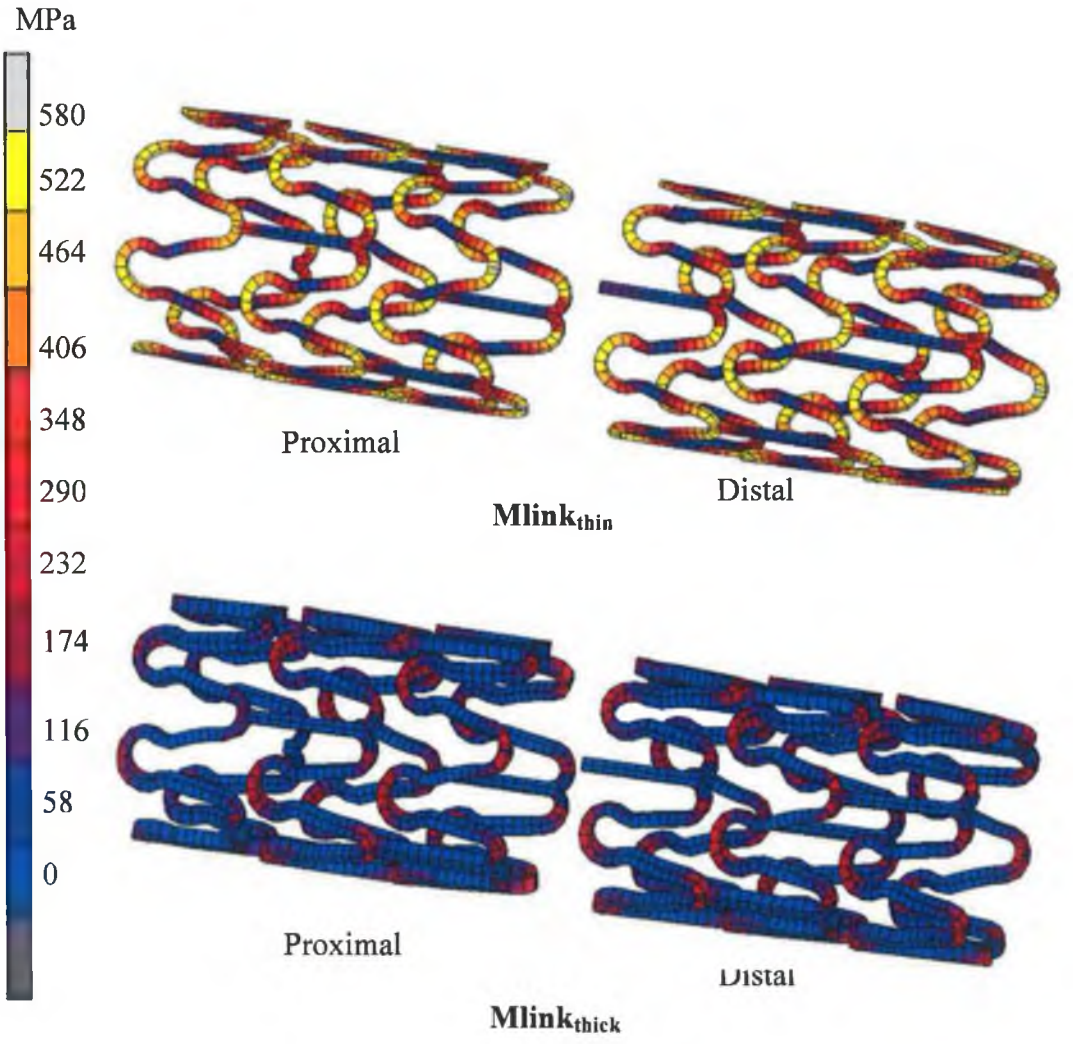

Figure 4.29 The resulting von Mises Stress contours throughout the structure of $Mlink_{thin}$ and $Mlink_{thick}$, under the influence of stenotic vessel of 0.8 mm thickness, achieving the same final vessel lumen diameter.

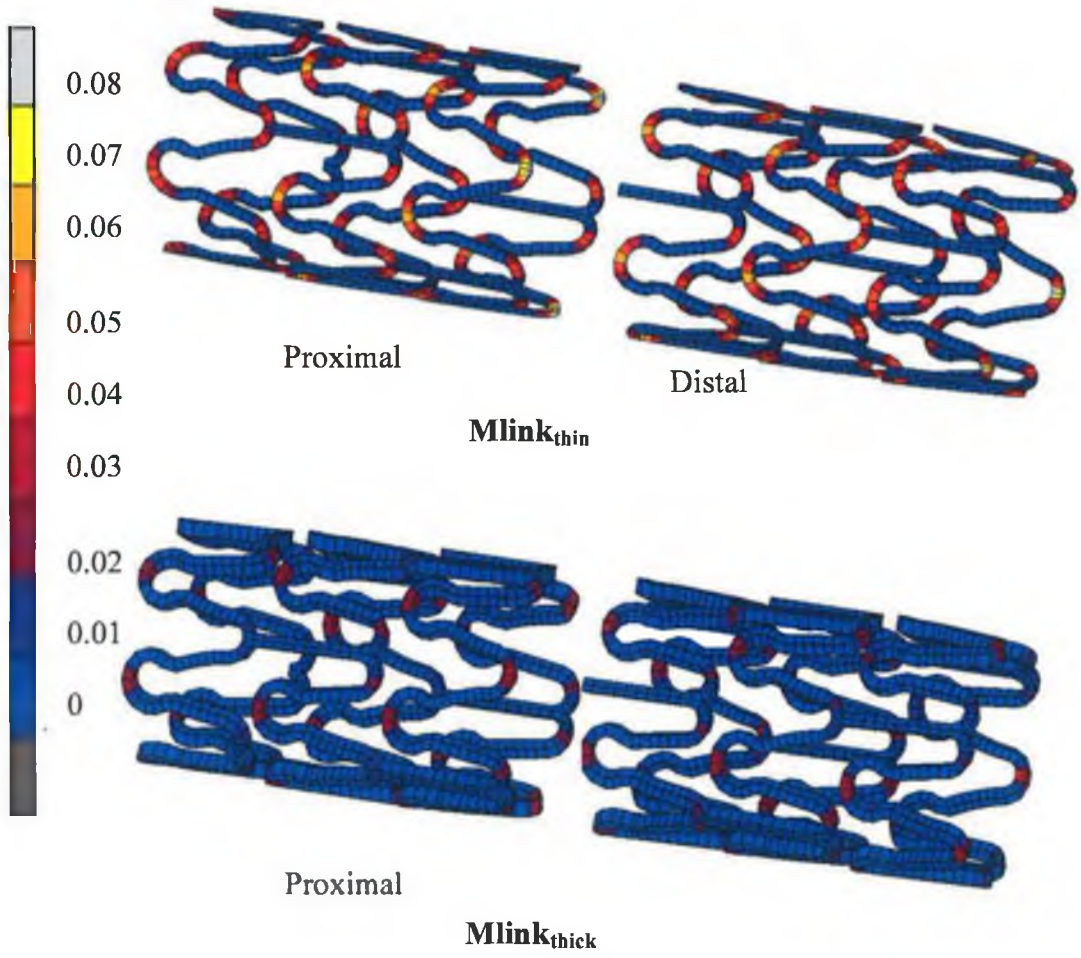

Figure 4.30 The resulting Total Equivalent Plastic Strain contours throughout the structure of Mlink$_{thin}$ and Mlink$_{thick}$, under the influence of stenotic vessel of 0.8 mm thickness, achieving the same final vessel lumen diameter.

4.4.1 Stress Analysis of the Stented Vessels

I. Stresses after stent loading: Stimulus for acute damage

The $Mlink_{thin}$ and $Mlink_{thick}$ were expanded and recoil to achieve a final lumen diameter of $Ø_F$ = 2.28 mm. The initial lumen diameter achieved by $Mlink_{thin}$ and $Mlink_{thick}$ were $Ø_{I\ thin}$ = 3 mm and $Ø_{I\ thick}$ = 2.48 mm. The stresses generated with the vessel wall on loading were examined to determine the degree of acute damage as it reached the initial lumen diameter.

Comparing the stresses induced in both vessels, it is evident that the vessel stented with $Mlink_{thin}$ has significant more tissue stressed at high levels than the vessel stented with $Mlink_{thick}$, see Figure 4.31-4.33.

The volume of tissue stressed to various levels was computed for specific stress values in the circumferential, radial and longitudinal directions within the stented stenotic vessels, see Figure 4.34 and Figure 4.35. Similar to case study 2, the tensile circumferential stress showed significantly higher magnitudes at 800 kPa, induced in the stented vessels compared with the other stresses. In contrast to the previous case study, $Mlink_{thin}$ was found to cause the greater volumes of tissue stressed at high levels when compared with $Mlink_{thick}$ in all directions. Similar to the previous case study, the lowest magnitude of stress was found to be the compressive longitudinal stress, where less than 5.1% volume of tissue was stressed above 40 kPa.

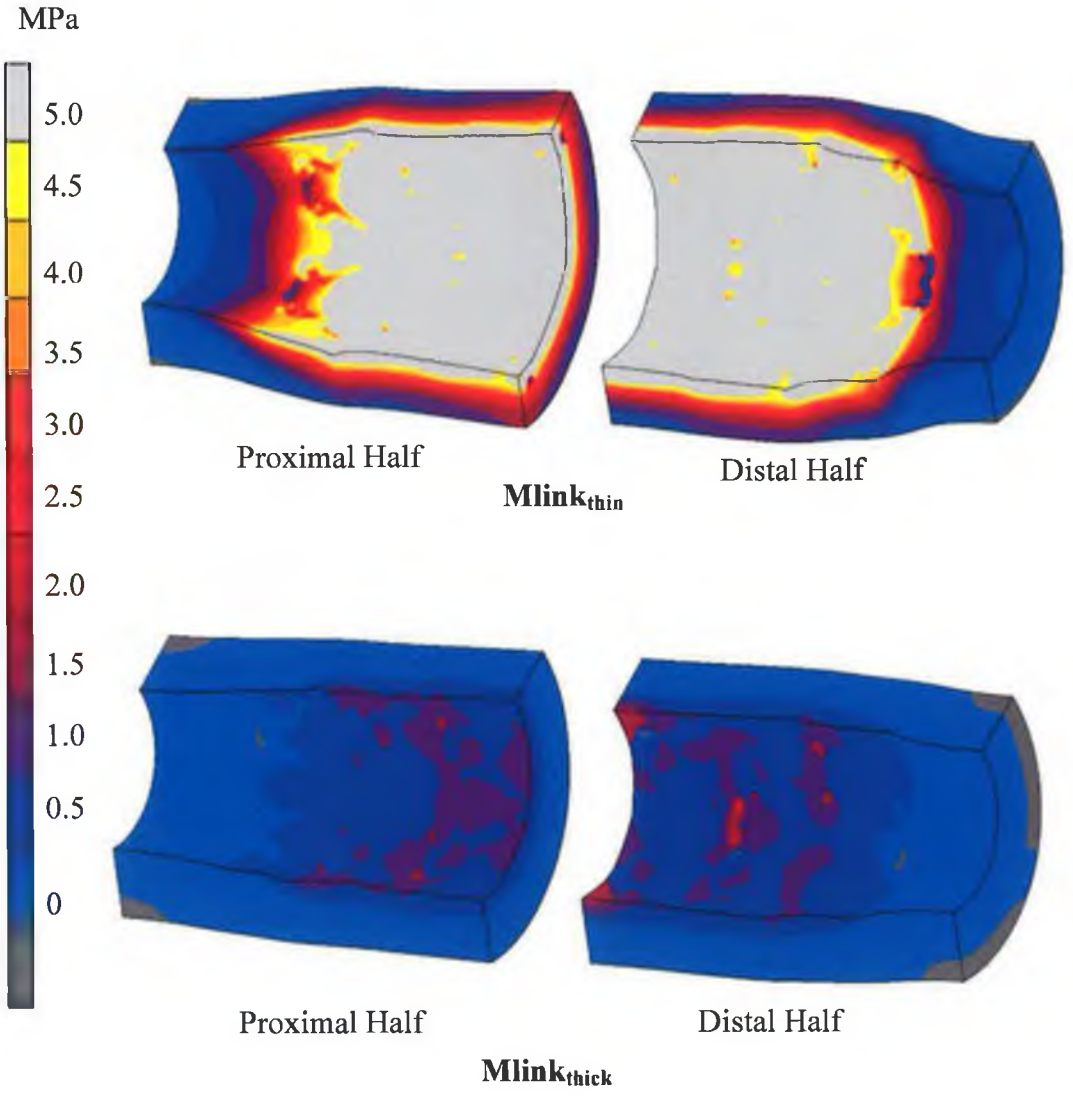

Figure 4.31 Tensile circumferential stresses induced in the arterial wall stented by $Mlink_{thin}$ and $Mlink_{thick}$, at loading, achieving different initial vessel lumen diameter.

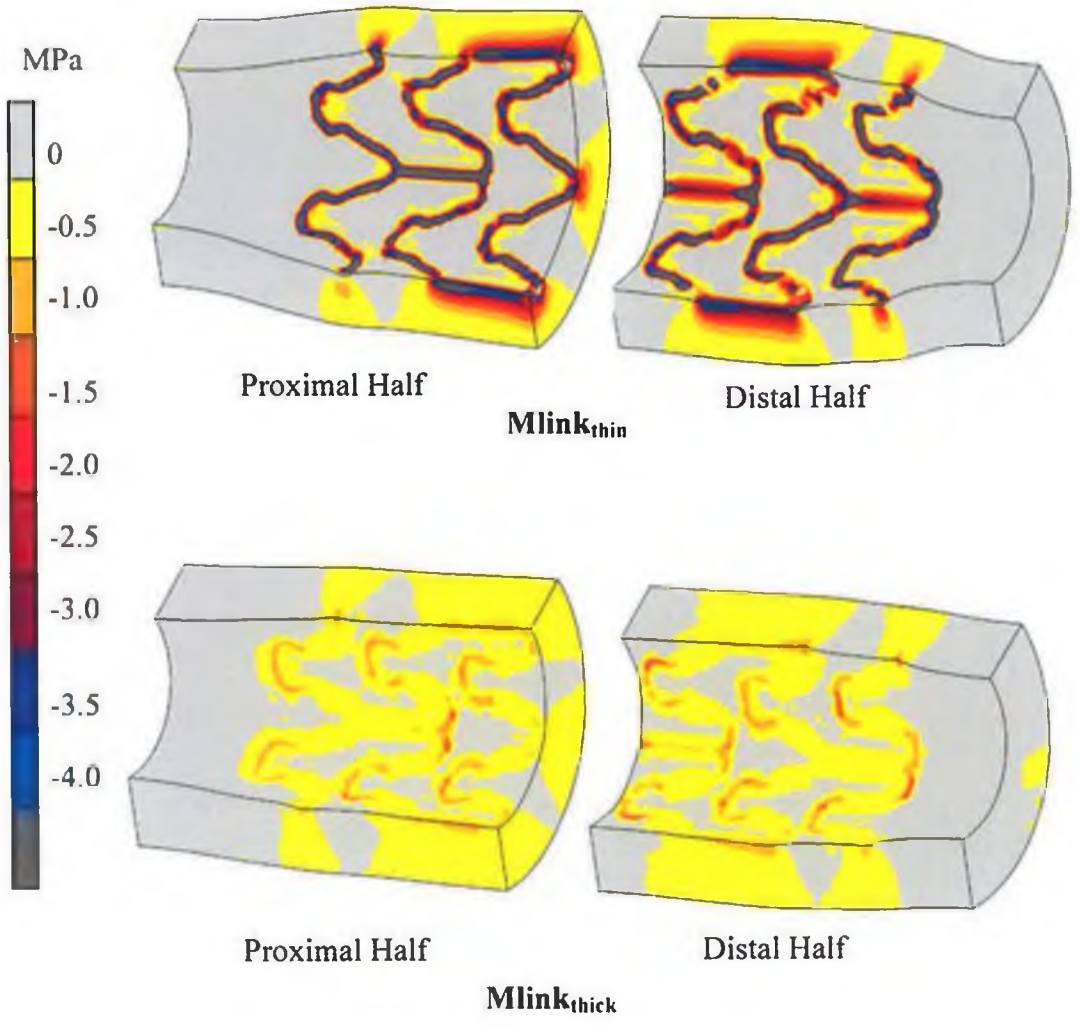

Figure 4.32 Compressive radial stresses induced in the arterial wall stented by $Mlink_{thin}$ and $Mlink_{thick}$, at loading, achieving different initial vessel lumen diameter.

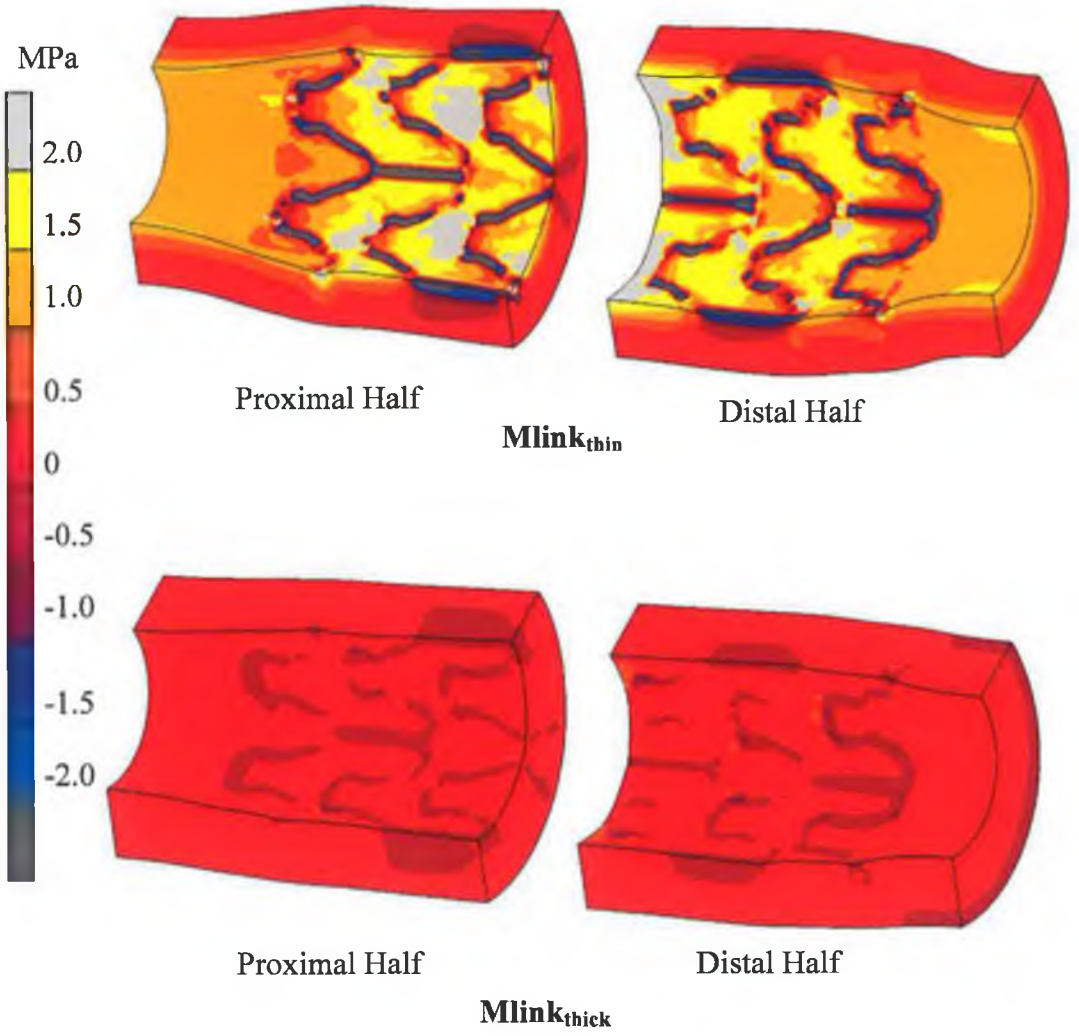

Figure 4.33 Tensile and compressive longitudinal stresses induced in the arterial wall stented by $Mlink_{thin}$ and $Mlink_{thick}$, at loading, achieving different initial vessel lumen diameter.

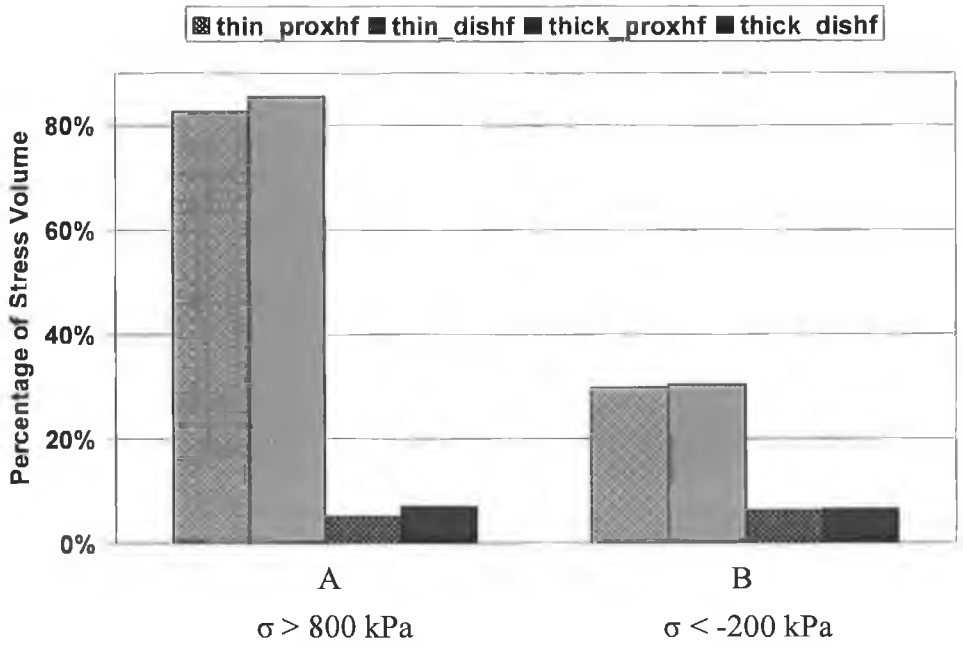

Figure 4.34 The percentage stress volumes by the tensile circumferential stress (A) and radial compressive stress (B), within the stented vessel by $Mlink_{thin}$ and $Mlink_{thick}$, at loading, achieving different initial vessel lumen diameter.

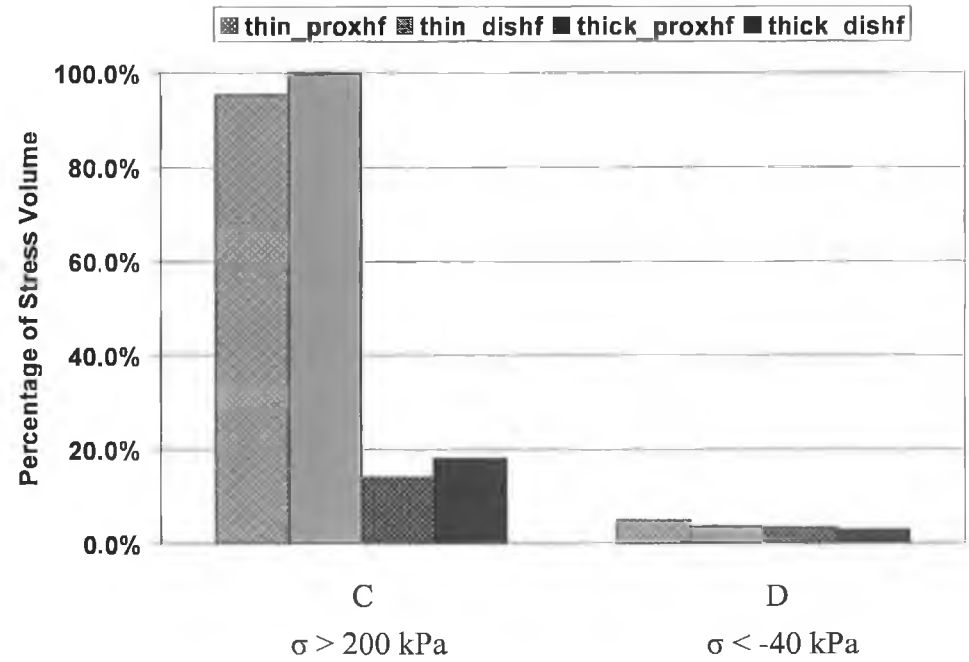

Figure 4.35 The percentage stress volumes by the tensile longitudinal stress (C) and longitudinal compressive stress (D), within the stented vessel by $Mlink_{thin}$ and $Mlink_{thick}$, at loading, achieving different initial vessel lumen diameter.

II. Stresses after stent unloading; Stimulus for long-term damage

The pressure was removed from the stents and the stents were allowed to recoil to a final lumen diameter of $Ø_F = 2.28$ mm. The stresses generated within the vessel wall on unloading were examined to determine the degree of long-term damage.

The stresses in the vessels were examined in the circumferential direction, see Figure 4.36, radial direction, see Figure 4.37, and the longitudinal direction, see Figure 4.38. A decrease in stresses in all direction was found in the stented stenotic vessels at unloading. The pattern of stresses induced in the stented vessels remained the same as loading, however, the difference in stresses in the two stented vessels on loading, was observed to reduce, as both stented vessels by $Mlink_{thin}$ and $Mlink_{thick}$ achieved the same final lumen diameter.

The volume of tissue stressed to various levels was computed for specific stress values in the circumferential, radial and longitudinal directions within the stented stenotic vessels, see Figure 4.39 and Figure 4.40. The tensile circumferential stress remained the highest magnitude of stress induced within the stented stenotic vessels, where some tissue was stressed above 0.5 MPa. Similar to loading, the longitudinal compressive stress was found to be the least magnitude of stress induced in the stented vessels with less than 4.1% stress volume at above 40 kPa.

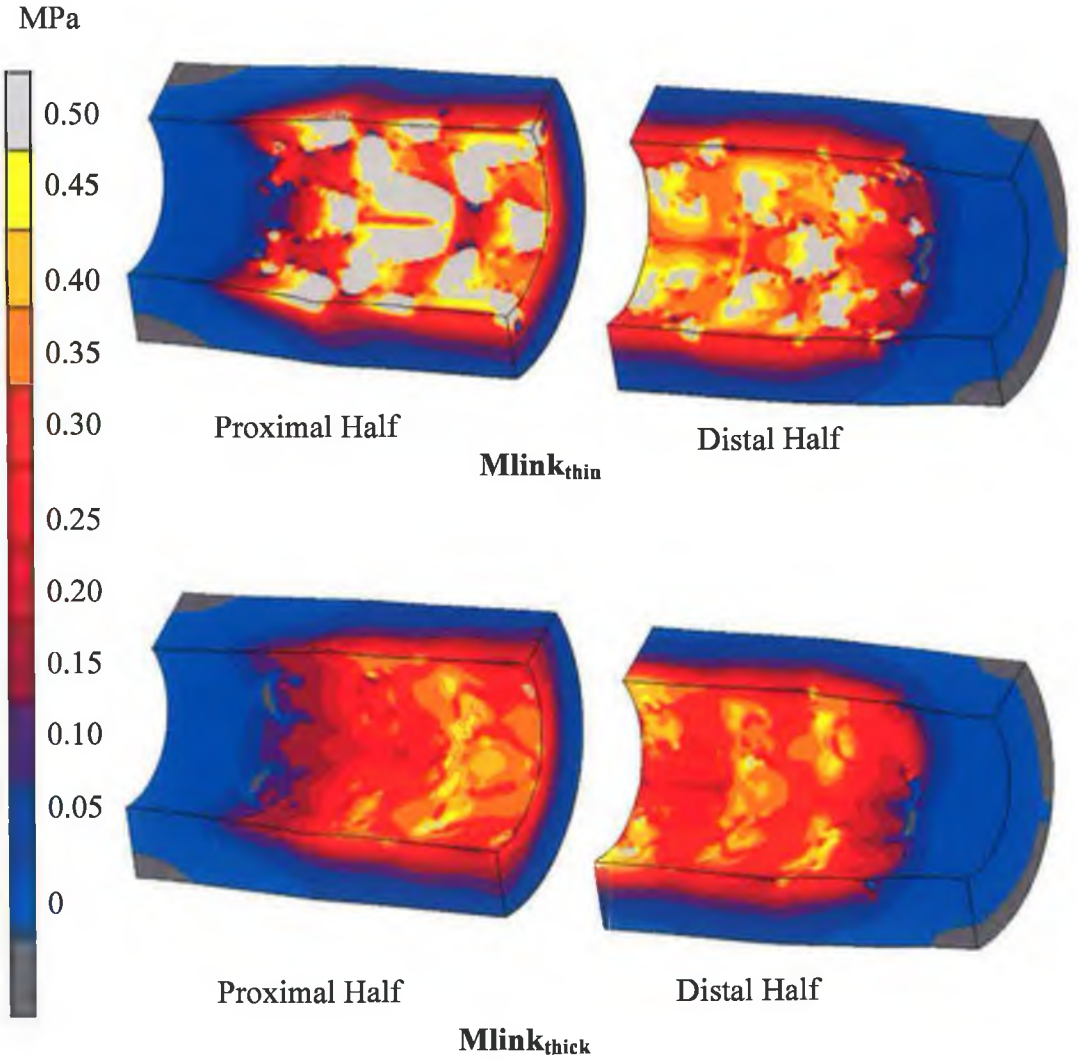

Figure 4.36 Tensile circumferential stresses induced in the arterial wall stented by $Mlink_{thin}$ and $Mlink_{thick}$, at unloading, achieving the same final vessel lumen diameter.

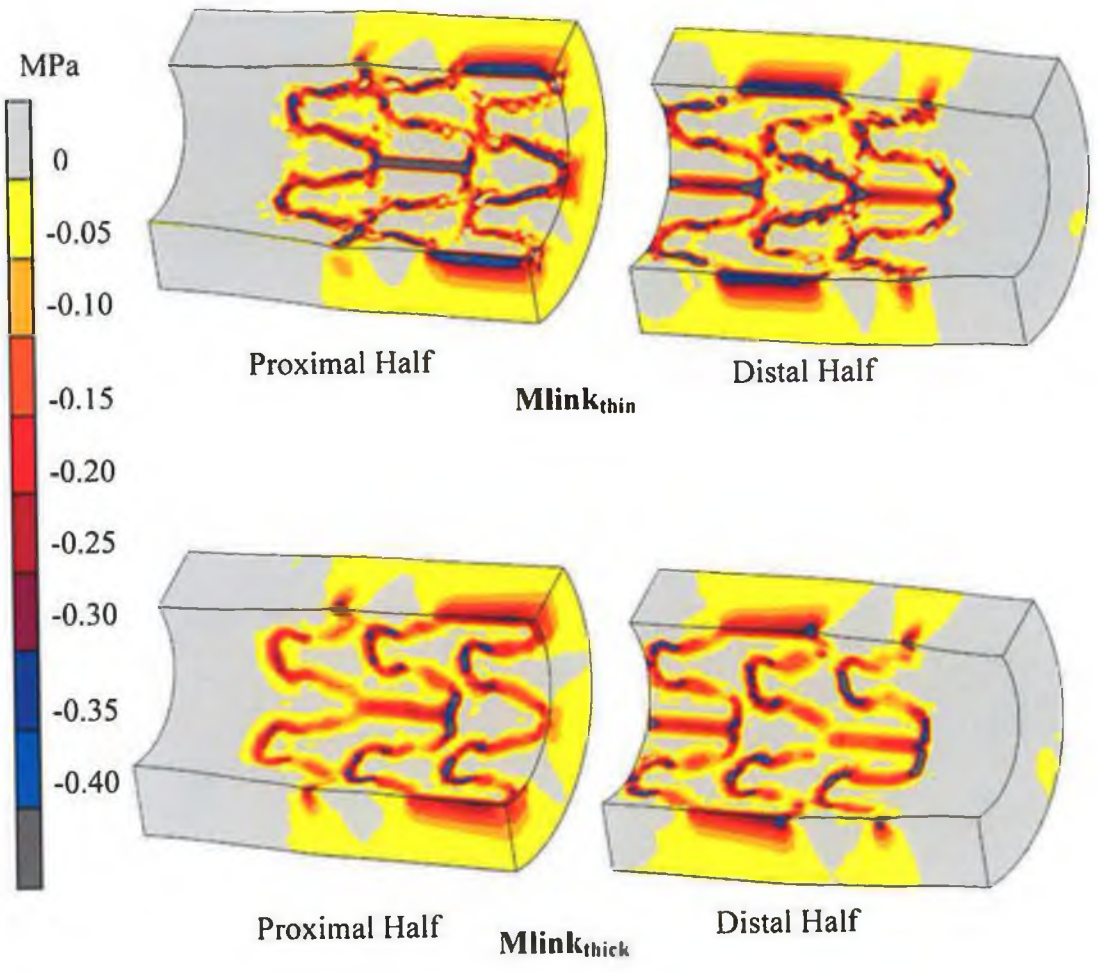

Figure 4.37 Compressive radial stresses induced in the arterial wall stented by $Mlink_{thin}$ and $Mlink_{thick}$, at unloading, achieving the same final vessel lumen diameter.

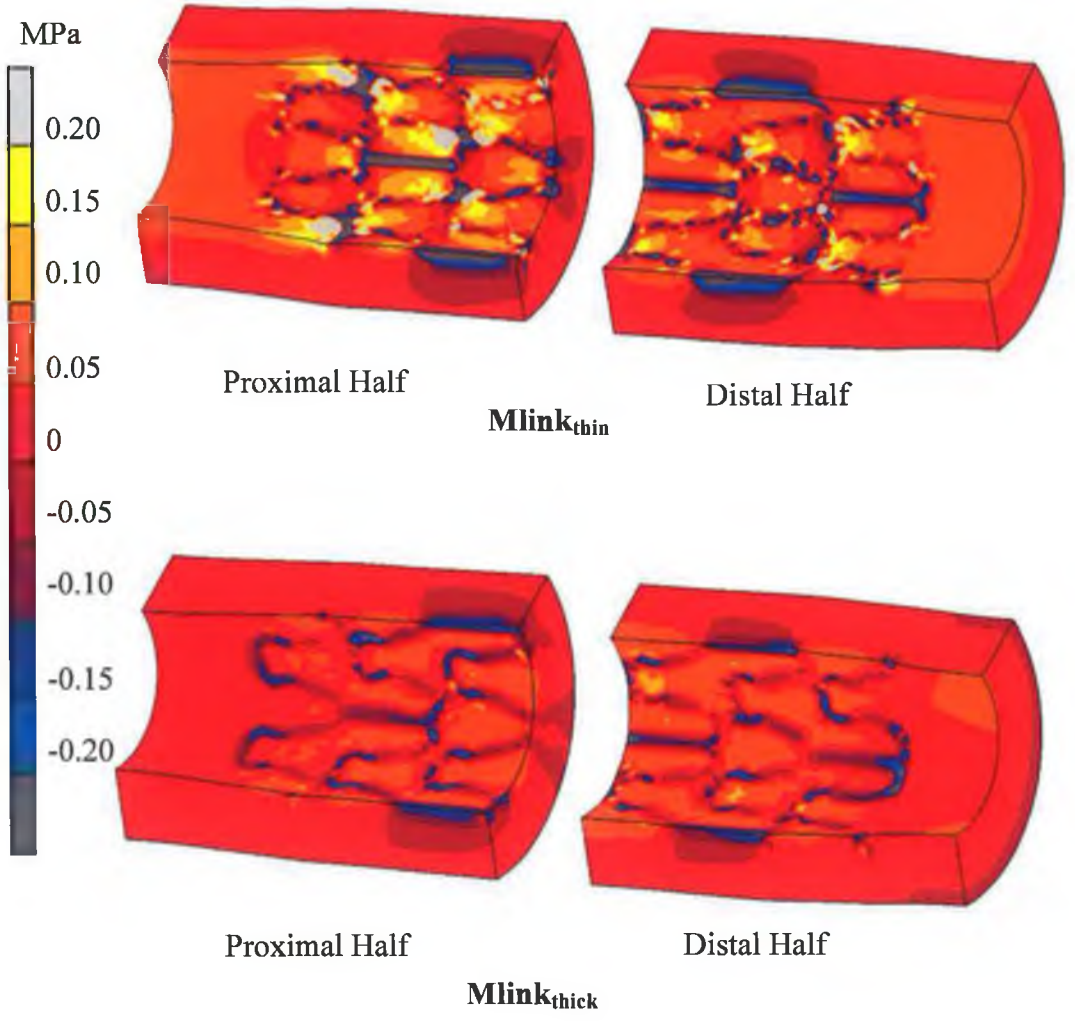

Figure 4.38 Tensile and compressive longitudinal stresses induced in the arterial wall stented by Mlink$_{thin}$ and Mlink$_{thick}$, at unloading, achieving the same final vessel lumen diameter.

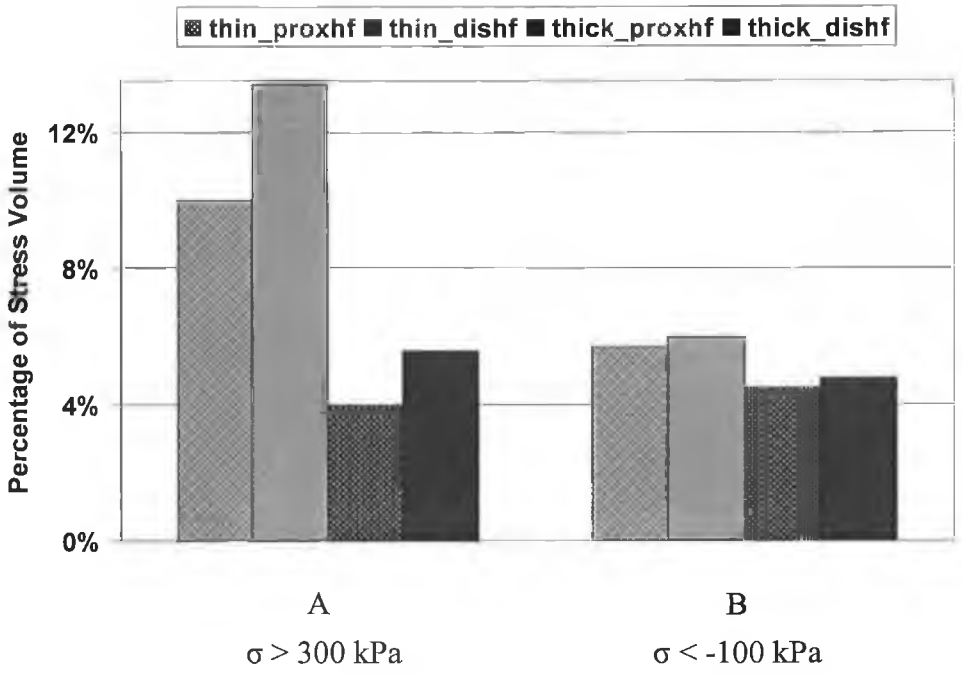

Figure 4.39 The percentage stress volumes by the tensile circumferential stress (A) and radial compressive stress (B), within the stented vessel by $Mlink_{thin}$ and $Mlink_{thick}$, at unloading, achieving the same final vessel lumen diameter.

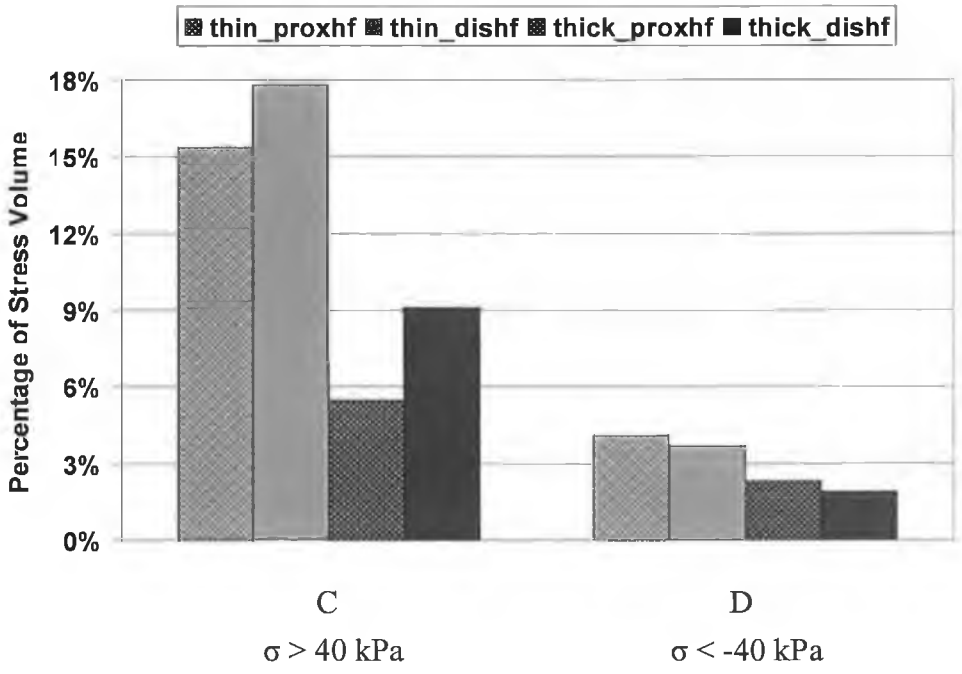

Figure 4.40 The percentage stress volumes by the tensile longitudinal stress (C) and longitudinal compressive stress (D), within the stented vessel by $Mlink_{thin}$ and $Mlink_{thick}$, at unloading, achieving the same final vessel lumen diameter.

4.5 Case Study 4:

Expansion of $Mlink_{thin}$ and $Mlink_{thick}$ inside a localised stenotic coronary artery achieving the same initial expanded lumen diameter

Two simulations were carried out, expanding the distal halves of $Mlink_{thin}$ and $Mlink_{thick}$ inside a localised stenotic coronary artery vessel, represented as a localised crescent-shaped axisymmetric stenosis. The vessel incorporated the properties of plaque and healthy porcine coronary arterial tissue. The pressure used to expand $Mlink_{thin}$ was 41 MPa and 45.7 MPa for $Mlink_{thick}$. Both $Mlink_{thin}$ and $Mlink_{thick}$ expansions achieved an initial lumen diameter, $Ø_I$, of 3.18 mm, see Figure 4.41.

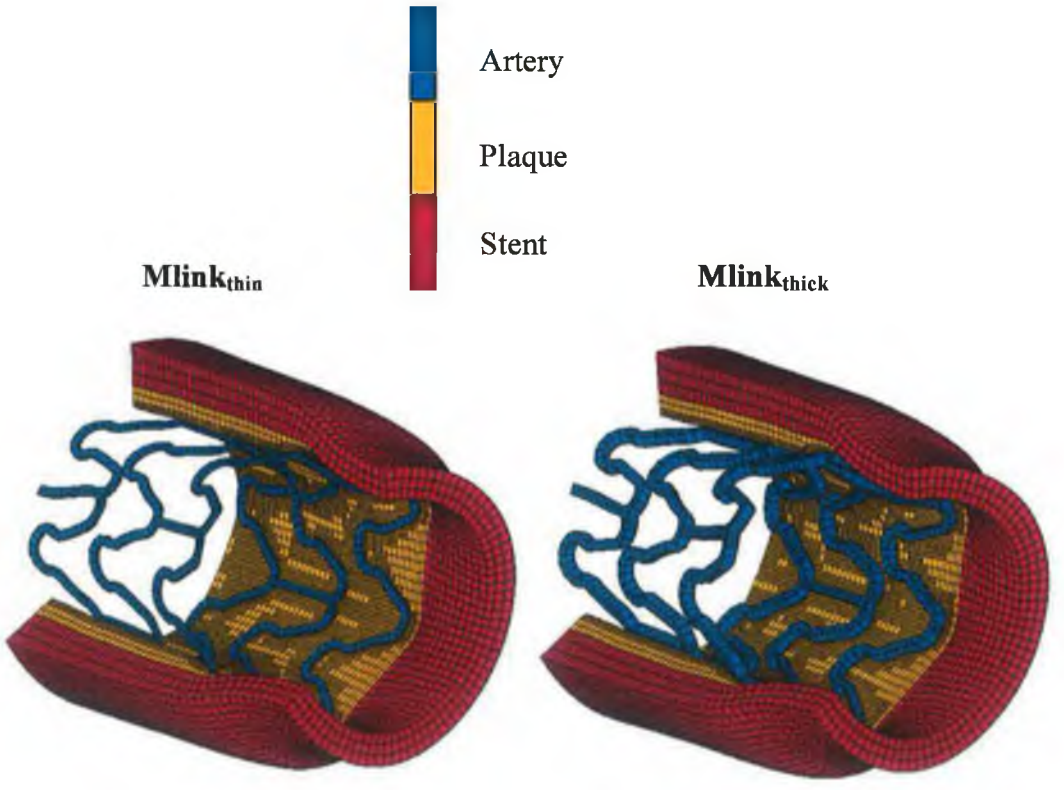

Figure 4.41 Deformed geometry of distal halves of $Mlink_{thin}$ and $Mlink_{thick}$, scaffolding a stenotic vessel, thickness of 0.8 mm, achieving the same initial vessel lumen diameter of $Ø_I = 3.18$ mm.

The radial expansion throughout the structures of both $Mlink_{thin}$ and $Mlink_{thick}$ was found to be highly non-uniform, see Figure 4.42. Due to the geometry of the local stenotic vessel (i.e. plaque geometry), the distal end of the stent structures were observed to experience the highest radial displacement.

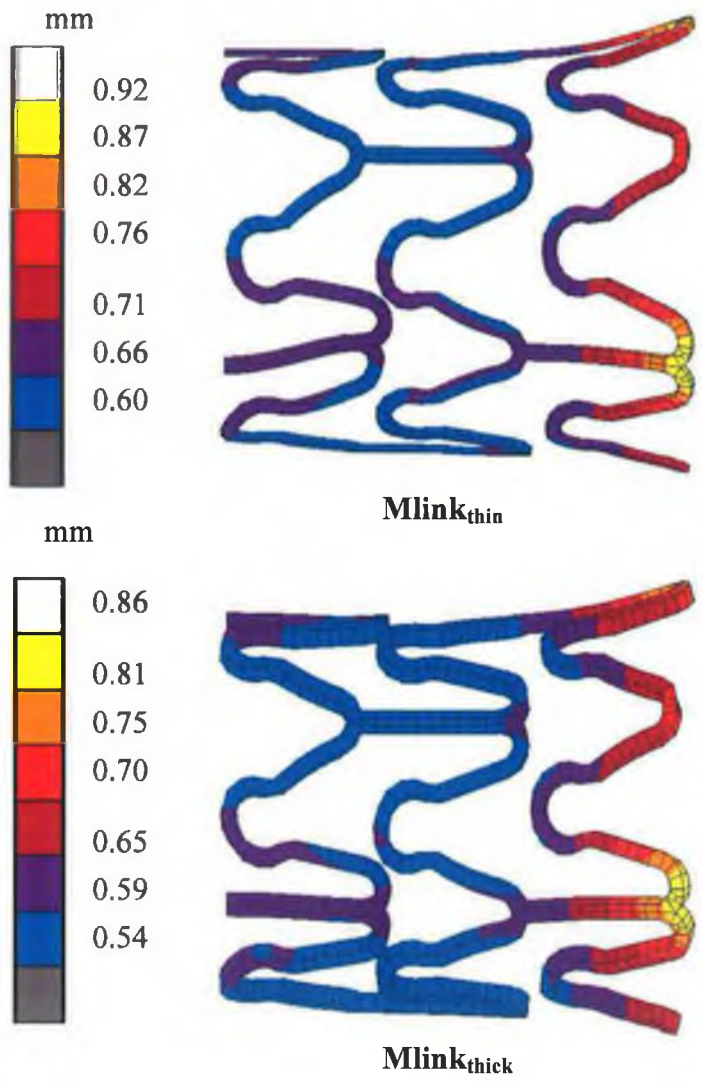

Figure 4.42 Radial displacement distribution throughout the stents' structure of $Mlink_{thin}$ and $Mlink_{thick}$, under the influence of a localised stenotic vessel, thickness of 0.8 mm, achieving the same initial vessel lumen diameter.

Radial displacement were measured at key locations on both the proximal and distal half of each stent, see Figure 4.10, in order to compute the structural characteristics of the stents through the loading and unloading process of the stents' expansion, see Table 4.4.

	$Mlink_{thin}$	**$Mlink_{thick}$**
▪ *Stent before expansion*	(mm)	(mm)
R_{orig}	0.77	0.86
L_{orig}	3.6	3.6
▪ *Stent after loading*		
$R_{load\ central}$	1.45	1.46
$R_{load\ distal}$	1.68	1.68
L_{load}	3.28	3.25
▪ *Stent after unloading*		
$R_{unload\ central}$	1.12	1.18
$R_{unload\ distal}$	1.27	1.3
L_{unload}	3.51	3.43
▪ *Calculated parameters*	(%)	(%)
Longitudinal recoil	-7.0	-5.5
Foreshortening	8.7	9.7
Dogboning	13.7	13.1

Table 4.4 Geometric data of $Mlink_{thin}$ and $Mlink_{thick}$ through loading and unloading, under the influence of localised stenotic vessel of 0.8mm thickness, achieving the same initial vessel lumen diameter of $Ø_I$ of 3.18 mm and a final lumen diameter, $Ø_F$ of 2.44 mm for $Mlink_{thin}$ and $Ø_F$ of 2.52 mm for $Mlink_{thick}$.

Both stents, $Mlink_{thin}$ and $Mlink_{thick}$ have the same pattern of radial displacement distribution. However, in contrast to case study 2 and 3, the central region was observed to experience lower radial displacement than the distal end, see Figure 4.43. For this analysis, both $Mlink_{thin}$ and $Mlink_{thick}$ were expanded to achieve an initial lumen diameter, $Ø_I$ of 3.18 mm while at the end of loading, the final lumen diameter for $Mlink_{thin}$ was found to be 2.44 mm and $Ø_F$ of 2.52 mm for $Mlink_{thick}$.

Foreshortening was observed at loading which was relatively high in magnitude in comparison to the other case studies. Unlike in the free expansion of stents, and the expansion of the stents in idealised stenotic vessels, dogboning was observed in $Mlink_{thin}$ and $Mlink_{thick}$ during expansion, whereby $Mlink_{thick}$ showed a slightly lower degree of dogboning.

Upon unloading, the radial recoil of $Mlink_{thin}$ was found to be greater than the recoil in the $Mlink_{thick}$ and the highest radial recoil was observed at the region where the highest radial displacement was observed, see Figure 4.44. Longitudinal recoil was found to be negative, indicating elongation occured.

The resulting von Mises stresses contours were examined and found to be similar for both stents, see Figure 4.45, whereby the arcs were subjected the high level of von Mises stress. The maximum Von Mises stress magnitude for $Mlink_{thin}$ was found to be 690.7 MPa and for $Mlink_{thick}$ was found to be 493.7 MPa.

The resulting contours of Total Equivalent Plastic strain throughout the expanded structures of $Mlink_{thin}$ and $Mlink_{thick}$, were taken at the end of loading. High plastic strains are evident on the arcs of the stent structures and the maximum Total Equivalent Plastic strain was found to be 0.156 for $Mlink_{thin}$ and 0.171 for $Mlink_{thick}$, see Figure 4.46.

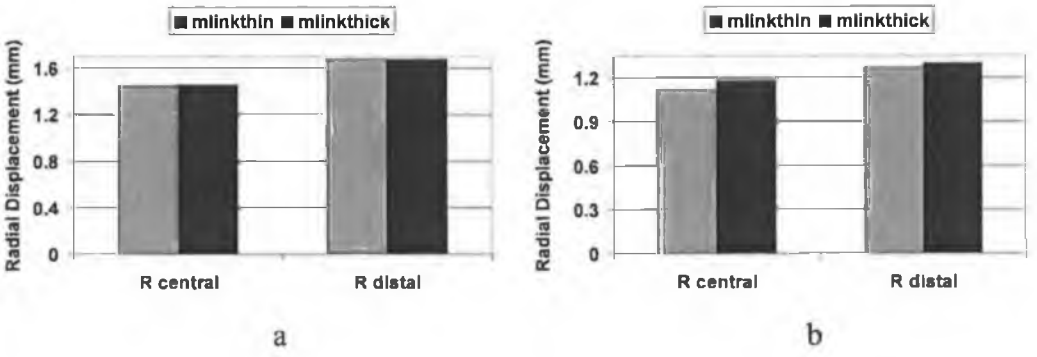

Figure 4.43 Comparison of radial displacement of $Mlink_{thin}$ and $Mlink_{thick}$ inside a localised stenotic vessel throughout the structure at (a) loading and (b) unloading, achieving an initial lumen diameter, $Ø_I$ of 3.18 mm and a final lumen diameter, $Ø_F$ of 2.44 mm for $Mlink_{thin}$ and $Ø_F$ of 2.52 mm for $Mlink_{thick}$.

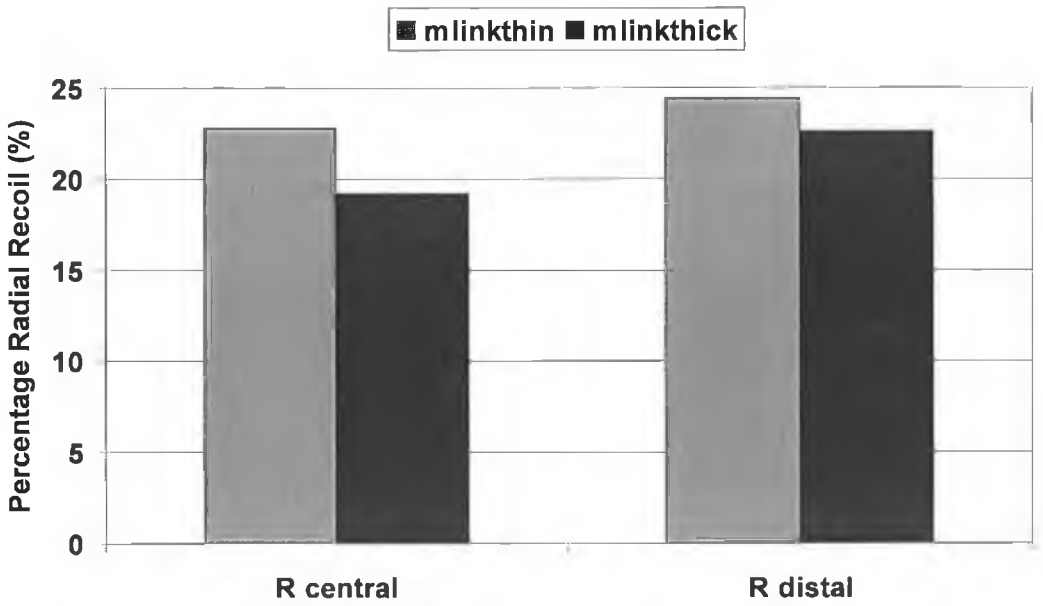

Figure 4.44 Comparison of percentage recoil of $Mlink_{thin}$ and $Mlink_{thick}$ inside a localised stenotic vessel, achieving an initial lumen diameter, $Ø_I$ of 3.18 mm.

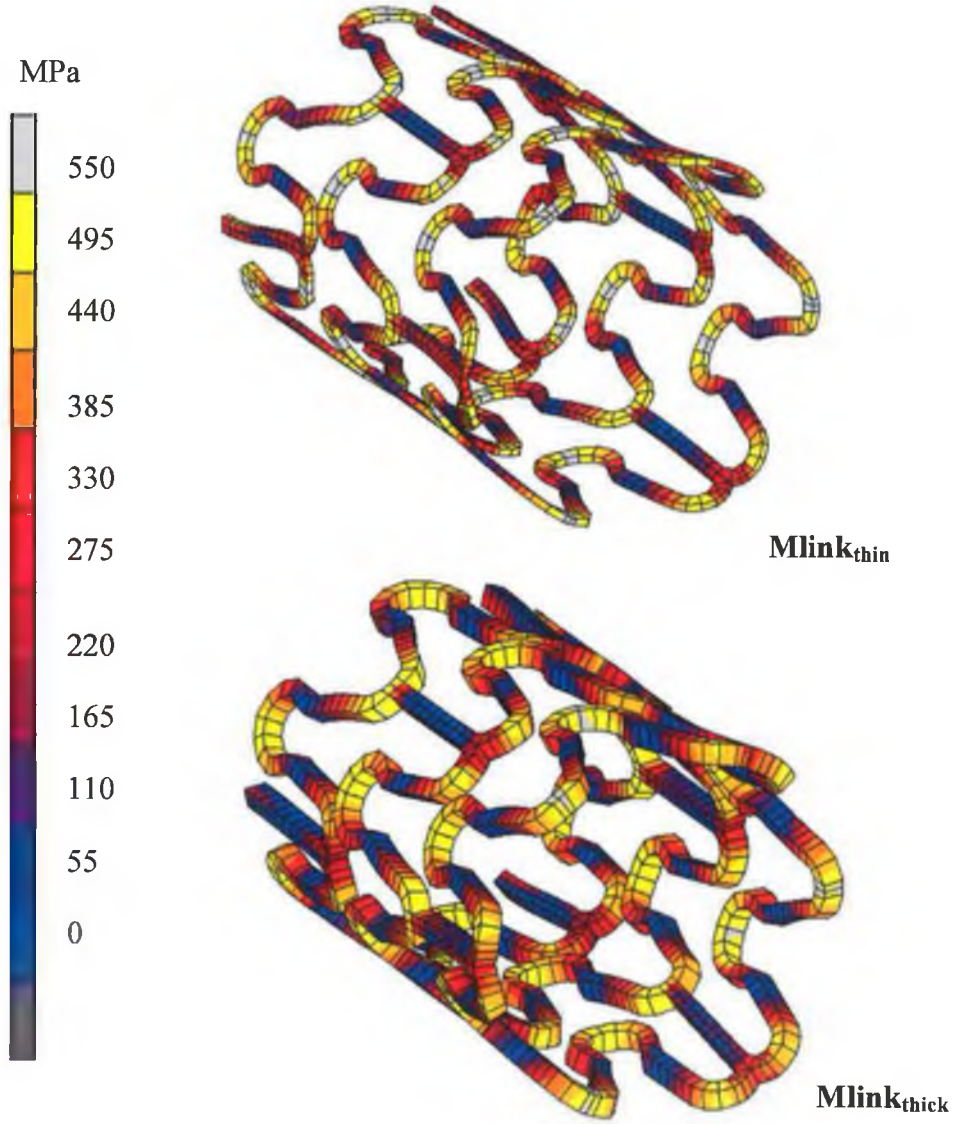

Figure 4.45 The resulting von Mises stress contours throughout the structure of Mlink$_{thin}$ and Mlink$_{thick}$, under the influence of a localised stenotic vessel, achieving an initial lumen diameter, $Ø_I$ of 3.18 mm and a final lumen diameter, $Ø_F$ of 2.44 mm for Mlink$_{thin}$ and $Ø_F$ of 2.52 mm for Mlink$_{thick}$.

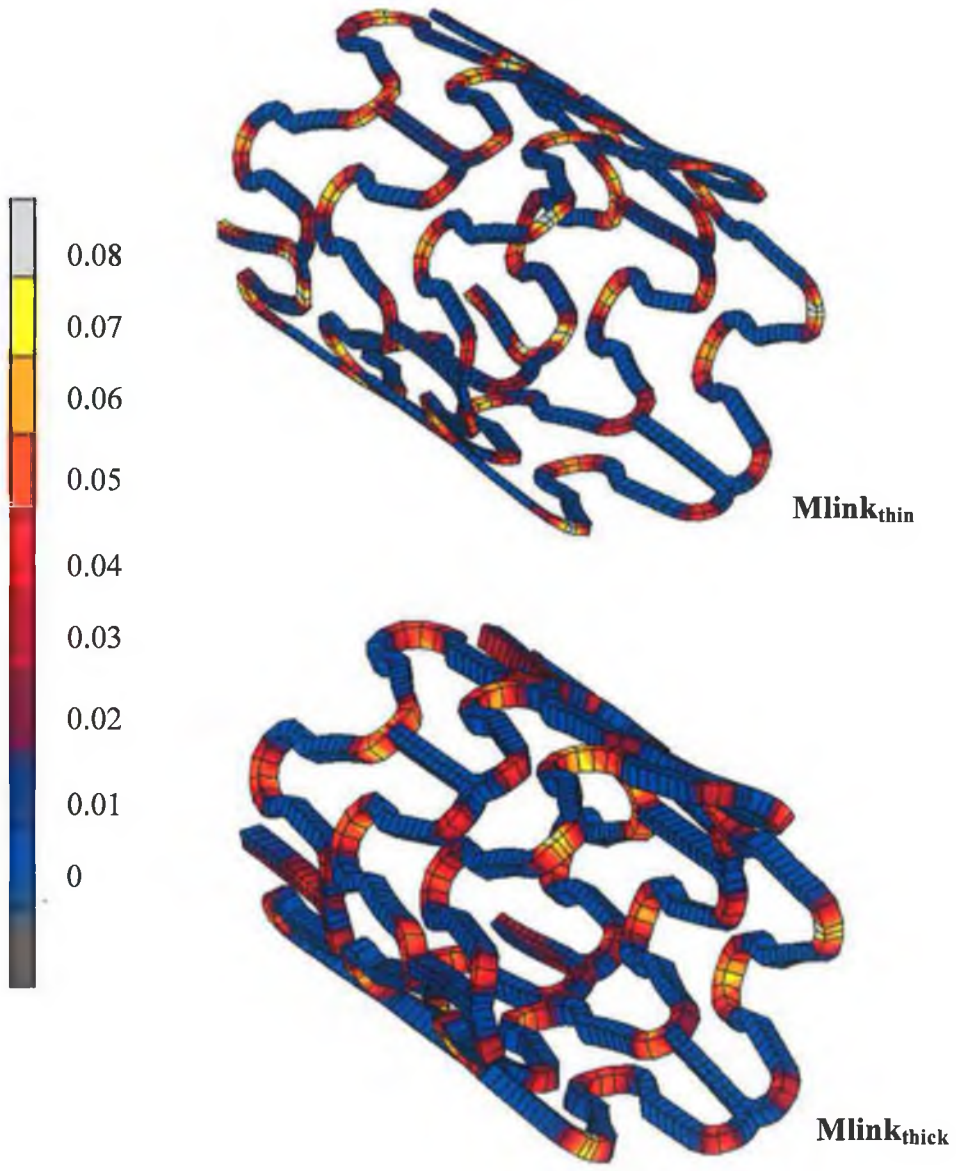

Figure 4.46 The resulting Total Equivalent Plastic strain contours throughout the structure of Mlink$_{thin}$ and Mlink$_{thick}$, under the influence of a localised stenotic vessel, achieving an initial lumen diameter, $Ø_I$ of 3.18 mm and a final lumen diameter, $Ø_F$ of 2.44 mm for Mlink$_{thin}$ and $Ø_F$ of 2.52 mm for Mlink$_{thick}$.

4.5.1 Stress Analysis of the Stented Vessels

I. Stresses after stent loading; Stimulus for acute damage

The $Mlink_{thin}$ and $Mlink_{thick}$ were expanded to achieve the same initial lumen diameter of $\emptyset_I$ = 3.18 mm. The stresses generated within the vessel wall on loading were examined to determine the degree of acute damage as it reached the initial lumen diameter.

The stresses in the vessels were examined in the circumferential, radial and longitudinal directions. Comparing the stresses induced in both vessel, it was found that there was a considerable more tissue stressed at high levels found in stented vessels by $Mlink_{thin}$ and $Mlink_{thick}$, see Figure 4.47-4.49. The same pattern was found in case study 2, where in both case studies, the stents were expanded to achieve the same initial expanded lumen diameter.

The volume of tissue stressed to various levels was computed for specific stress values in the circumferential, radial and longitudinal directions within the stented stenotic vessels, see Figure 4.50. In contrast to other case studies, the magnitude of stresses induced within the stented vessels was found to be significantly higher. The highest magnitude of stress induced within the stented stenotic vessels was produced by the tensile stresses in the circumferential and longitudinal direction, whereby some tissue was stressed above 60 MPa and 20 MPa respectively. The least magnitude of stress was found to be the compressive longitudinal stress, where less than 5% volume of tissue at a high magnitude of 0.5 MPa. Meanwhile, there was some tissue stressed experiencing compressive radial stress at above 10 MPa.

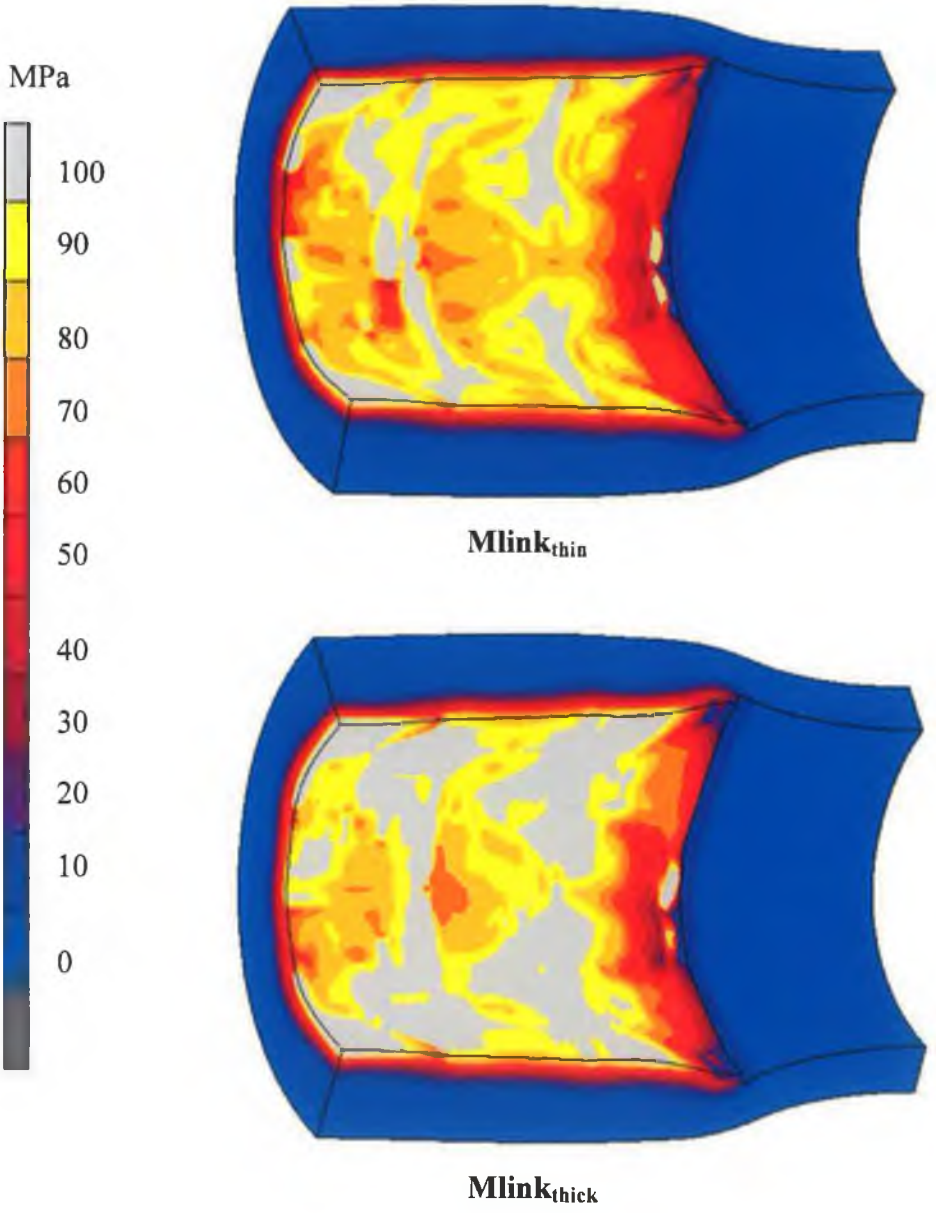

Figure 4.47 Tensile circumferential stresses induced in the arterial wall stented by Mlink$_{thin}$ and Mlink$_{thick}$, at loading, achieving the same initial lumen diameter, $Ø_l$ of 3.18 mm.

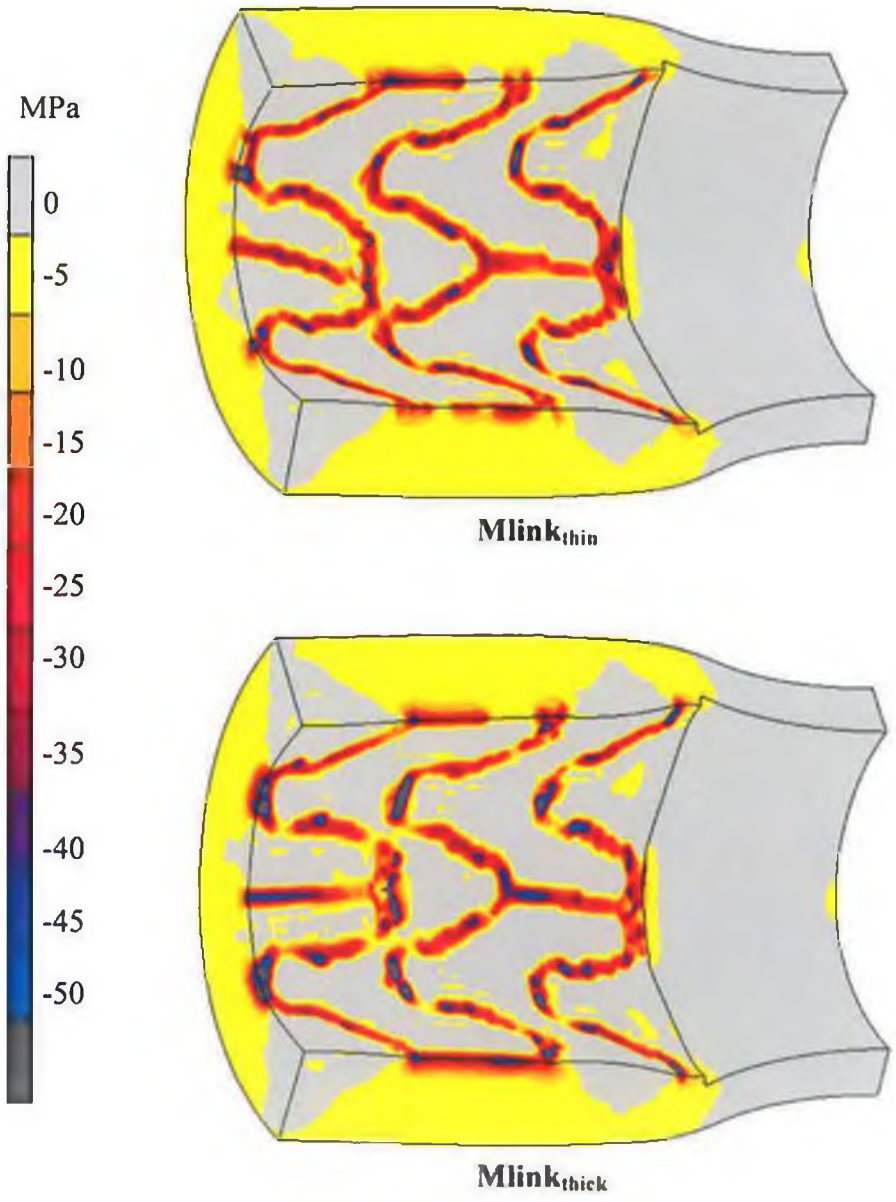

Figure 4.48 Compressive radial stresses induced in the arterial wall stented by Mlink$_{thin}$ and Mlink$_{thick}$, at loading, achieving the same initial lumen diameter, $Ø_l$ of 3.18 mm.

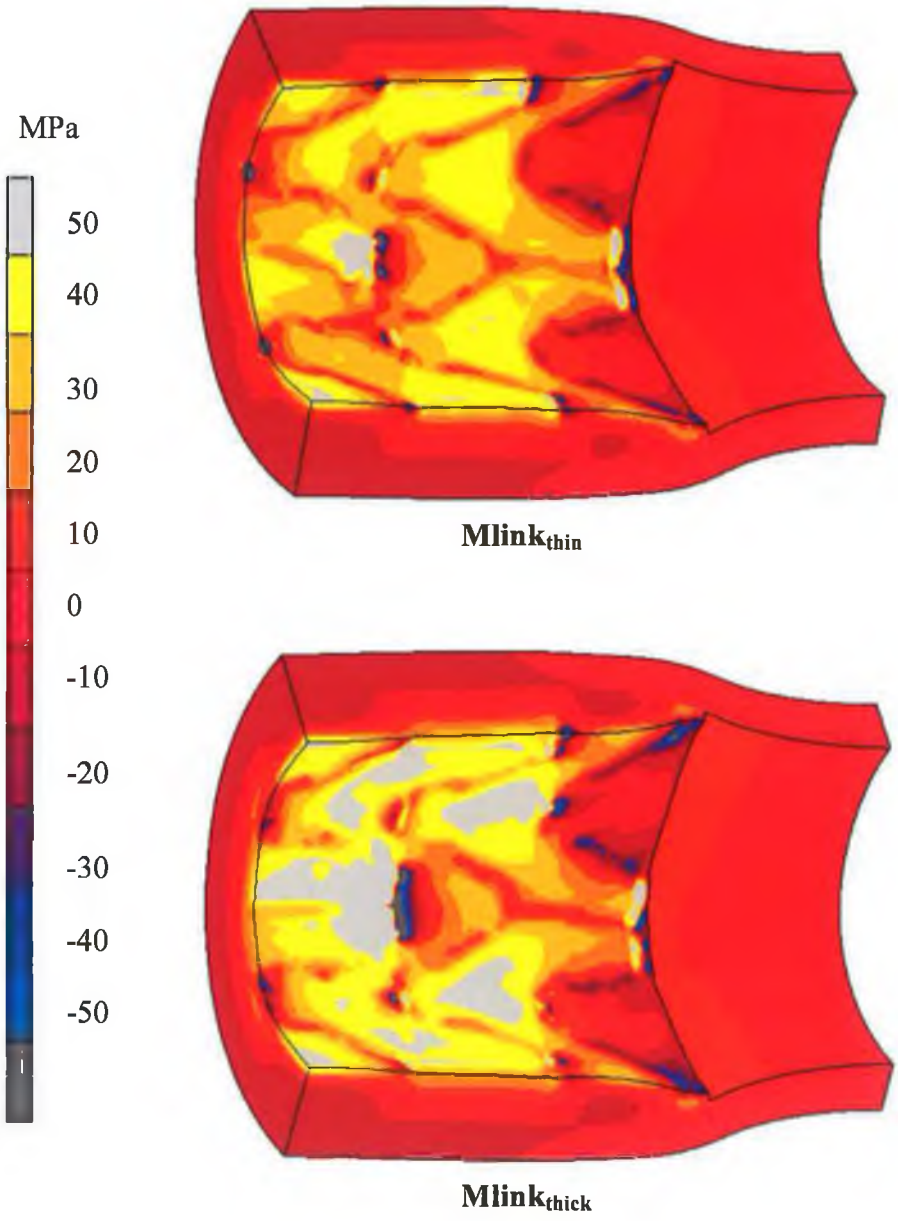

Figure 4.49 Tensile and compressive longitudinal stresses induced in the arterial wall stented by $Mlink_{thin}$ and $Mlink_{thick}$, at loading, achieving the same initial lumen diameter, $Ø_I$ of 3.18 mm.

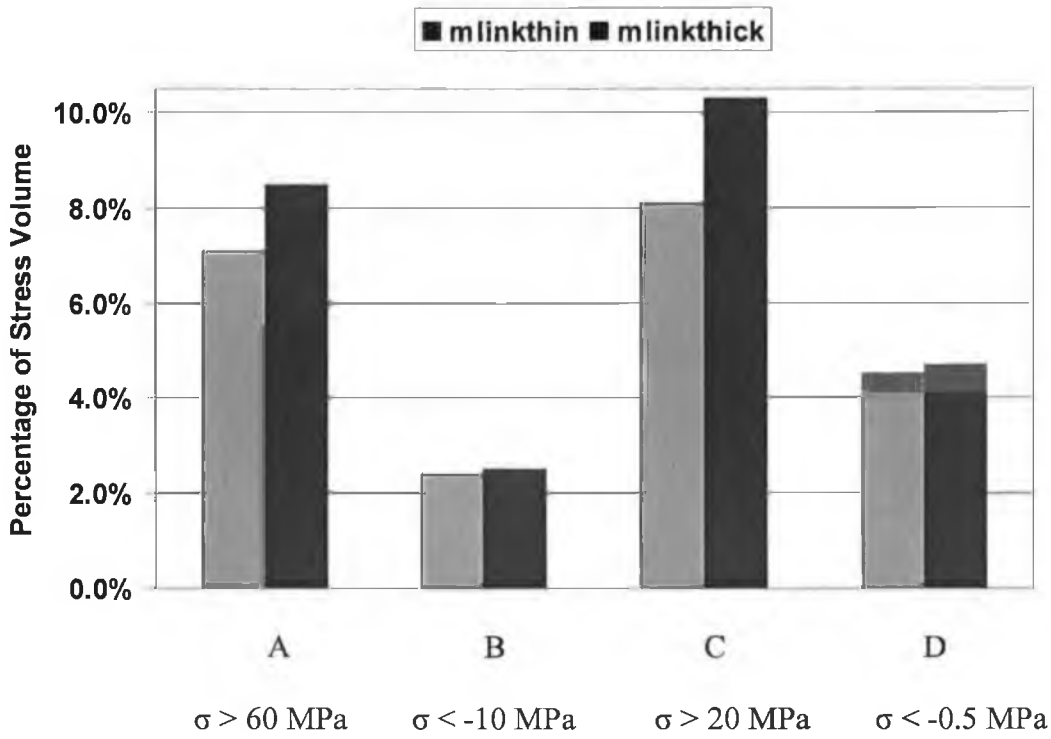

Figure 4.50 The percentage volume stress by the tensile circumferential stress (A), radial compressive stress (B), tensile longitudinal stress (C) and compressive longitudinal stress (D), at loading, within the stented vessel by $Mlink_{thin}$ and $Mlink_{thick}$, achieving an initial lumen diameter, $\emptyset_I = 3.18$ mm at loading.

II. Stresses after stent unloading; Stimulus for long-term damage

The pressure was removed from the stent once the 3.18 mm diameter lumen was achieved. The resulting final arterial lumen diameter, $Ø_F$, was found to be different for vessels stented with $Mlink_{thin}$ and $Mlink_{thick}$. The localised stenotic vessel stented with $Mlink_{thin}$ produced a final lumen diameter of $Ø_F$ = 2.44 mm while $Mlink_{thick}$ produced a final lumen diameter of $Ø_F$ = 2.52 mm. These variations in the final lumen diameter were the as a result of the difference in the radial recoil of both stent structures, where $Mlink_{thin}$ was found to have higher recoil than $Mlink_{thick}$.

The stresses in the vessels were examined in the circumferential direction, see Figure 4.51, radial direction, see Figure 4.52, and the longitudinal direction, see Figure 4.53, and similar stress patterns were observed in the stented vessels as those observed on loading. A decrease in stresses in all direction was found in the stented stenotic vessels. In contrast to loading, the difference between the stented vessels by $Mlink_{thin}$ and $Mlink_{thick}$ was found more prominent.

As the stents structures were left scaffolding open the arterial wall, the volume of tissue stressed to various levels was computed for specific stress values in the circumferential, radial and longitudinal directions within the stented stenotic vessels, see Figure 4.54. Similar to case study 2, whereby the stents were expanded to the same initial expanded lumen diameter, which resulted in different final lumen diameter, the stented vessel by $Mlink_{thick}$ showed a significant higher volume of tissue stressed at high levels at unloading.

Similar to loading, the tensile stresses were found higher than the compressive stress found in the stented vessels. Some tissue was stressed above 1 MPa by the tensile circumferential stress and 0.5 MPa by the tensile longitudinal stress found in the stented vessels by $Mlink_{thin}$ and $Mlink_{thick}$. Meanwhile the stress volume was computed above 0.1 MPa for the compressive stress in the radial and longitudinal direction. There was more tissue stressed at this level by the compressive radial stress, see Figure 4.54.

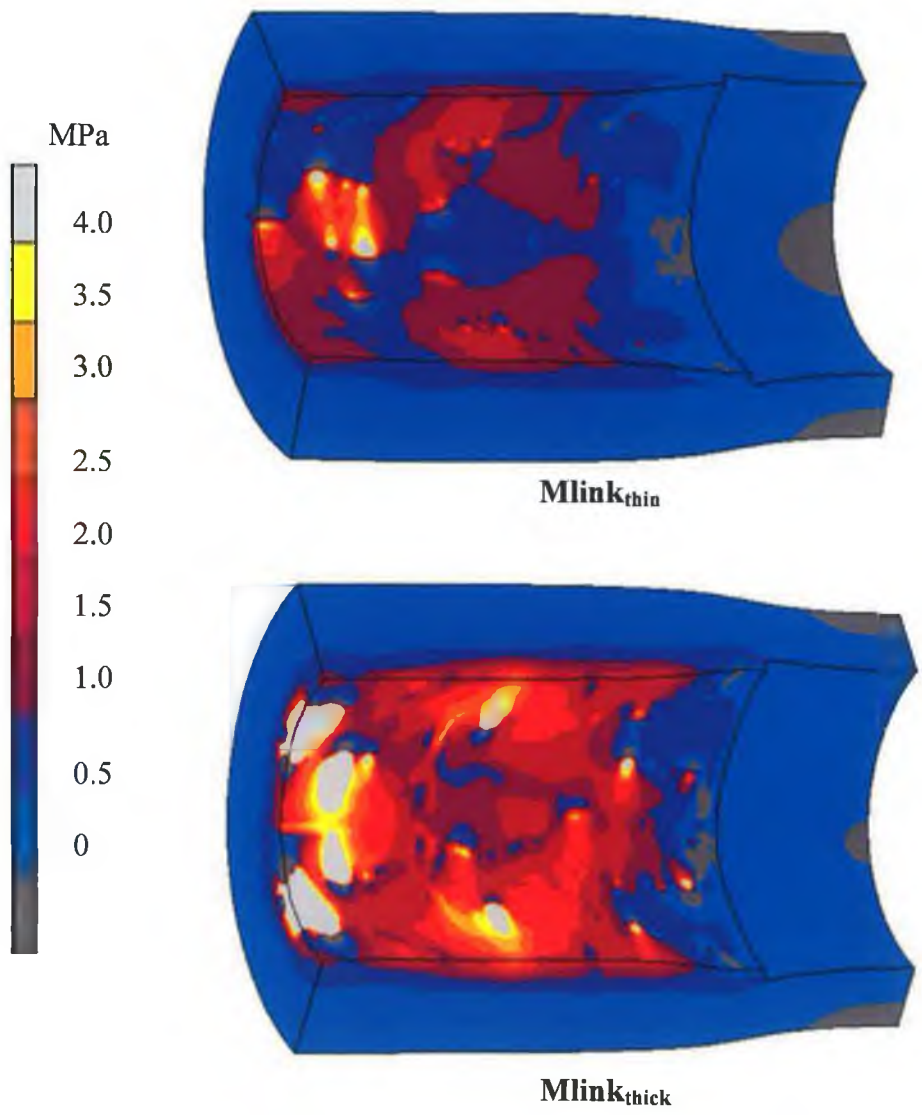

Figure 4.51 Tensile circumferential stress induced in the localised stenotic vessel wall stented by $Mlink_{thin}$ and $Mlink_{thick}$, at unloading, achieving a final lumen diameter, $Ø_F$ of 2.44 mm for $Mlink_{thin}$ and $Ø_F$ of 2.52 mm for $Mlink_{thick}$.

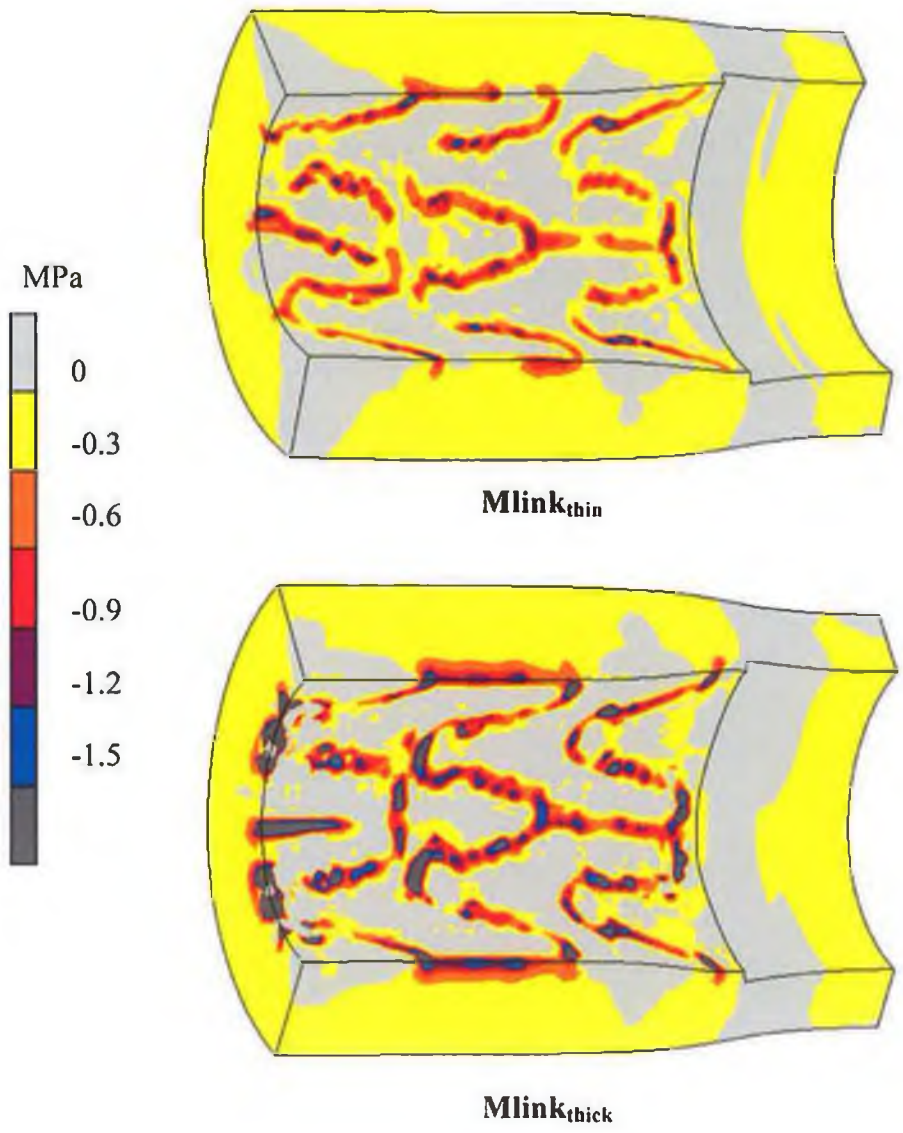

Figure 4.52 Compressive radial stress induced in the localised stenotic vessel wall stented by $Mlink_{thin}$ and $Mlink_{thick}$, at unloading, achieving a final lumen diameter, $Ø_F$ of 2.44 mm for $Mlink_{thin}$ and $Ø_F$ of 2.52 mm for $Mlink_{thick}$.

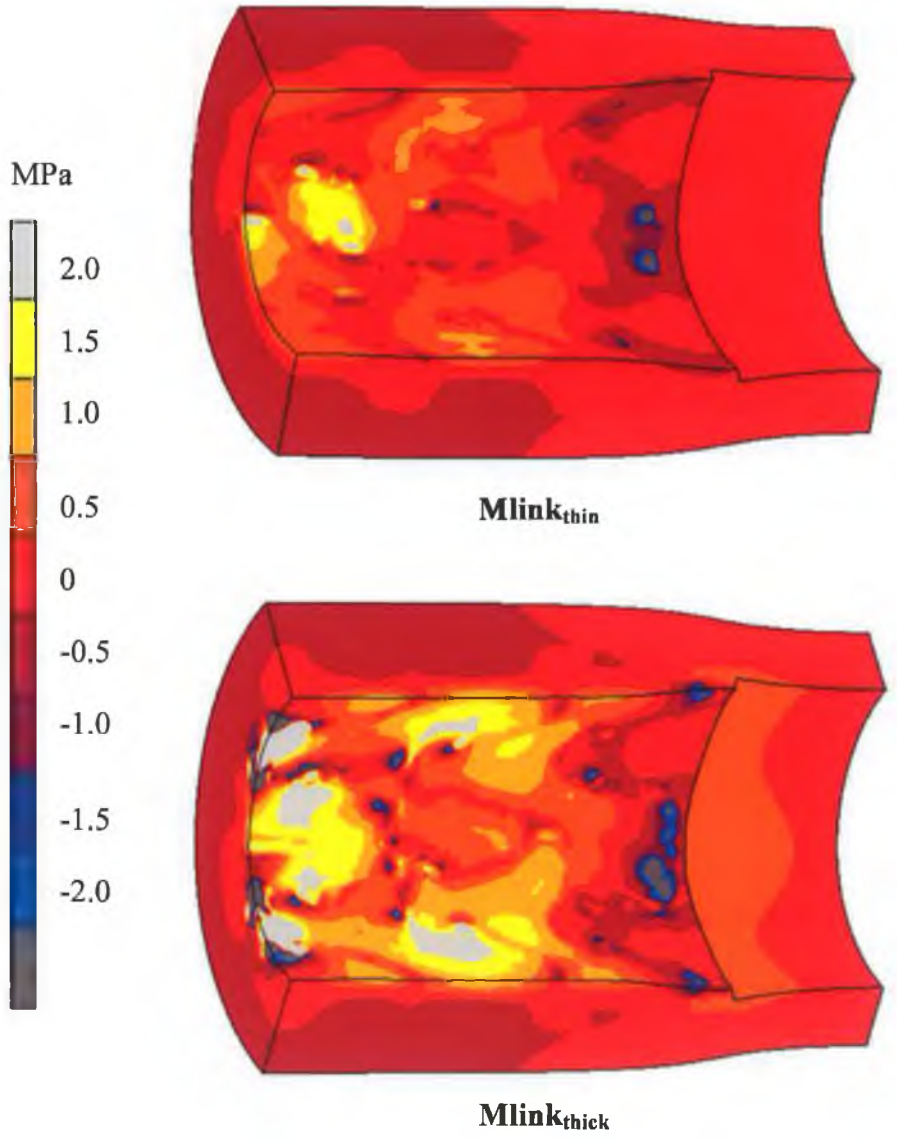

Figure 4.53 Tensile and compressive longitudinal stress induced in the localised stenotic vessel wall stented by Mlink$_{thin}$ and Mlink$_{thick}$, at unloading, achieving a final lumen diameter, $Ø_F$ of 2.44 mm for Mlink$_{thin}$ and $Ø_F$ of 2.52 mm for Mlink$_{thick}$.

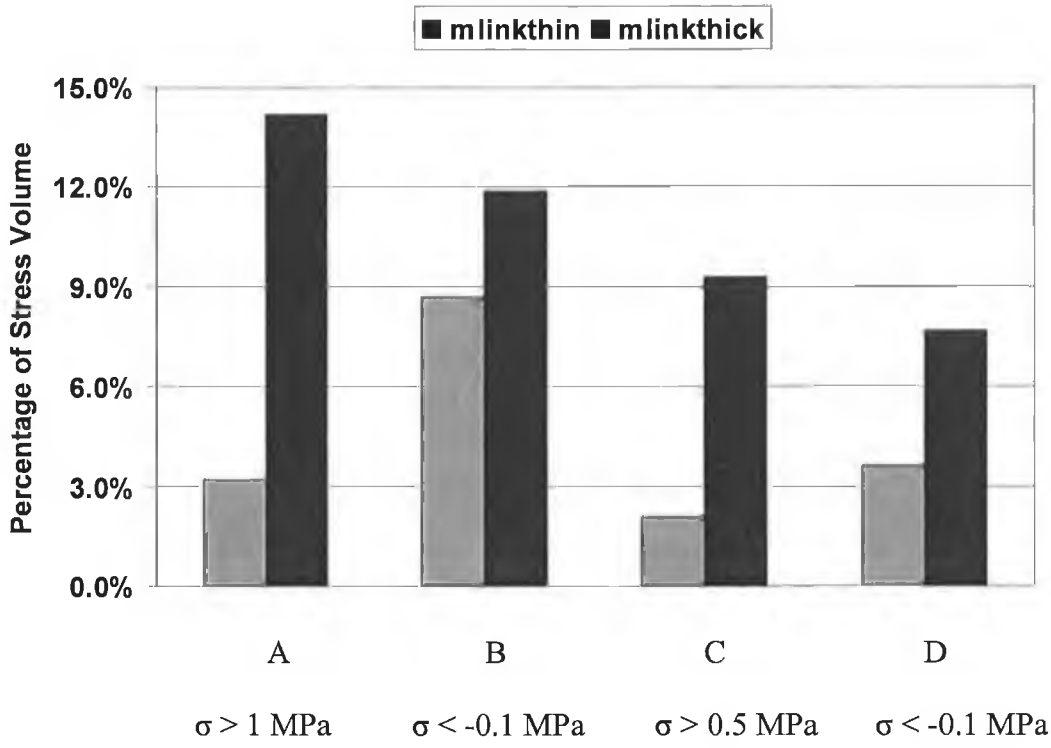

Figure 4.54 The percentage volume stress by the tensile circumferential stress (A), radial compressive stress (B), tensile longitudinal stress (C) and compressive longitudinal stress (D), at unloading, within the stented vessel by $Mlink_{thin}$ and $Mlink_{thick}$, achieving a final lumen diameter, $Ø_f$ of 2.44 mm for $Mlink_{thin}$ and $Ø_f$ of 2.52 mm for $Mlink_{thick}$.

4.6 Summary

This chapter has evaluated the results following the four case studies to investigate the influence of stent's expansion on stents characteristics. The stresses induced within the stented vessels were thoroughly examined, identifying the difference in the magnitude at loading and unloading, which provided a greater insight into the mechanical stimuli for restenosis.

Chapter 5

DISCUSSION

5.1 Introduction

The ISAR STETREO Trial by Kastrati *et al.* [26] examined the clinical restenosis outcome of the ACS RX Multilink and the ACS Multilink RX Duet. These MultiLink stents are similar in design but have with different strut thicknesses. The expansion characteristics of the thinner strut stent ($Mlink_{thin}$) and the thicker strut stent ($Mlink_{thick}$) were examined during this study using FE analyses. The stents were compared under free expansion and also expanded in different vessels geometries. The vessel geometry and the material properties of the arterial tissue and plaque resulted in significantly different expanded stent structures. The stresses induced within the stented vessel walls by the two stents were also thoroughly examined since these stresses are believed to potentially act as the mechanical stimuli for in-stent restenosis. This chapter therefore discusses the FE analyses carried out as follows:-

1. Comparison of pressure deployment of $Mlink_{thin}$ and $Mlink_{thick}$ for each case study.
2. Comparison of the expanded $Mlink_{thin}$ and $Mlink_{thick}$ stents
3. Comparison of the radial recoil of $Mlink_{thin}$ and $Mlink_{thick}$ after deployment.

4. Comparison of the stresses induced within the stented vessels through loading and unloading of pressure, determining the volume of tissue stressed at high levels in each stented vessel and hence the level of damage caused by $Mlink_{thin}$ and $Mlink_{thick}$.

Finally, issues of stent design are discussed in terms of the results obtained from this study.

5.2 Limitations of this Study

The accuracy and the reliability of the results from a finite element study are highly dependent upon the inputs, such as the geometry, the boundary conditions applied to represent the problem adequately, and the materials properties assigned to each component. The deployment of a stent involves the interaction between a balloon, stent and atherosclerotic coronary artery. The modelling of this process using finite element analysis is a complicated and challenging study. To completely describe the problem involves modelling the interaction between the balloon and stent, and the stent and artherosclerotic artery. This analysis did not include the influence of the balloon in expanding the stents and this is therefore a limitation of this work. The inclusion of a balloon in the expansion of the stent may result in a more uniform stent's structure. However the balloon's material is believed to contribute largely to the uniformity of stent's expansion. Future work could include determining the influence of different balloon types on the expansion characteristics of stents.

Coronary stents are placed in coronary arteries where the blood is pulsatile in nature and hence the stented vessel is subjected to a dynamic pressure environment after implantation. The blood flow inside the coronary vessel also creates a shear stress on the wall of the arteries that may alter upon implantation of the stents. Although stented vessels may exhibit a biological response to changes in shear stresses, fluid flow dynamics were beyond the scope of this study.

One of the major limitations of the finite element models in this study is the geometrical representation of the stents and the artery. The geometric measurements of the stents, the ACS RX MultiLink and the ACS MultiLink RX Duet, were extrapolated from a handbook of coronary stents [89]. The stents could have been more accurately described using stent dimensions obtained from the manufacturer of these stents (Guidant), however, this information could not be obtained from the manufacturer. The idealised representation of the stenotic vessel geometry also represents another limitation to this study. Different vessel geometries were adopted in the analyses, although all of the geometries were idealised representations of real vessels. This study focuses on examining the role of strut thickness in generating stresses in the stented vessel, whereby the absolute magnitude of these stresses was not the primary concern, but rather the difference in the stresses generated by the two different stents. Therefore, the finite element models used for this comparative study were adequate in order to identify the different levels of stresses induced within stented stenotic vessels by the thinner and thicker struts stents. The study can also clearly indicate the influence of changes in vessel geometry on the magnitude of the stresses that would be induced in a stented vessel.

The stents's structures were discretised by means of eight-noded isoparametric, three-dimensional brick elements with one element through the thickness, see Figure 3.3. The mesh of the stent structure represents another limitation to this study. A higher order element and finer mesh density may contribute to the accuracy of the magnitude of expansion and stresses found in the stent's structure. Contact analysis for Marc/Mentat requires a finer mesh on the most deformable body of the contact bodies, i.e. the stenosed artery in this case. Therefore this mesh density of the stent was chosen to minimise the number of elements and was found reasonable. A finer mesh of the stent structure would lead to a finer mesh density needed for the artery. The use of a higher order element and a finer mesh density of the stent structure would consequently result in much greater heavy computational time and resources.

The material models represent another limitation to this study. The arterial wall was represented by an isotropic Mooney-Rivlin model, instead of an anisotropic viscoelastic model that includes the hysteresis exhibited by arterial

tissue and the anisotropy observed in the composition of the arterial wall. Residual stress was also absent in the constitutive model defined for the arterial wall properties. The Mooney-Rivlin model has been found to adequately represent arterial tissue when determined by fitting to published experimental data from uniaxial and equibiaxial tension test data as it includes the stress-stiffening behaviour of arterial tissue [41]. Although the plaque tissue was described using a constitutive model defined by fitting to published data on the stress-strain behaviour of human atherosclerotic plaque obtained from uniaxial tension test data alone, to the authors knowledge no other uniaxial tensile test data on human plaques has been published and no data on the biaxial tensile behaviour of human atherosclerotic plaques could be found in the literature. The material data present a direct link to the magnitude of stresses examined for these analyses. Different material data are likely to result in a different magnitude of stresses. However, this study has successfully identified the major stress contributor found in the stented vessel.

The limitations outlined may be accepted for the purpose of comparative analyses such that the models limit the complexity of modelling the process of stent expansion within an artery vessel. However, the models still provide valuable information on the influence of stent design on stent expansion and vessel stresses. For this purpose all parameters, for example, the materials used for these analyses and the geometrical representations of the stenotic vessels and the stents' structures were kept identical, with the only variation being the strut thicknesses of the stents for each case study.

5.3 Comparison of Pressure Deployment

The lumen pressure applied to the stents was ramped up for a small time step size. The size of time step depended upon the amount of pressure applied for each analysis and was therefore found to be highly dependant on the stent structure. The pressure was unloaded by half the time it took to load it. High time step sizes were found to cause too much pressure to be applied in a single increment resulting in the simulation not converging.

5.3.1 Comparison of thinner strut stent vs. thicker strut stent

The analyses found that the thicker strut stent needed a higher amount of pressure compared with the thinner strut stent, in order to expand both stents to the same initial expanded outer diameter, as seen for case study 1, 2 and 4, see Figure 5.1. Under free expansion, there was a significant difference in the pressure required to expand both stents to achieve the same outer diameter of 3 mm. It was found that the pressure required to expand $Mlink_{thick}$ was approximately three times higher than the pressure required to expand $Mlink_{thin}$ to the same diameter. Under the influence of a stenosed straight vessel, $Mlink_{thin}$ required approximately 78% of the pressure required to expand the $Mlink_{thick}$ and 90% under the influence of a localised stenosed. However, in case study 3, whereby $Mlink_{thin}$ and $Mlink_{thick}$ were expanded and allowed to recoil to achieve the same final outer diameter, under the influence of a stenosed vessel, the pressure required to expand $Mlink_{thick}$ was found to be significantly lower, whereby $Mlink_{thick}$ required approximately 27% of the pressure required to expand the $Mlink_{thin}$.

5.3.2 Comparison of each stent design under free expansion and under the influence of various stenosed vessels

The pressure required to expand the same stent design under free expansion and under the influence of a stenotic straight vessel was found to be significantly different, see Figure 5.1. For example, to expand $Mlink_{thin}$ under free expansion, the pressure required was significantly lower at only 5.3% of the pressure required to deploy $Mlink_{thin}$ under the influence of a stenotic straight vessel to achieve the same outer diameter. In case study 4, whereby $Mlink_{thin}$ and $Mlink_{thick}$ were expanded inside a localised stenotic vessel with plaque and arterial properties, the pressures required to expand both $Mlink_{thin}$ and $Mlink_{thick}$ were significantly higher than for the straight stenosed vessel. This high pressure has also been shown to be associated with the magnitude of stresses found in the stented vessels. Clearly, the pressure required for stent deployment is highly dependant on the

stent design, the material properties of the atherosclerotic coronary arteries, and the geometry of the vessel wall.

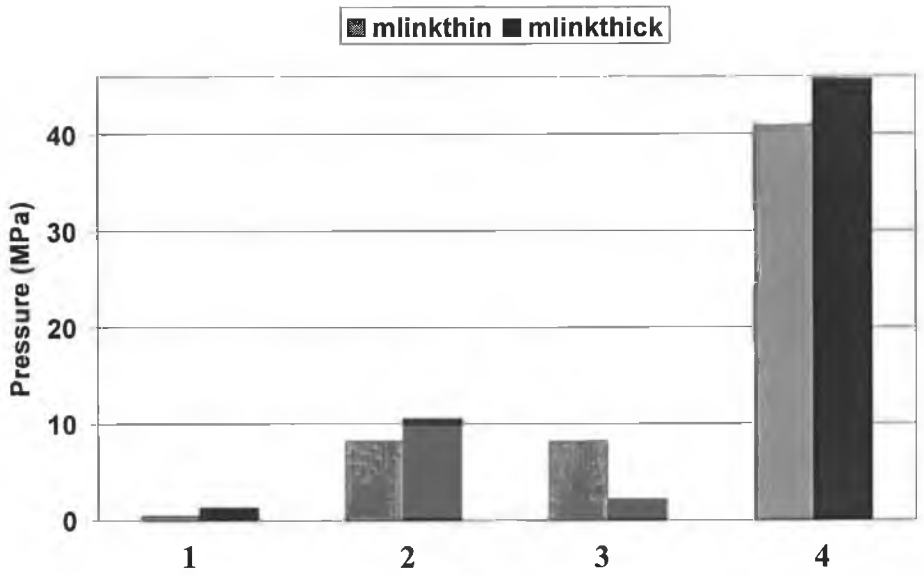

Figure 5.1 Comparison of pressure deployment of $Mlink_{thin}$ and $Mlink_{thick;}$ for 1) free expansion (Case study 1); 2) within the straight stenotic vessel achieving the same initial lumen diameter (Case study 2); 3) within the straight stenotic vessel achieving the same final lumen diameter (Case study 3); and 4) within the localised stenotic vessel achieving the same initial lumen diameter (Case study 4).

5.4 Comparison of the $Mlink_{thin}$ and $Mlink_{thick}$ stents after deployment

5.4.1 von Mises stress and plastic strain

The von Mises stresses and plastic strain distributions within the deployed stents showed similar patterns for all of the simulations. It is interesting to note the comparison of maximum von Mises stress in each stent design under different influence of expansion, see Figure 5.2.

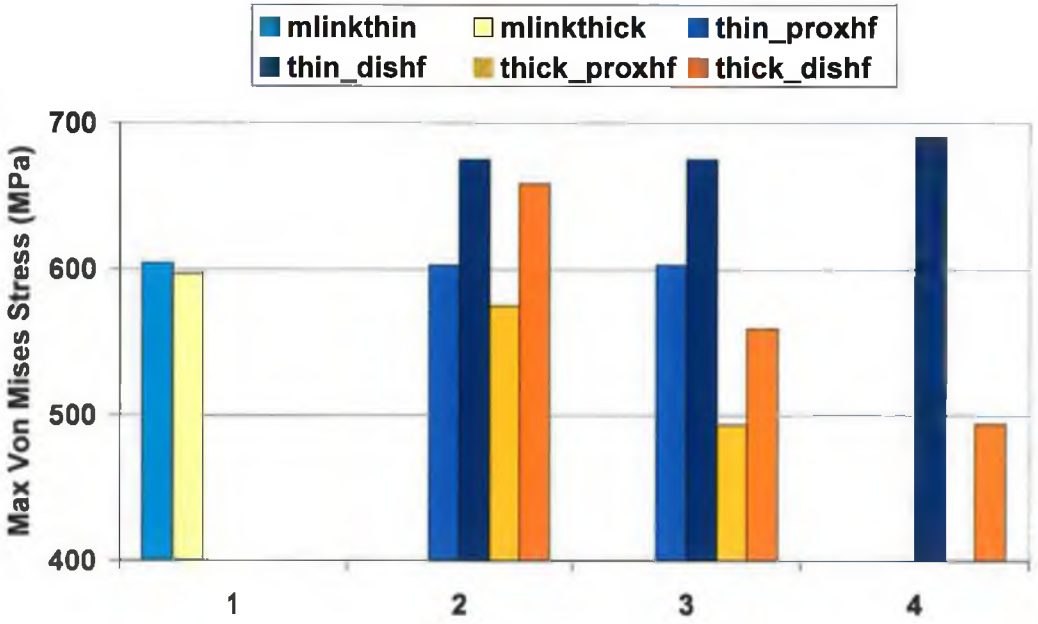

Figure 5.2 Comparison of max von Mises stress found in the structures of $Mlink_{thin}$ and $Mlink_{thick}$, upon deployment for 1) free expansion (Case study 1); 2) in a straight stenotic vessel achieving the same initial lumen diameter (Case study 2); 3) in a srtaight stenotic vessel achieving the same final lumen diameter (Case study 3); and 4) in a localised stenotic vessel achieving the same initial lumen diameter (Case study 4).

Murphy *et al.* [88] reported that the stress-strain behaviour of 316L stainless steel stent struts is size dependent. That study suggested that certain areas of thinner stent struts could experience local failure, which would not be detected if bulk stress-strain curves were used to describe the material behaviour. They proposed that any analysis of a stent with strut thickness below 0.05 mm should use a size based stress-strain relationship.

Under free expansion, the specific stress-strain behaviour of 316L stainless steel was incorporated into the analyses, according to the stent's strut size. The resulting maximum von Mises stresses were found only marginally higher for $Mlink_{thin}$ at 604.4 MPa compared with 597 MPa for $Mlink_{thick}$. However, the failure stress for the thinner strut stent was found to 693.2 MPa

compared with 730.4 MPa for thicker strut stent from the data by Murphy *et al.* [88]. The $Mlink_{thin}$ was therefore at a greater risk of failure than the $Mlink_{thick}$.

As discussed earlier, the pressure required to expand the stent structures under the influence of stenosed vessels was significantly higher than that required to expand the stents under free expansion. In order to run the simulations the failure stress of the thinner strut stent had to be brought up to same failure point as thicker strut stent. For these case studies, where the stent was expanded inside a stenosed vessel, the max von Mises stress for the $Mlink_{thin}$ was found to exceed the failure stress found by Murphy *et al.* [88], see Figure 5.2.

Clearly therefore, the thin strut stent is highly susceptible to failure and the use of a material with higher failure strength may be necessary to prevent this risk of failure in thin strut stents; examples include cobalt chromium which has been successfully used for thin strut stents in recent years [91].

5.4.2 Foreshortening

Foreshortening is a common problem in metallic stents. It is the contraction of a stent in the axial direction during deployment. In general foreshortening is not desirable, as accurate placing and optimum longitudinal vessel coverage is compromised with increasing foreshortening in stents. Foreshortening was found to vary considerably for all of the case studies evaluated in this thesis, see Table 5.1.

Under free expansion, foreshortening was absent in both stent designs. In fact, the stents were found to elongate by 2% of their original lengths. However, when the stents were subjected to high pressure they exhibited foreshortening, see Table 5.1. This table also shows that the larger the radial expansion the greater the degree of foreshortening, when expanding from the crimped low profile stent to an expanded larger profile. This characteristic behaviour was confirmed by case study 3, where the $Mlink_{thick}$ exhibited lower foreshortening whilst achieving a lower initial lumen diameter compared with $Mlink_{thin}$.

	Foreshortening (%)			
	Thin_proxhf	thin_dishf	thick_proxhf	thick_dishf
Case study 1	-2		-2	
Case study 2	6	5	4	5
Case study 3	6	5	2	2
Case study 4		9		10

Table 5.1 Foreshortening of $Mlink_{thin}$ and $Mlink_{thick}$ after deployment, for all of the case studies evaluated in this thesis.

Under the influence of the straight and localised stenotic vessels, both stent designs exhibited foreshortening. In case study 2 and 4, the foreshortening experienced by $Mlink_{thin}$ and $Mlink_{thick}$ was found to be similar for both stents, where both stents were expanded to achieve the same initial lumen diameter. This illustrates that the different strut thicknesses, for the same stent design, do not have a major influence on the degree of foreshortening exhibited by the stents. However, in case study 4, foreshortening was found approximately twice that observed in case study 2. This is due to the variation in the vessel geometry, whereby the stents conform to the geometry resulting in greater foreshortening around the localised stenosis.

5.4.3 Dogboning

Dogboning may be observed in stents during loading, whereby the ends expand to a higher radial displacement than the middle of the stent, causing the stent to 'flare' at the ends. This behaviour is undesirable as the flare is likely to cause

damage through the arterial wall. Dogboning was evaluated in all of the case studies, see Table 5.2.

Dogboning was not observed in either the $Mlink_{thin}$ or $Mlink_{thick}$ during free expansion, in fact, a high degree of radial retraction was observed at the proximal ends of both stents, see Table 5.2. This behaviour is due to the fact that there is less metal surface area at the proximal end of the stent's structure. Pressure is uniformly applied on the internal surface of the stent, and therefore the net force applied in the proximal end of the stent is lower than in the other areas of the stent structure. This consequently led to lower expansion seen at the proximal end. The radial displacement distributions throughout the stents were found to be highly non-uniform. It was clear that the proximal end resulted in the least radial displacement under free expansion. The proximal end of both stents underwent approximately 74% of the maximum radial displacement. This 'negative dogboning' was found to occur to a similar degree in both stents.

Similar to free expansion, both stent designs showed 'negative dogboning' when expanded inside a straight stenotic vessel. However, the degree of retraction was lower in the stenotic straight vessel than during free expansion. The proximal end underwent approximately 88% of the maximum radial displacement.

	Dogboning (%)			
	Thin_proxhf	thin_dishf	thick_proxhf	thick_dishf
Case study 1	-34.9	-16	-34.5	-8
Case study 2	-15.1	-3.4	-14.1	-5.4
Case study 3	-15.1	-3.4	-7.6	-0.8
Case study 4		13.7		13.1

Table 5.2 Dogboning of $Mlink_{thin}$ and $Mlink_{thick}$ after deployment, for all of the case studies evaluated in this thesis.

In case study 4, however, under the influence of a localised stenotic vessel geometry, a similar degree of dogboning was exhibited by $Mlink_{thin}$ and $Mlink_{thick}$, see Table 5.2. This is due to the geometry of the localised stenosed vessel geometry, whereby the stents conformed to the plaque geometry, resulting in the ends experiencing more radial displacement.

It is clear therefore that the degree of dogboning of a stent is dependant on the strut thickness and design of the stent but is more highly depentant on the host vessel geometry.

5.5 Radial Recoil

Radial recoil is a common characteristic of metallic stents whereby the stents radially retract during the recovery of elastic deformation after the removal of the balloon pressure. Radial recoil is generally regarded as undesirable since it results in lumen loss after stent deployment. Radial strength is one of the fundamental characteristics of a stent since it defines the ability of stent to withstand the elastic recoil and collapsing force of a vessel wall and it is therefore needed to ensure the vessel is maintained open. Radial recoil of $Mlink_{thin}$ and $Mlink_{thick}$ was found to be consistently higher for $Mlink_{thick}$ compared with $Mlink_{thick}$ for all of the case studies, see Figure 5.3.

It is interesting to note the deviation of radial recoil within each stent. For example, in case study 1, the $Mlink_{thin}$ was found to have radial recoil of 4-5% in the central and distal regions, whilst the proximal end was found to radially recoil by 7%. The same pattern of radial recoil was observed within the thicker strut stent.

Whilst the radial recoil was consistently higher in $Mlink_{thin}$, the vessel geometry also had an influence on the magnitude of the recoil. Radial recoil was found to be significantly higher under the influence of a stenotic vessel compared with free expansion, see Figure 5.3.

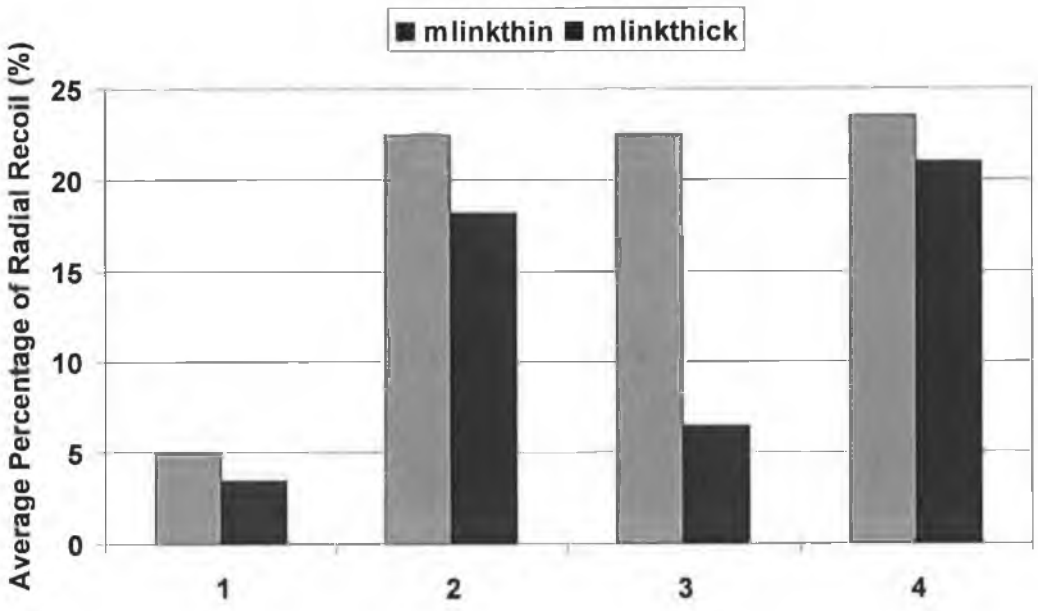

Figure 5.3 Comparison of radial recoil of $Mlink_{thin}$ and $Mlink_{thick}$; 1) free expansion (Case study 1); within a straight stenotic vessel achieving the same initial lumen diameter (Case study 2); within a straight stenotic vessel achieving the same final lumen diameter (Case study 3); and within a localised stenotic vessel achieving the same initial lumen diameter (Case study 4).

5.6 Stresses Induced Within The Stented Vessels

Three case studies were carried out to establish the relationship between the strut thicknesses and vessel stresses. The stresses induced within the vascular wall by $Mlink_{thin}$ and $Mlink_{thick}$ were examined in each case study. Migliavacca *et al.* [86] and Petrini *et al.* [48] have previously reported the stresses found in a stented vessel during stent deployment. In addition, Lally *et al.* [41] and Holzapfel *et al.* [32] have further suggested that these stresses found in the vascular wall may be used as a measure of restenosis outcome.

The differences in the levels of stresses in the circumferential, radial and longitudinal direction were examined for both $Mlink_{thin}$ and $Mlink_{thick}$. In addition, the von Mises stress was also examined. The stresses found within the vascular wall at loading were taken as a measure of acute damage and those at

unloading as a measure of long-term damage. The acute damage is predicted to cause the initial laceration to the arterial wall whilst the long-term damage must be minimized, as the stent scaffolds the vascular wall, to prevent an aggressive long-term vascular response to this damage and ultimately restenosis.

All of the stress analyses carried out indicated that the tensile circumferential stresses were of highest magnitude in comparison to radial, longitudinal and von Mises stresses. Lally *et al.* [41] investigated the maximum principal stresses, which were noted to act in the circumferential direction, whilst Holzapfel *et al.* [32] also investigated changes in circumferential stress with variations in stent design. It is most likely, therefore, that the stresses acting in the circumferential direction are most important in terms of restenosis outcome.

Generally it was noted that as the stent expanded out against the vessel wall, with greater expansion of the vessel lumen higher stresses were induced within the vessel wall. The results also show that there is a significant difference between acute damage and long-term damage, where the magnitude of stresses were greatly reduced due to stent and vessel recoil. The reduced stresses found at unloading, or the long-term stresses, are those that would contribute to long-term damage, and hence the long-term restenotic response of the vessel. Clearly, therefore, theses stresses are of most interest in this study.

5.6.1 Stress Analysis: Case Study 2

Expansion of $Mlink_{thin}$ and $Mlink_{thick}$ inside a stenotic artery vessel geometry with arterial material properties, achieving the same initial expanded lumen diameter, $Ø_{I\ thin} = Ø_{I\ thick}$

$Mlink_{thin}$ and $Mlink_{thick}$ were expanded inside a stenotic vessel where they achieved the same initial expanded lumen diameter. The circumferential, radial and longitudinal stresses in the stented vessels were examined at loading and unloading, see Figure 5.4. It is clear that the tensile circumferential stress are the stresses of highest magnitude in the stented vessels, whilst the compressive longitudinal stresses are low and appear insensitive to loading and unloading.

The difference in percentage volumes of tissue stressed to high levels is more prominent at unloading than at loading, for all of the stresses induced in the stented vessels. It was found that $Mlink_{thick}$ caused significantly higher percentage volume of tissue to be stressed at high levels than the $Mlink_{thin}$. This result correlates with the findings of the ISAR Stereo Trial where the clinical result showed that the used of a thinner strut stent was associated with a significant reduction of angiographic restenosis than the thicker strut stent [26], whereby the thinner strut stent resulted in 15% angiographic restenosis compared with 25.8% for the thicker strut stent.

It is interesting to note that this significant difference in the volume stresses for the two stents is due to the fact that as discussed earlier, $Mlink_{thin}$ resulted in a higher level of recoil and consequently produced a smaller expanded final lumen vessel than $Mlink_{thick}$. During the clinical intervention, x-ray angiography was used as a visual aid for the operators and it was left to the operators' discretion to achieve the desired luminal gain observed through angiography [26]. The luminal gain observed by the operators would be the initial expanded lumen diameter before the pressure was removed. Due to the thin geometry struts of the $Mlink_{thin}$, the stent has a higher degree of recoil and consequently results in a lower expanded final lumen diameter than the $Mlink_{thick}$ lowering the stresses induced within the vessel. As a result, the stresses within the vessel stented with the thinner strut stent were found to be lower than the vessel stented with a thicker strut stent.

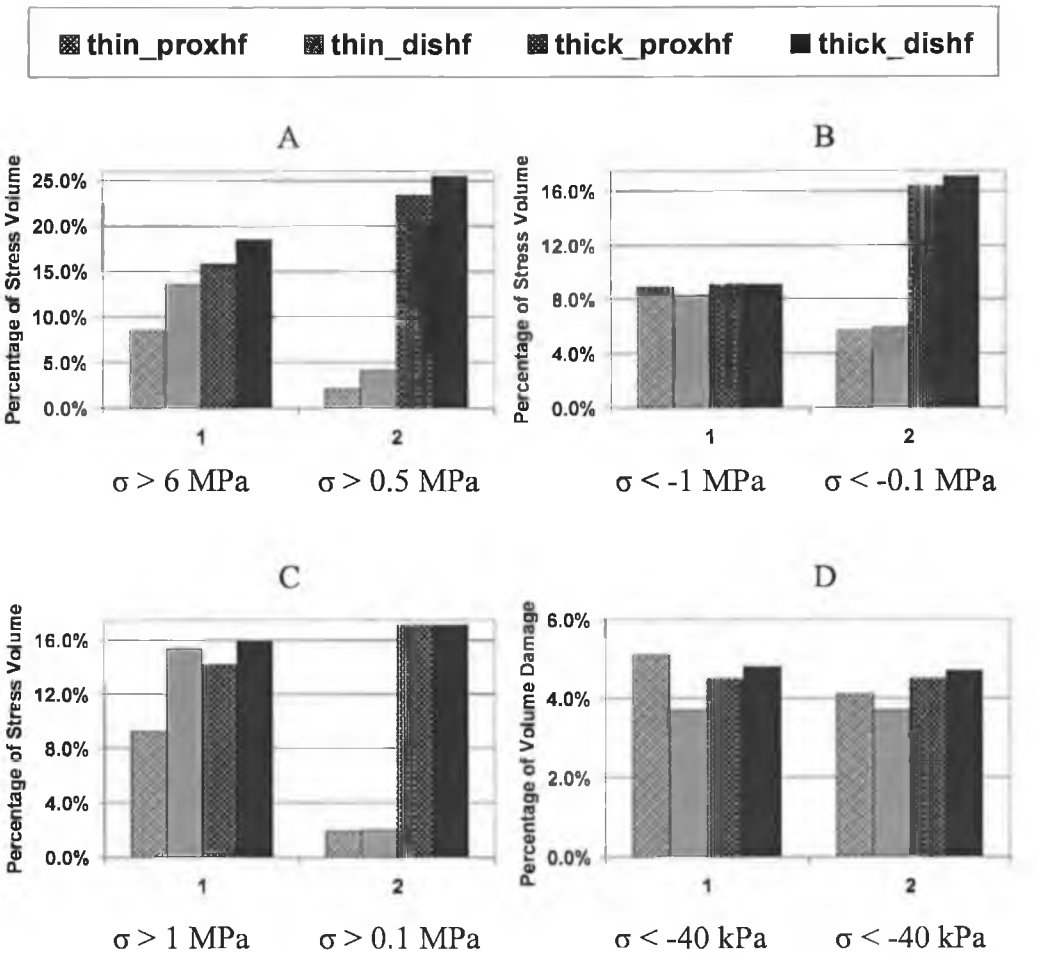

Figure 5.4 Comparison of tensile circumferential stresses (A), compressive radial stresses (B), tensile longitudinal stresses (C) and compressive longitudinal stresses (D), at loading (1) and unloading (2), in vessels by $Mlink_{thin}$ and $Mlink_{thick}$, whereby the stents were expanded to achieve the same initial lumen diameter of 3 mm, and at unloading $Mlink_{thin}$ and $Mlink_{thick}$ achieved a final lumen diameter of 2.28 mm and 2.54 mm respectively.

5.6.2 Stress Analysis: Case Study 3

Expansion of $Mlink_{thin}$ and $Mlink_{thick}$ inside a stenotic artery vessel geometry with arterial material properties as in Case Study 2, however, achieving the same final lumen diameter, $Ø_{F\ thin} = Ø_{F\ thick}$

Finite element simulations were carried out where $Mlink_{thin}$ and $Mlink_{thick}$ were expanded inside a stenotic vessel identical to that used in the previous analyses but where the stents were allowed to recoil to achieve the same expanded final lumen diameter. The circumferential, radial and longitudinal stresses in the stented vessels were examined at loading and unloading, see Figure 5.5. The tensile circumferential stresses were again found to be the stresses of highest magnitude in the vessels.

However, in this case, the difference in percentage of tissue volume damage at loading is more prominent than at unloading. As it was established earlier that stresses increase with luminal gain, this prominent difference in the stresses found at loading was due to the fact that the $Mlink_{thin}$ had to be expanded more to produce a higher initial lumen diameter than the $Mlink_{thick}$, as $Mlink_{thin}$ recoiled more to achieve the same final lumen diameter. At unloading, the amounts of volume stressed at specific magnitudes were analysed. In this case, it was clear that $Mlink_{thin}$ resulted in a marginally higher percentage volume of tissue stressed to high levels when compared with $Mlink_{thick}$, see Figure 5.5.

This resulting higher volume damage found in $Mlink_{thin}$ may be explained by the fact that the vessel load to be supported, to maintain the vessel open at the same vessel lumen diameter, is supported by a lower area in the thin strut stent compared with the thick strut stent since the artery-stent contact area is lower for the $Mlink_{thin}$.

In addition, the magnitude of the pressure used for stents's expansion for these analyses was higher for $Mlink_{thin}$ at 8.2 MPa compared with 2.2 MPa for $Mlink_{thick}$. Clearly, this difference in the pressure applied to the stents causes the difference in the stresses found in the stented vessel wall on loading.

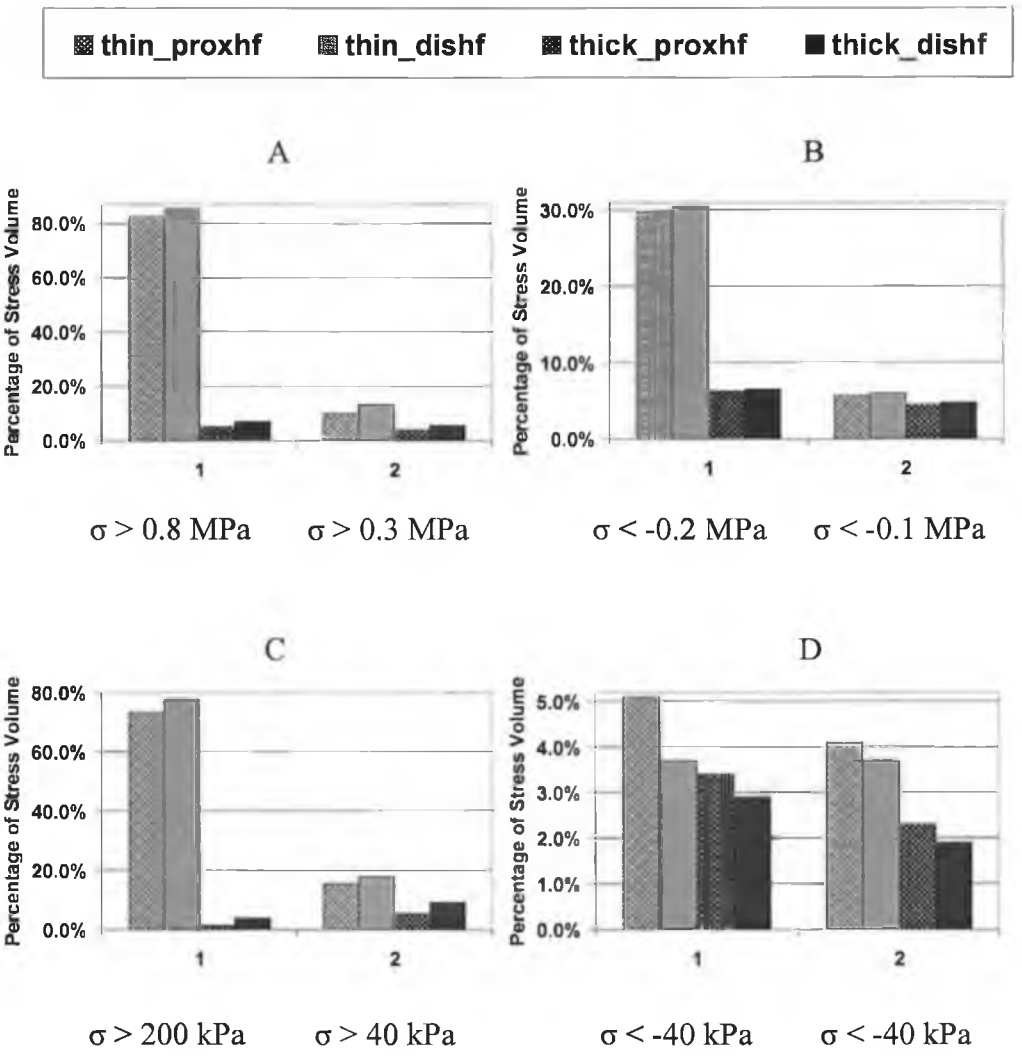

Figure 5.5 Comparison of (A) tensile circumferential stresses; (B) compressive radial stresses; (C) tensile longitudinal stresses; and (D) compressive longitudinal stresses, at loading (1) and unloading (2), in stented vessels by $Mlink_{thin}$ and $Mlink_{thick}$, whereby they were expanded to achieve the same final lumen diameter of 2.28 mm, whereby at loading $Mlink_{thin}$ achieved the inital lumen diameter of 3 mm and 2.48 mm for $Mlink_{thick}$.

5.6.3 Stress Analysis: Case Study 4

Expansion of $Mlink_{thin}$ and $Mlink_{thick}$ inside a localised stenotic artery, achieving the same initial expanded lumen diameter, $Ø_{I\ thin} = Ø_{I\ thick}$

Finite element simulations were carried out where $Mlink_{thin}$ and $Mlink_{thick}$ were expanded inside a localized stenotic vessel achieving the same initial lumen diameter. The circumferential, radial and longitudinal stresses in the stented vessels were examined at loading and unloading, see Figure 5.6. In these analyses, the tensile circumferential stresses were also found to be the stresses of highest magnitude in both stented vessels.

As for case study 2, the $Mlink_{thick}$ caused greater volumes of tissue to be stressed at high levels compared with $Mlink_{thin}$. It was noted that the magnitudes at which the vascular wall was stressed were significantly higher than the previous analyses, particularly on loading. The type of plaque and the geometry of the vessel wall greatly influenced the results in terms of the magnitude and the distribution of the resulting stresses found in the vascular wall. The pressures used to expand the stents inside the vessels were approximately five times the pressures used in the previous analyses. These high pressures resulted in the significantly higher stresses induced within the vessel wall, see Figure 5.6.

These analyses illustrate the relationship between the stresses induced in the vascular wall and the results obtained in the clinical study, the ISAR STEREO Trial [26]. Although the stress analyses do not identify the exact percentage of restenosis they do show that there is a much greater volume of tissue stressed to elevated levels in the vessels stented by $Mlink_{thick}$ particularly in the circumferential direction at unloading. This difference in the stresses found within the stented vessels can be identified as the potential mechanical stimuli for in-stent restenosis. Theses stresses, which are markedly different for the two stents on unloading, are deemed to act as a long-term stimulus for in-stent restenosis.

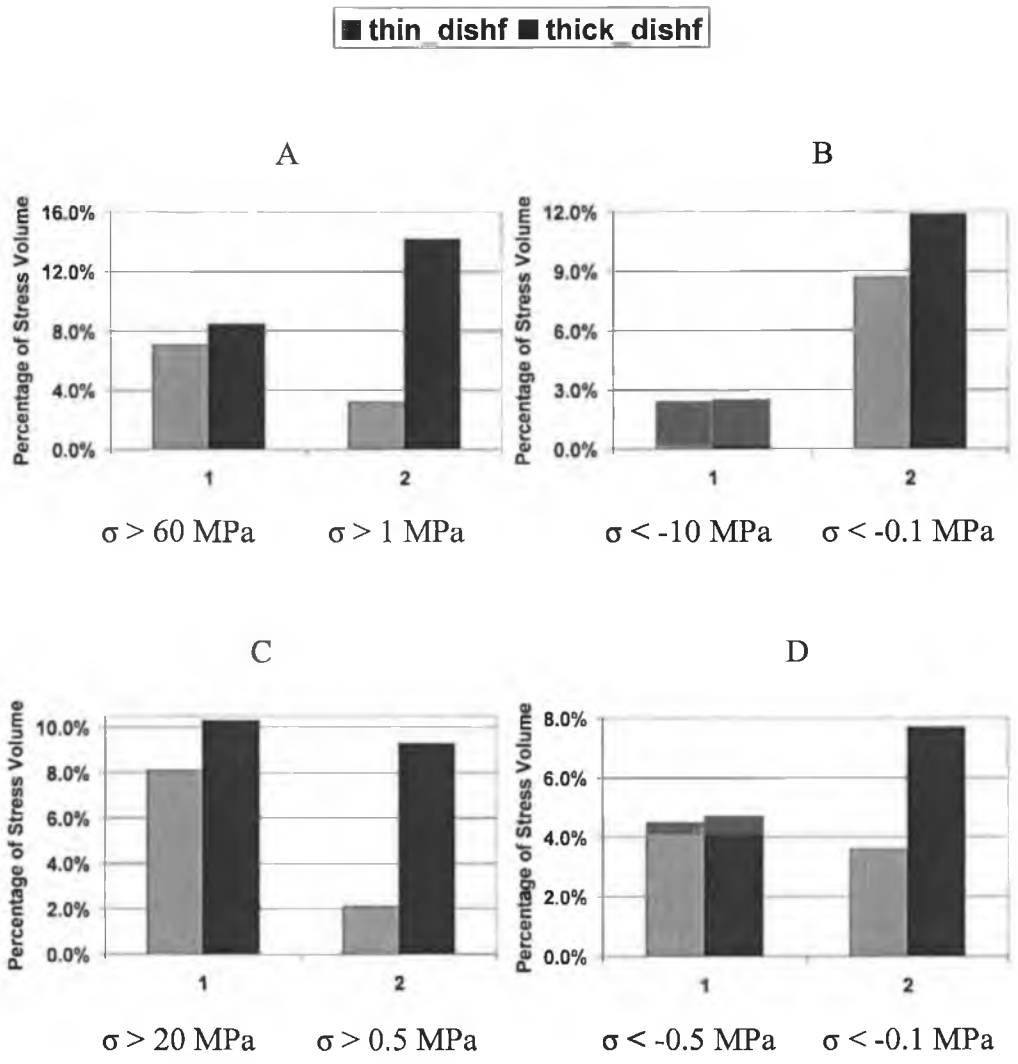

Figure 5.6 Comparison of (A) tensile circumferential stresses; (B) compressive radial stresses; (C) tensile longitudinal stresses; and (D) compressive longitudinal stresses at loading (1) and unloading (2), in stented vessels by $Mlink_{thin}$ and $Mlink_{thick}$ The stents were expanded to achieve the same initial lumen diameter of 3.18 mm, and at unloading $Mlink_{thin}$ and $Mlink_{thick}$ achieved a final lumen diameter of 2.44 mm and 2.52 mm, respectively.

5.7 Preclinical Testing Of Stents And Stent Design

Intravascular stenting has emerged over the years as among the most successful treatment of coronary artery disease. However, this promising intervention presents in-stent restenosis as the major limitation to stenting procedure. Stent design has been identified as a major factor in determining restenosis outcome. This finite element study is used as a preclinical tool to investigate the expansion of stent's complex structure and identify the influence of stent design on the resulting stresses found in the stented arteries, thus direct comparison was made to clinical study by Kastrati *et al.* [26].

The stent's structure after deployment is highly dependent on the geometry of the stenosed artery. The complex geometry of the stent's structures resulted in a non-uniform radial displacement distribution. Thinner strut stent exhibits greater radial recoil than the thicker strut stent under free expansion. This may serve as a disadvantage in obtaining the adequate luminal gain. Both stents were then expanded inside a various stenosed arteries to examine the effects of different strut thickness stents on their structures expansion and the resulting stresses induced within the stented vessels. Since radial recoil play a major role in obtaining the sufficient luminal gain, the stresses within the stented vessels were examined at the end of loading, where the initial luminal gain is achieved and at the end of unloading, where the luminal loss is observed as radial recoil takes place.

These stresses in the former are believed to act as a stimulus for acute damage while long-term stresses are of most interest in this study since these stresses must contribute to the long-term growth of in-stent restenosis. The acute loading of the vessel may cause damage to the vessel however acute loading is also observed in balloon angioplasty. In balloon angioplasty restenosis is not due to neotimal growth but primarily due to vessel recoil. Therefore, it may be the recoil of the vessel that lowers the stresses in balloon angioplasty such that the vessel does not respond with high neointimal growth.

Clearly therefore, for stenting there may be an optimal level of vessel expansion that achieves a sufficiently large lumen to restore blood flow but does

not illicit an aggressive restenotic response and subsequently restenosis in stented vessels. The high radial recoil of the thin strut stent may enable this optimum vessel diameter to be more easily achieved when compared with the $Mlink_{thick}$ and therefore result in the thin strut stent having a lower propensity for restenosis.

Overall therefore, there may be an optimum expansion pressure for all stent designs that is required to achieve this optimum diameter and which depends upon the vessel wall geometry as well as the arterial material properties.

Chapter 6

CONCLUSIONS

6.1 Main Findings

The main objective of this thesis was to identify the mechanical stimuli for in-stent restenosis. This study focused on examining the role of strut thickness on restenosis outcome. Finite element analyses were used to examine the expansion of a thinner strut stent and a thicker strut stent in various stenosed vessel geometry. Stress analyses were carried out on the stented vessels and a comparison was made to the clinical data. The main conclusions of this study are as follows:-

1. There is a significant difference between the expansion characteristics of a stent on free expansion compared with the stent when it is expanded inside a stenotic vessel. Free expansion of the stents in this study showed no foreshortening and gave rise to elongation whereas elongation was not observed when the stent was expanded inside a stenotic vessel.
2. The geometry of the stenotic vessel has a significant influence on a stent's expansion. In this study dogboning of the stent was observed when it was expanded inside a localised stenotic vessel whilst 'negative dogboning' was seen under free expansion and under the influence of an idealised straight stenotic vessel.

3. For the same stent design, a thinner strut stent has a higher level of recoil than a thicker strut stent. This leads to lower final luminal gain in a vessel stented by a thinner strut stent, when both stents are expanded to achieve the same initial luminal gain. Since the analyses show that the magnitude of stresses increases with luminal gain, the thicker strut stent resulted in a higher luminal gain and hence higher stresses in the vascular wall.

4. Higher stresses occurred in the vessel wall of the thicker strut stent for the same initial lumen diameter. Since available clinical data indicates that a thicker strut stent has a greater propensity for restenosis, this indicates that wall stresses may act as the stimulus for restenosis. The difference in stress magnitudes and volumes of tissues stressed at high levels in the vessels stented with the different strut stents was found to be most pronounced in the circumferential direction but was also evident in the radial and longitudinal directions. The tensile circumferential stresses may therefore be the main stimulus for in-stent restenosis.

5. The analyses indicate that long-term damage, or stresses on stent unloading, may be the critical stresses for stimulating the progression of restenosis.

6. The stenting analyses, where both stents were expanded such that they achieved the same final lumen diameter, suggest that thicker strut stent, or any stent design, may have the potential to be expanded to an optimal diameter whereby the proliferation of neointima is minimised. Therefore, the use of preclinical testing tools, such as finite element modelling, could be used to predetermine the level of expansion that a particular stent should be subjected to in order to achieve the optimum luminal gain and minimise the stimuli for in-stent restenosis.

7. Vessel wall stresses, induced through stent expansion, are highly dependant on the stent design, the luminal pressure, the vessel geometry and the vessel material properties.

6.2 Future Work

The main findings of this thesis have determined the role of strut thickness on restenosis outcome. This knowledge could improve the development of intravascular stenting. The following recommendations are proposed:-

1. Cell tests could be carried out on vascular smooth muscle and endothelial cells to identify the specific level of stress at which neointima starts to proliferate in an aggressive manner. This data could then be used in finite element studies to determine the optimum vessel diameter which would not reach those critical stress levels for various stent designs. The balloon pressures required to achieve these vessel diameters, in different vessel geometries with different material properties, could also be established using finite element techniques.
2. Realistic stenosed vessel geometries could be obtained from in-vivo imaging, such as Intravascular Ultrasound, and used in the finite element preclinical tests of stents to determine the stent most suited to particular host vessel geometries.
3. Finite element analyses are highly dependent upon the accuracy of the material models used in the analyses. Further tests could be carried out on human atherosclerotic plaque tissue to add to the limited data currently available. This would enable the range of properties of plaque tissues to be determined and the influence that changes in these properties have on the outcome of stenting procedures to be determined. Further data would also enable more accurate constitutive models for the tissue to be implemented in preclinical tests of intravascular stents.
4. Ultimately, preclinical testing could lead to patient-specific analyses capable of determining the optimum stent design and stent deployment protocol that reduces the likelihood of in-stent restenosis for a particular stenotic vessel with specific material properties.

REFERENCES

[1] Ward, M., (2005), "Implementation of secondary prevention of coronary heart disease in primary care", Heartwise, Irish Heart Foundations magazine, Volume 8, Issue 1, Spring 2005.

[2] Central Statistics Office, [online], http://www.cso.ie/statistics/ (Accessed 7th March 2005).

[3] Irish Heart Foundation, Cardiovascular Mortality Rates, [online], http://www.irishheart.ie/iopen24/catalog/pub//CVDMortalityRates04.pdf (Accessed 2nd March 2005).

[4] Heart Centre, [online], http://heart.healthcentersonline.com (Accessed 12th December 2004).

[5] Rankin, J.M. and Penn, I.M., (1998), "Coronary stenting: A global perspective", Journal of the American College of Cardiology, pp.22-25.

[6] American Heart Association, [online], http://www.americanheart.org/presenter.jhtml?identifier=1200026 (Accessed 8th December 2004).

[7] Medline, [online], http://www.nlm.nih.gov/medlineplus/ency/presentations/100160_1.htm (Accessed 15th November 2004).

[8] PTCA, [online], http://www.ptca.org/ (Accessed 11th November 2004).

[9] Hospital In-Patient Enquiry (HIPE) System Unit, [online], http://www.esri.ie (Accessed 14th April 2005)

[10] Colombo, A. and Tobis, J., (2001), "Techniques in Coronary Artery Stenting", (2nd ed.), Martin Dunitz Lt., United Kingdom.

[11] Banka, V.S., Kochar, G.S., Maniet, A.R., D.O., Voci, G., (1993), "Progressive coronary dilation: An angioplasty technique that creates controlled arterial injury and reduces complications", American Heart Journal, Vol. 125, pp. 61-71.

[12] Guidant, http://www.guidant.com (Accessed 15th December 2004).

[13] Adam, [online], http://www.adam.com/ (Accessed 20th November 2004).

[14] Edelmen, E.R. and Rogers, C., (1998), "Pathobiologic responses to stenting", American Journal of Cardiology, Vol. 81, pp. 4E-6E.

[15] Sigwart, V.J., Puel, J. and Mirkovitch, V., (1987), "Intravascular stents to prevent occlusion and restenosis after transluminal angioplasty", N Engl J Med, Vol. 316, pp. 701-706.

[16] Moscucci, M., Mansour, K.A., Kent, K.C., Kuntz, R.E., Senerchia, C., Baim, D.S. and Carrozza, J.P., (1994), "Peripheral vascular complication of directional coronary atherectomy and stenting: Predictors, management, and outcome", American Journal of Cardiology, Vol. 74 (5), pp. 448-453.

[17] David, H., 1998, "Renal angioplasty and stenting", Asia Pacific Heart Journal, Vol. 7 (3), pp. 215-218.

[18] Sachar, R., Yadav, J.S. and Roffi, M., (2004), "Severe Bilateral Carotid Stenosis", Journal of the American College of Cardiology, Vol. 43 (8), pp. 1358-1362.

[19] Levin, T., Holloway, S. and Feldman, T., (2000), "Use of intracoronary stents for the prevention of restenosis", Interventional Cardiology.

[20] Fischman, D.L., Leon, M.B. and Baim, D.S., (1994), "A randomized comparison of coronary-stent implantation with balloon angioplasty in patients with coronary artery disease, New England Journal of Medicine, Vol. 331, pp. 496-501.

[21] Bult, H., (2000), "Restenosis: a challenge for pharmacology", Trends in Pharmacological Sciences, Vol. 21 (7), pp. 274-279.

[22] McClean, R. and Eigler, N.L., (2002), "Stent design: implications for restenosis", Reviews in Cardiovascular Medicine, Vol. 3, pp. S16-S22.

[23] Hausleiter, J., Kastrati, A, Mehilli, J., Schuhlen, H., Pache, J., Dotzer, F., Dirschinger, J. and Schomig, A., (2002), "Predictive factors for early cardiac events and angiographic restenosis after coronary stent placement

in small coronary arteries", Journal of the American College of Cardiology, Vol. 40, pp. 882-889.

[24] Escaned, J., Goicolea, J., Alfonso, F., Perez-Vizcayno, M.J., Hernandez, R., Fernandez-Ortiz, A., Banuelos, C. and Macaya, C., (1999), "Propensity and mechanism of restenosis in different coronary stent designs, Journal of the American College of Cardiology, Vol. 34 (5), pp. 1490-1497.

[25] Hoffmann, R., Mintz, G.S., Haager, P.K., Bozoglu, T., Grube, E., Michael Gross, Beythien, C., Mudra, H., vom Dahl, J. and Hanrath, P., (2002), "Relation of stent design and stent surface material to subsequent in-stent intimal hyperplasia in coronary arteries determined by intravascular ultrasound", American Journal of Cardiology, Vol. 89, pp. 1360-1364.

[26] Kastrati, A., Mehili, J. and Dirschinger, J., (2001), "Intracoronary stenting and angiographic results: Strut thickness effect on restenosis outcome (ISAR-STEREO) trial", Circulation, Vol. 103, pp. 2816-2821.

[27] Dumoulin, C. and Cochelin, B., (2000), "Mechanical behaviour modelling of balloon-expandable stents", Journal of Biomechanics, Vol. 33, pp. 1461-1470.

[28] Chua, S. N. D, Mac Donald, B. J. and Hashmi, M. S. J., (2002), "Finite element simulation of stent expansion", Journal of Materials Processing Technology, Vol. 120, pp. 335-340.

[29] Migliavacca, F., Petrini, L., Colombo, M., Auricchio, F. and Pietrabissa, R., (2002), "Mechanical behaviour of coronary stents investigated through the finite element method", Journal of Biomechanics, Vol. 35, pp. 803-811.

[30] Petrini, L., Migliavacca, F., Auricchio, F. and Dubini, G., (2004), "Numerical Investigation of the Intravascular Coronary Stent Flexibility", Journal of Biomechanics, Vol. 37, pp. 495-501.

[31] Lally, C., Dolan, F. and Prendergast, P.J., (2005), "Cardiovascular stent design and vessel stresses: a finite element analysis", Journal of Biomechanics, Vol. 38, pp. 1574-1581.

[32] Holzapfel, G.A., Stadler, M. and Gasser, T.C., (2005), "Changes in the mechanical environment of stenotic arteries during interaction with stents:

computational assessment of parametric stent designs", AMSE, Vol. 127, pp. 166-180.

[33] Humphrey, J.D., (2002), "Cardiovascular solid mechanics: cells, tissues, and organs", Springer, New York.

[34] Hayashi, K., (2003), "Mechanical properties of soft tissues and arterial walls, Biomechanics of soft tissue in cardiovascular systems", Wien, Springer.

[35] Ozolanta, I., Tetere, G., Purinya, B. and Kasyanov, V., (1998), "Changes in the mechanical properties, biomechanical contents and wall structure of the human coronary arteries with age and sex", Medical Engineering and Physics, Vol. 20, pp. 523-533.

[36] Frederick, H.S., (1994), "Biomaterials, Medical Devices and Tissue Engineering: An Intergrated Approach", Chapman & Hall, United Kingdom.

[37] van Andel, C.J., Pistecky, P.V. and Borst, C., (2003), "Mechanical properties of porcine and human arteries: implications for coronary anastomotic connectors, Annals of Thoracic Surgery, Vol. 76, pp. 58-65.

[38] Ahlgren, A.R., Astrand, H., Sandgren, T., Vernersson, E., Sonesson, B. and Lanne, T., (2001), "Dynamic behaviour of common femoral artery: age and gender of minor importance", Ultrasound in Medicine & Biology, Vol. 27 (3), pp. 181-188.

[39] Cheng, K.S., Tiwari, A., Baker, C.R., Morris, R., Hamilton, G. and Seifalian, A.M., (2002), "Impaired carotid and femoral viscoelastic properties and elevated intima-media thickness in peripheral vascular disease", Atherosclerosis, Vol. 164 (1), pp. 113-120.

[40] Vito, R.P. and Dixon, S.A., (2003), "Blood vessel constitutive models – 1995-2002", Annual Review of Biomedical Engineering, Vol. 5, pp. 413-439.

[41] Lally, C., Reid, A.J. and Prendergast, P.J., (2004), "Elastic behaviour of porcine coronary artery tissue under uniaxial and equibiaxial tension", Annals of Biomedical Engineering, Vol. 32 (10), pp. 1355-1364.

[42] Holzapfel, G.A., Gasser, T.C. and Stadler, M., (2002), "A structural model for the viscoelastic behaviour of arterial walls: continuum formulation and finite element analysis", European Journal of Mechanmics A/Solids, Vol. 21, pp. 441-463.

[43] Rachev, A. and Greenwalf, S.E., (2003), "Residual strains in conduit arteries", Journal of Biomechanics, Vol. 36 (5), pp. 661-670.

[44] Holzapfel, G.A., Gasser, T.C. and Stadler, M., (2000), "A new constitutive framework for arterial wall mechanics and a comparative study of material models", Journal of Elasticity, Vol. 61, pp. 1-48.

[45] Menzel, A., (2005), "Modelling of anisotropic growth in biological tissues: a new approach and computational aspects", Biomechanical Model Mechanobiology, Vol. 3, pp. 147-171.

[46] Lally, C. and Prendergast, P.J., (2003), "An investigation into the applicability of a mooney-rivlin constitutive equation for modelling vascular tissue in cardiovascular stenting procedures", In Proceedings of the International Congress on Computational Biomechanics, Zaragoza, Spain, pp. 542-550.

[47] Fung, Y.C., (1993), "Biomechanics: Mechanical Properties of Living Tissues", Springer, New York.

[48] Petrini, L., Migliavacca, F., Dubini, G. and Auricchio, F., (2003), "Numerical Analysis of Vascular Stents Exploiting Shape-Memory-Alloy Behavior", 16th AIMETA Congress of Theoretical and Applied Mechanics.

[49] Carmines, D.V., McElhaney, J.H. and Stack, R., (1991), "A piece-wise non-linear elastic stress expression of human and pig coronary arteries tested in vitro", Journal of Biomechanics, Vol. 24, pp. 899-906.

[50] Rogers, C., Tseng, D.Y., Squire, J.C. and Edelman, E.R., (1999), "Balloon-artery interactions during stent placement: a finite element analysis approach to pressure, compliance, and stent design as contributors to vascular injury", Circulation Research, Vol. 84, pp. 378-383.

[51] Berry, J.L., Manoach, E., Mekkaoui, C., Rolland, P.H., Moore, J.E. Jr, Rachev, A., (2002), "Hemodynamics and wall mechanics of a compliance

matching stent: in vitro and in vivo analysis", Journal of Vascular Interventional Radiology, Vol. 13, pp. 97-105.

[52] Chua, S. N. D., MacDonald, B.J. and Hashmi, M.S.J., (2004), "Finite element simulation of slotted tube (stent) with the presence of plaque and artery by balloon expansion", Journal of Materials Processing Technology, pp. 1772-1779.

[53] Auricchio, F., Di Loreto, M. and Sacco, E., (2001), "Finite-element analysis of a stenotic artery revascularisation through a stent insertion", Computer Methods in Biomechanics and Biomedical Engineering, Vol. 4, pp.249-263.

[54] Loree, H.M., Grodzinsky, A.J., Park, S.Y., Gibson, L.J. and Lee, R.T., (1994), "Static and circumferential tangential modulus of human atherosclerotic tissue", Journal of Biomechanics, Vol. 27, pp. 195-204.

[55] Macaya, C., Serruys, P.W., Ruygrok, P., Suryapranata, H., Mast, G., Klugmann, S., Urban, P., den Heijer, P., Koch, K., Simon, R., Morice, M.C., Crean, P., Bonnier, H., Wijns, W., Danchin, N., Bourdonnec, C. and Morel, M.A., (1996), "Continued Benefit of Coronary Stenting Versus Balloon Angioplasty: One Year Clinical Follow-Up of Benestent Trial", Journal of the American College of Cardiology, Vol. 27, pp. 255-261.

[56] Kiemeneij, F., Serruys, P.W., Macaya, C., Rutsch, W., Heyndrickx, G., Albertsson, P., Fajadet, J., Legrand, V., Materne, P., Belardi, J., Sigwart, U., Colombo, A., Goy, J.J., Disco, C.M. and Morel, M.A., (2001), "Continued benefit of coronary stenting versus balloon angioplasty: five-year clinical follow-up of Benestent-I trial", Journal of the American College of Cardiology, Vol. 37, pp. 1598-1603.

[57] Rubartelli, P., Niccoli, L., Verna, E., Giachero, C., Zimarino, M., Fontanelli, A., Vassanelli, C., Campolo, L., Martuscelli, E. and Tommasini, G., (1998), "Stent implantation versus balloon angioplasty in chronic coronary occlusions: results from the GISSOC trial", Journal of the American College of Cardiology, Vol. 32, pp. 90-96.

[58] Pratsos, A., Fischman, D.L. and Savage, M.P., (2001), "Restenosis in SaphenousVein Grafts", Current Interventional Cardiology Reports, Vol. 3, pp. 287-295.

[59] Schwartz, R.S. and Henry, T.D., (2002), "Pathophysiology of coronary artery restenosis", Review of Cardiovascular Medicine, Vol. 3 (5), pp. S4-9.

[60] Zimmermann, A., Pollinger, B., Rieber, J., Konig, A., Erhard, I., Krotz, F., Sohn, H.Y., Kantlehner, R., Haimerl, W., Duhmke, E., Leibig, M., Theisen, K., Klauss, V. and Schiele, T.M., (2005), "Early time course of neointima formation and vascular remodelling following percutaneous coronary intervention and vascular brachytherapy of in-stent restenotic lesions as assessed by intravascular ultrasound analysis", Journal of Cardiology, Vol. 94 (4), pp. 239-246.

[61] Moreno, P.R., Palacios, I.F., Leon, M.N., Rhodes, J., Fuster, V. and Fallon, J.T., (1999), "Histopathologic comparison of human coronary in-stent and post-balloon angioplasty restenotic tissue", Am J. Cardiol, Vol. 84 (4), pp. 462-466.

[62] Horne, McD., (2005), "Overview of hemostasis and thrombosis; current status of antithrombotic therapies", Thrombosis Research, in press.

[63] Bauters, C. *et al.*, (1996), "Mechanism and prevention of restenosis: from experimental models to clinical practice", Cardiovascular Research, Vol. 31, pp. 835-846.

[64] Bauters, C. and Isner, J.M., (1997), "The biology of restenosis", Progress in Cardiovascular Diseases, Vol. 40 (2), pp. 107-116.

[65] Lowe, H.C., Schwartz, R.S., Mac Neill, B.D., Jang, I.K., Hayase, M., Rogers, C. and Oesterle, S.N., (2003), "The porcine coronary model of in-stent restenosis: current status in the era of drug-eluting stents", Catheterisation and Cardiovascular Interventions, Vol. 60, pp. 515-523.

[66] Dangas, G. and Fuster, V., (1996), "Management of restenosis after coronary intervention", Am Heart J, Vol. 132, pp. 428-436.

[67] Schwartz, R.S., Chronos, N.A. and Virmani, R., (2004), "Preclinical restenosis models and drug-eluting stents, still important, still much to learn", Journal of the American College of Cardiology, Vol. 44 (7), pp. 1373-1385.

[68] Waksman, R., (2002), "Drug-eluting stents, from bench to bed", Cardiovascular Radiation Medicine, Vol. 3, pp. 226-241.

[69] Morton, A.C., Crossman, D. and Gunn, J., (2004), "The influence of physical stent parameters upon restenosis", Pathologie Biologie, Vol. 52, pp. 196-205.

[70] Schachter, L.G. and Bakarat, A.I., (2001), "Computational study of arterial flow disturbance induced by intravascular stents", The ASME Bioengineering Conference, Vol. 50.

[71] Carter, A.J., Lee, D.P. and Yeung, A.C., (2001), "Metaling with new stent designs", Catheterisation and Cardiovascular Interventions, Vol. 53, pp. 426-428.

[72] Colombo, A., Stankovic, G. and Moses, J.W., (2002), "Selection of coronary stents", Journal of the American College of Cardiology, Vol. 40 (6), pp. 1021-1033.

[73] Stoeckel, D., Bonsignore, C. and Duda, S., (2002), "A survey of stent designs", Min Invas Ther & Allied Technology, Vol. 11 (4), pp. 137-147.

[74] Hautmann, H. and Huber, R.M., (1996), "Stent flexibility: an essential feature in the treatment of dynamic airway collapse", European Respiratory Journal, Vol. 9, pp. 609-611.

[75] Kuntz, R.E., Safian, R.D., Levine, M.J., Reis, G.J., Diver, D.J. and Baim, D.S., (1992), "Novel approach to the analysis of restenosis after the use of three new coronary devices", Journal of American College of Cardiology, Vol. 19, pp. 1493-1499.

[76] Ferrero, V., Ribichini, F., Heyndrickx, G.R., De Bruyne, B., Piessens, M., Carlier, S., Buchi, M., Matullo, G., Vassanelli, C. and Wijns, W., (2004), "Angiographic and three-dimensional intravascular ultrasound analysis of combined intracoronary beta radiation and self-expanding stent implantation in human coronary arteries", Am J Cardiol, Vol. 94, pp. 1237-1242.

[77] Lansky, A.J., Mintz, G.S., Mehran, R., Popma, J.J., Pichard, A.D., Kent, K.M., Satler, L.F. and Leon, M.B., (1998), "Insights into the mechanism of restenosis after PTCA and stenting", Indian Heart J., Vol. 50, Suppl 1, pp. 104-108.

[78] Carrozza, J.P. Jr, Hosley, S.E., Cohen, D.J. and Baim, D.S., (1999), "In *Vivo* Assessment of Stent Expansion and Recoil in Normal Porcine

Coronary Arteries: Differential Outcome by Stent Design", Circulation, Vol. 100, pp. 756-760.

[79] Stankovic, G., Briguori, C., Sarais, C., Pagnotta, P., Liistro, F., Montorfano, M., Chieffo, A., Sgura, F., Corvaja, N., Albiero, R., Toutoutzas, C., Bonizzoni, E., Di Mario, C. and Colombo, A., (2001), "Effect of Strut Thickness on Angiographic Restenosis Rate After Coronary Stenting", Journal of the American College of Cardiology, Vol. 40, pp. 403-409.

[80] Costa, M.A., Sabate, M., Kay, I.P., de Feyter, P.J., Kozuma, K., Serrano, P., de Valk, V., Albertal, M., Ligthart, J.M., Disco, C., Foley, D.P. and Serruys, P.W., (2000), "Three-Dimensional Intravascular Ultrasonic Volumetric Quantification of Stent Recoil and Neointimal Formation of Two New Generation Tubular Stents", Journal of the Americal College of Cardiology, Vol. 85, pp. 135-139.

[81] Taylor, A.J., Gorman, P.D., Kenwood, B., Hudak, C., Tashko, G. and Virmani, R., (2001), "A comparison of four stent designs on arterial injury, cellular proliferation, neointima formation, and arterial dimensions in an experimental porcine model", Catheterisation and Cardiovascular Interventions, Vol. 53, pp. 420-425.

[82] Edelman, E.R., Seifert, P., Groothuis, A., Morss, A., Bornstein, D. and Rogers, C., (2001), "Gold-Coated NIR Stents in Porcine Coronary Arteries", Circulation, Vol. 103, pp. 429-434.

[83] Pache, J., Kastrati, A., Mehilli, J., Schuhlen, H., Dotzer, F., Hausleiter, J., Fleckenstein, M., Neumann, F.J., Sattelberger, U., Schmitt, C., Muller, M., Dirschinger, J. and Schomig, A., (2003), "Intracoronary Stenting and Angiographic Results: Strut Thickness Effect on Restenosis Outcome (ISAR-STEREO-2) Trial", Journal of the American College of Cardiology, Vol. 41.

[84] Chua, S. N. D., MacDonald, B.J. and Hashmi, M.S.J., (2003), "Finite element simulation of stent and balloon interaction", Journal of Materials Processing Technology, Vol. 143-144, pp. 591-597.

[85] McGarry, J.P., O'Donnell, B.P., McHugh, P.E. and McGarry, J.G., (2004), "Analysis of the mechanical performance of a cardiovascular stent design based on micromechanical modelling", Computational Materials Science, Vol. 31, pp. 421-438.

[86] Migliavacca, F., Petrini, L., Colombo, M., Auricchio, F. and Pietrabissa, R., (2003), "Deployment of an intravascular stent in coronary stenotic arteries: a computational study", Summer Bioengineering Conference, 25-29 June.

[87] Liang, D.K., Yang, D.Z., Qi, M., Wang, W.Q., (2005), "Finite element analysis of the implantation of a balloon-expandable stent in a stenosed artery", International Journal of Cardiology, Vol. 104, pp. 314-318.

[89] Serruys, P.W. and Kutryk, M.J.B., (2000), "Handbook of Coronary Stents", (3rd ed.), Martin Dunitz Lt., United Kingdom.

[90] Wilms, G., van Calenbergh, F., Stockx, L., Demaerel, P., van Loon, J. and Goffin, J., (2000), "Endovascular treatment of a ruptured paraclinoid aneurysm of the carotid syphon achieved using endovascular stent and endovascular coil placement", AJNR Am J Neuroradiol, Vol. 21, pp. 753-756.

[91] Kereiakes, D.J., Cox, D.A., Hermiller, J.B., Midei, M.G., Bachinsky, W.B., Nukta, E.D., Leon, M.B., Fink, S., Marin, L. and Lansky, A.J., (2003), "Usefullness of a cobalt chromium coronary stent alloy", The American Journal of Cardiology, Vol. 92 (4), pp. 463-466.

Appendix A

Simulation of a Full Model of $Mlink_{thick}$ inside a Stenotic Straight Vessel.

A.1 Introduction

Intravascular stenting procedure involves in the deployment of the stent inside a stenotic coronary artery. Full three-dimensional model of the stent expanded within a stenotic vessel were developed to determine more realistically the expansion of the stent and to quantify the stresses induced within stented stenotic coronary arteries. The finite element modelling of this procedure is a challenging study that involves large displacements and deformation, geometric and material non-linearity. Depending on the complications of the model, finite element simulation can be rather expensive on time consumption.

The purpose of this work is to study the movement of the artery vessel relative to the stent during stent expansion inside a stenotic vessel. This is for the purpose of providing justification in dividing the model into two halves models for the purpose of saving computational time and resources.

A.2 Materials and Method

Full three-dimensional model of $mlink_{thick}$ was developed to expand inside a stenotic coronary artery which was modelled as a straight vessel. The model composed of two bodies, the stent ($mlink_{thick}$) and the stenotic artery. The stent has an internal radius of 0.72 mm and outer radius of 0.86 mm. The straight

vessel has an internal radius of 1 mm and thickness of 0.8 mm, see Figure A.1. A uniform, linearly increasing radial pressure (P) of 10.5 MPa was applied as a surface load to the internal surface of the stent to deploy the stent within the vessel, which was subsequently removed.

The stent is made of 316L stainless steel with Young's modulus of 196 GPa and Poisson ratio of 0.3. The inelastic stress-strain behaviour was incorporated into the analysis through a Von Mises-Hill plasticity model with isotropic hardening using data obtained from Murphy *et al.* [88]. The non-linear stress-strain relationship of the arterial wall was described using a third order Mooney-Rivlin hyperelastic constitutive equation determined by fitting to data from uniaxial and equibiaxial tension tests of porcine coronary tissue by Lally ***et al.*** [41].

Figure A.1 Finite element mesh of $mlink_{thick}$ inside a stenotic vessel.

Due to symmetry, only 120 degrees in circumferential direction (one-third) was modelled. Cyclic symmetry boundary conditions were imposed on the nodes of the stent and the stenotic vessel in the circumferential plane of symmetry. Both ends of the stenotic vessel were constraint in the longitudinal direction. Two nodes in the middle of the stent were constraint in the longitudinal direction and one node of the stenotic vessel was constraint in the circumferential direction to prevent rigid body rotations, allowing the nodes movement relative to the constraint node.

Five elements were assigned through the thickness of the vessel, thirty elements were assigned in the circumferential length and ninety-six elements were assigned in the longitudinal length. There were 14,400 elements in total for the stenotic vessel and 532 elements were assigned to the stent. The element type used was a full integration, three-dimensional eight-node isoparametric arbitrary hexahedral element (Type 7 in Marc Mentat). A non-linear, large displacement analysis was performed using Msc Marc Mentat.

A.3 Results and Discussion

The radial displacement throughout the structure was found to be highly non-uniform, see Figure A.2. The stent was expanded to achieve 3 mm diameter. The movement of the artery relative to stent expansion in the middle plane were examined. The measurements were taken at full loading. It was found that the circumferential movement in the middle plane ranged from -0.02 mm to 0.03 mm, see Figure A.3 and the longitudinal movement ranged from 0.02 mm to 0.06 mm, see Figure A.4.

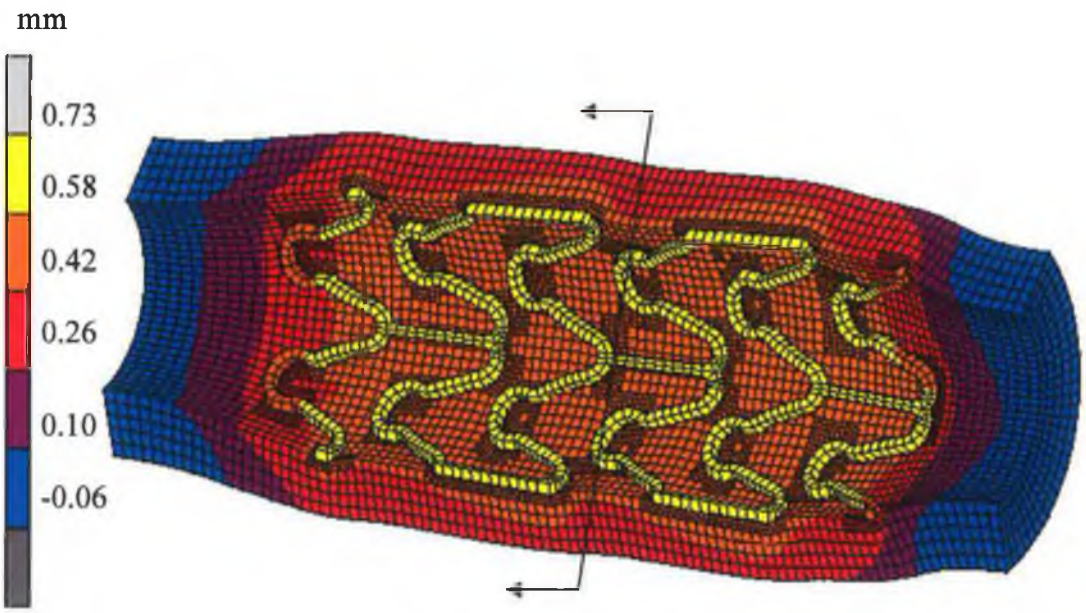

Figure A.2 Radial displacement distribution throughout mlinkthick scaffolding a stenotic vessel.

Figure A.3 Circumferential distribution throughout the middle plane of the vessel.

Figure A.4 Longitudinal distribution throughout the middle plane of the vessel.

A.4 Conclusions

The result shows that the displacement in the middle plane of the artery relative to the stent expansion was found minimal. The computational time for this model took 20 days to obtain 100% loading with a system of the following specification; Pentium 4 CPU, 1 GB of RAM and 2.6 GHz of speed. Therefore the full model was divided into two halves of proximal half and distal half.